

Time series analysis of wrist
accelerometry and cardiorespiratory
signals during sleep

DISSERTATION

zur Erlangung des Doktorgrades der Naturwissenschaften
(Dr. rer. nat.)

der

Naturwissenschaftlichen Fakultät II
Chemie, Physik und Mathematik

der Martin-Luther-Universität
Halle-Wittenberg

vorgelegt von

Herrn JOHANNES ZSCHOCKE

Erstgutachter: Herr PD Dr. J. Kantelhardt
Zweitgutachter: Herr PD Dr. V. Ivanov
Drittgutachterin: Frau Prof. Dr. D. Krefting

Tag der Abgabe: 26.01.2023

Tag der Öffentlichen Verteidigung: 05.09.2023

Vorsitzender der Promotionskommission: Herr Prof. Dr. Kay Saalwächter

ABSTRACT

This cumulative dissertation deals with the analysis of cardiorespiratory biosignals in combination with high resolution accelerometry. Today smartwatches and smartphones can often record similar data, albeit at slightly lower quality, opening up a huge field of possible applications.

In the first part, we have focused on biosignals hidden in acceleration measurements with high resolution that come as a by-product besides the quantification of physical activity and the detection of sleep, wake, and non-wear times, in large cohort studies like the “NAKO Gesundheitsstudie”. For wrist accelerometer data we have developed algorithms to extract the pulse wave propagating through the wrist, and also detect respiration movements during sleep. We found that pulse waves can be better reconstructed than respiration signals. Comparing sleep stages we found best reconstruction during deep sleep, while during wakefulness the reconstruction quality drops due to movement artifacts. We used the advantage of three dimensional accelerometry to identify the best axis for 30 second epochs and to identify epochs with poor signal quality.

The second part of the thesis investigates the scaling behavior of cardiorespiratory signals, in order to better understand the regulatory pathways in the human cardiorespiratory system. Therefore, detrended fluctuation analysis was applied, differentiating between short-term (6-16 seconds) and long-term (50-200 seconds) correlations. We found that heart and pulse rates are characterized by sex- and age-dependent short-term fluctuations, while their long-term fluctuations exhibit a clear sleep stage dependence: weak long-term correlations during non-REM sleep and pronounced long-term correlations during REM sleep and wakefulness. In contrast, pulse transit times do not show differences between short-term and long-term scaling behavior; their short-term fluctuations are less correlated and hardly depend on age or sex. The long-term scaling of all observed systems seems to be modulated by sleep stage patterns generated in the brain, while short-term control differs between the organ systems. Furthermore, fluctuation analysis of hip and wrist accelerometry were analyzed and compared on scales of 50 to 200 seconds, 5 to 20 minutes and 0.5 to 2 hours. We found that with increasing activity, the correlation increases on all mentioned scales. Moreover hip accelerometry appears to vary more on different scales than wrist accelerometry.

ZUSAMMENFASSUNG

Diese kumulative Dissertation befasst sich mit der Analyse von kardiorespiratorischen Biosignalen in Kombination mit hochauflösender Akzelerometrie. Smartwatches und Smartphones können ähnliche, wenn auch qualitativ etwas schlechtere, Daten aufzeichnen, wodurch sich ein riesiges Feld möglicher Anwendungen ergibt.

Im ersten Teil haben wir uns auf Biosignale konzentriert, die in hochaufgelösten Beschleunigungsmessungen verborgen sind. Diese Beschleunigungsmessungen werden eigentlich zur Quantifizierung der körperlichen Aktivität und der Erkennung von Schlaf-, Wach- und Nicht-Tragezeiten in großen Kohortenstudien eingesetzt, wie zum Beispiel in der NAKO-Gesundheitsstudie.

Für Beschleunigungsmessungen am Handgelenk haben wir Algorithmen entwickelt, die das Handgelenk durchlaufende Pulswellen extrahieren, sowie Atmungsbewegungen während des Schlafs detektieren. Wir konnten zeigen, dass sich Pulswellen besser rekonstruieren lassen als Atmungssignale. Bei dem Vergleich von Schlafstadien fanden wir die beste Rekonstruktion im Tiefschlaf, während im Wachzustand die Rekonstruktionsqualität aufgrund von Bewegungsartefakten abnimmt. Wir nutzten den Vorteil dreidimensionaler Beschleunigungsmessung, um die beste Achse für 30-Sekunden-Epochen zu identifizieren und Epochen mit schlechter Signalqualität zu erkennen.

Der zweite Teil der Arbeit behandelt das Skalenverhalten kardiorespiratorischer Signale, um die Regulationswege im menschlichen kardiorespiratorischen System besser zu verstehen. Dafür wurde die trendbereinigte Fluktuationsanalyse (DFA) verwendet, wobei zwischen kurzzeitigen (6–16 Sekunden) und langzeitigen (50–200 Sekunden) Korrelationen unterschieden wurde. Wir fanden heraus, dass Herz- und Pulsrate durch geschlechts- und altersabhängige kurzzeitige Fluktuationen gekennzeichnet sind, während ihre langzeitigen Fluktuationen eine klare Schlafstadienabhängigkeit aufweisen: schwache Langzeitkorrelationen während des Non-REM-Schlafs und ausgeprägte Langzeitkorrelationen während des REM-Schlafes und der Wachphase. Im Gegensatz dazu zeigen Pulslaufzeiten keine Unterschiede zwischen kurzzeitigem und langfristigem Skalenverhalten; ihre kurzzeitigen Fluktuationen sind weniger korreliert und kaum alters- oder geschlechtsabhängig. Das Langzeitskalenverhalten aller beobachteten Systeme scheint durch im Gehirn generierte Schlafstadienmuster moduliert zu werden, während die kurzzeitige Regulation zwischen den Organsystemen unterschiedlich ist. Weiterhin wurden die Fluktuationen der Hüft- und Handgelenkakkzelerometrie analysiert und auf Skalen von 50 bis 200 Sekunden, 5 bis 20 Minuten und 0,5 bis 2 Stunden verglichen. Wir fanden heraus, dass mit zunehmender Aktivität der Skalierungsexponenten auf allen genannten Skalen zunimmt. Darüber hinaus scheint die Hüftakkzelerometrie auf den verschiedenen Skalen stärker zu variieren als die Handgelenkakkzelerometrie.

CONTENTS

ABSTRACT	i
ZUSAMMENFASSUNG	iii
1 INTRODUCTION	1
1.1 Motivation	1
1.2 Goals	3
1.3 Outline	4
1.4 Remark to the term “pulse transit time”	4
2 METHODOLOGY	5
2.1 Polysomnography	5
2.1.1 Historic development	5
2.1.2 Modern polysomnography	6
2.1.3 Sleep stages	7
2.2 Accelerometry	8
2.2.1 Historic development	8
2.2.2 Technical details	9
2.2.3 Accelerometer devices	9
2.2.4 Advantages of accelerometry	10
2.3 Data acquisition studies	12
2.3.1 NAKO Gesundheitsstudie	12
2.3.2 Detection of the sleep-wake structure at night from actimetry and ECG recordings	13
3 PART I: HIDDEN SIGNALS IN ACCELEROMETER DATA	15
3.1 Introduction to signal reconstruction	15
3.1.1 A first hint - power spectra of accelerometry data	15
3.1.2 How to compare signals	18
3.2 Publication: Pulse wave reconstruction	19
3.3 Publication: Respiration reconstruction	39
3.4 Publication: Reconstruction dependencies on sleep stages	53
4 PART II: FLUCTUATION ANALYSIS STUDIES	67
4.1 Introduction to detrended fluctuation analysis	67
4.1.1 Cardiorespiratory regulation	67
4.1.2 Detrended fluctuation analysis	68
4.2 Publication: DFA of cardiorespiratory and brain signals.	71

4.3	Preliminary results of DFA in accelerometry data	85
4.3.1	Preprocessing of accelerometry data	85
4.3.2	Classification of accelerometry data	85
4.3.3	Results and discussion of accelerometry DFA	87
5	CONCLUSION AND OUTLOOK	91
6	BIBLIOGRAPHY	95
6.1	Publication List	95
6.2	References	98
7	CURRICULUM VITAE	107
8	DECLARATION UNDER OATH	
	EIDESSTATTLICHE ERKLÄRUNG	109
9	ACKNOWLEDGEMENTS	111

1 | INTRODUCTION

1.1 Motivation

Accelerometry. The use of accelerometers increased over the last years not only in personal devices, like smartphones and smartwatches, but also in huge studies like “NAKO Gesundheitsstudie”[1], “SHIP studies”[2], and “UK Biobank”[3]. Basically, this data is collected to score physical activity, to differentiate between lying, sedentary behavior or standing, but also to measure circadian rhythms.

However, highly time resolved (≥ 100 Hz) accelerometer data contain much more valuable information. It is possible to distinguish between wake, sleep and non-wear times based on the accelerometer measurements. Recent results show that modern machine learning approaches can even detect sleep stages [4]. Furthermore, pattern recognition can be used to distinguish between different kinds of physical activities, like jogging, cycling or rowing [5]–[7]. But that is not the end of the possibilities.

A deeper look into the raw accelerometer data of Fig. 1.1 unfolds a new world of hidden information and interesting areas. The upper plots show a typical 24 hour three dimensional (3D) accelerometry measurement for wrist (Fig. 1.1 a.1, blue) and hip (a.2, blue), extended by an activity parameter derived from the 3D acceleration values (a.1 and a.2, orange). High amplitudes indicate high activity, while low values indicate rest, sleep or non-wear time. In addition, the heart rate is shown (a.3, red).

The mentioned hidden information is revealed on the lower left hand side in Fig. 1.1. The y axis wrist accelerometry signal is chosen as an example (i.1 and ii.2, blue) and plotted in a 60 second (i.1, blue) and a 10 second (ii.1, blue) window, an episode during sleep. In Fig. 1.1 i.1 respiratory flow is shown together with the raw acceleration signal, and besides of a phase shift and a high-frequency component, the signal matches perfectly the respiratory flow. The high-frequency component of the acceleration signal, which seems to disturb the hidden respiratory signal, is shown in detail in Fig. 1.1 i.2. It shows multiple spindles perfectly aligned with the R peaks of the electrocardiography (ECG) signal with respect to pulse transit time (PTT) approximately 0.2 seconds after the R peak.

Detrended fluctuation analysis (DFA). Besides hidden information in accelerometry data, the structure of the biosignals itself is of interest, which could give a clue about regulation mechanisms in the human body. Temporal fluctuations in the cardiorespiratory system indicate adaptations to external or internal stimuli. Fluctuations may also be seen in accelerometry data during sleep as implied in the paragraph above.

1. INTRODUCTION

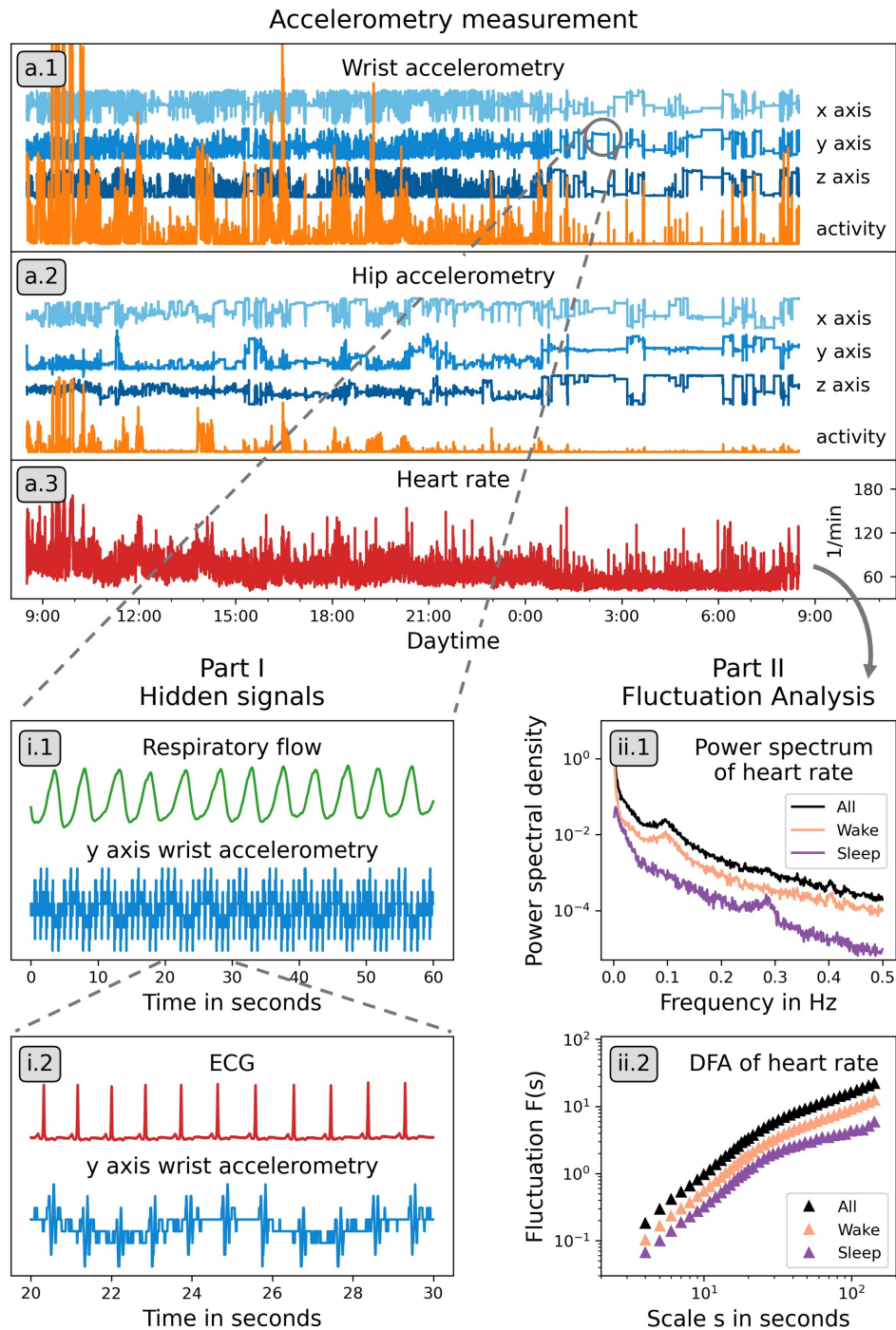


Figure 1.1: **Complexity of accelerometry data.** Upper plot (a) shows 3D accelerometry measurements for wrist (a.1, blue) and hip (a.2, blue), expanded by an activity norm (mean amplitude deviation, MAD, orange), and the heart rate (a.3, red). Lower left panel (i) reveals the potential of accelerometry data, which contains information about respiration and the pulse. In i.1 a snippet of respiratory flow (green) during sleep is plotted together with the same time window of the y axis of the wrist accelerometer data (blue), similarly for i.2 with ECG (red) and accelerometer data (blue). The lower right panel (ii) gives a brief idea of fluctuation analysis of the heart rate time series for sleep, wake and both together. The curves have been shifted vertically for better visualization. ii.1 is showing a power spectrum of the heart rate. ii.2 presenting the primary results of a DFA analysis, the scaling behavior of the heart rate.

Figure 1.1 ii.1 and ii.2 show the scaling behavior of heart rate data, for wake, sleep and both together.

In the power spectrum during sleep (Fig. 1.1 ii.1, purple) a peak around 0.3 Hz can be seen, indicating parasympathetic activity (relaxing), but also respiratory activity (respiratory sinus arrhythmia), while during wake (ii.1, orange), we see a 0.1 Hz peak, corresponding to sympathetic activity (physical activity) [8]. Since the subject is awake most of the day, the 0.1 Hz peak is present in the spectrum of the whole time series (ii.1., black), while the 0.3 Hz peak disappears.

Figure 1.1 ii.2 shows the results of DFA, which is used in this work. Here, the focus is on the different slopes of the fluctuation function $F(s)$, which differs between the ranges of 10 seconds and 100 seconds, but also between sleep and wake, indicating different regulation mechanisms on short and long time scales, but also between sleep and wake.

All together, acceleration measurements have a huge potential. Besides, heart rate, pulse waves and respiration have to be investigated at the same time, to know what to expect from acceleration data.

1.2 Goals

This thesis will focus on the unused potential of accelerometry data and scaling behavior of cardiorespiratory biosignals. This results in the following goals for this thesis:

- (i) Establish a method to extract pulse waves from wrist worn accelerometry during sleep, in order to reconstructed pulse to pulse beats, which allows to estimate pulse rate, pulse rate variability and therefore heart rate and heart rate variability.
- (ii) Develop an algorithm to reconstruct breathing activities via wrist worn accelerometers during sleep.
- (iii) Evaluate pulse wave and breathing reconstruction during different sleep stages, and find possible improvements. In addition, the influence of apneas shall be examined.
- (iv) Investigate the scaling behavior of PTT, and compare to the scaling behavior of heart rate, pulse rate, respiration rate and EEG alpha-band amplitudes.
- (v) Characterize the scaling behavior of hip and wrist accelerometry data.

1.3 Outline

The following Chapter 2 covers the basic methods and devices used for data acquisition, data analysis and evaluation. First, Section 2.1 presents the-state-of-the-art data recording and monitoring of human biosignals during sleep - known as polysomnography (PSG) - consisting in particular of recording respiration, ECG, electroencephalography (EEG), photoplethysmography (PPG), etc.. In Section 2.2 accelerometry and its technical components are introduced. The data used in this thesis was provided by two studies, which are described in Section 2.3.

Chapter 3, “Part I: Hidden signals in accelerometer data” is the first main part of this cumulative thesis. In the beginning, Section 3.1 gives a brief introduction to the idea behind signal reconstruction from accelerometry data. This introduction is followed by three publications (Section 3.2 - 3.4) considering the reconstruction of pulse wave and breathing activity from accelerometer data [JZ1], [JZ2] and its evaluation during different sleep stages [JZ3], which correspond to the goals (i), (ii) and (iii).

Chapter 4, “Part II: Fluctuation analysis studies”, investigates the scaling behavior of biosignals. In Section 4.1, DFA and its relevance on this work is introduced. Results of DFA are presented in Section 4.2, which contains a publication about DFA of heart rate, pulse rate, PTT, respiration rates and EEG alpha band amplitudes [JZ4]. Here, for the first time the scaling behavior of PTT is investigated, which corresponds to the goal (iv). Furthermore, we present in Section 4.3 preliminary results for investigating accelerometry data with DFA, which correspond to the goal (v).

Finally, this work ends with a conclusion in Chapter 5. The results of this thesis will briefly be summarized and an outlook on promising projects related to this work is given.

1.4 Remark to the term “pulse transit time”

We note that the term “pulse transit time” (PTT) is used in a colloquial way in this thesis as well as in the publications. We use PTT to describe the time between the R peak in the ECG, and a pulse wave peak at the finger tip or at the wrist, which is denoted as pulse arrival time in other works [9], [10]. More exactly, PTT is the time, that the pressure wave takes to travel from the heart to the extremities. The time we measured, pulse arrival time, includes the pre-ejection time, the time between the R peak (polarization) and the ejection of the blood in the heart.

Unfortunately, literature is mostly not clear about this, and, PTT is often misused for the term pulse arrival time, e.g. as in [11], [12]. To be consistent with our publications, the term “pulse transit time” is used in this thesis.

2 | METHODOLOGY

2.1 Polysomnography

Polysomnography (PSG) is the most important tool in sleep medicine. Subsection 2.1.1 presents a brief summary of the development of sleep scoring. More details can be found in “The History of Polysomnography” by Deak and Epstein [13]. The state of the art of PSG and its technical terms will be explained in the Subsection 2.1.2. Lastly, Subsection 2.1.3 explains the different sleep stages.

2.1.1 Historic development

For long times humankind was wondering about sleep, its meaning and regulation. Systematic research of sleep began in the 20th century. In 1929 Berger recorded electrical brain activity in humans, introducing the term “electroencephalogram” and demonstrated changes in the electrical activity between wake and sleep [14]. In 1957, Dement and Kleitman provided a further basis with their publication on the description of sleep stages using EEG and electrooculography (EOG) [15].

Unfortunately, sleep stage scoring reliability between sleep laboratories was poor because of the lack of “standardization of recording techniques and scoring criteria” as Monro *et al.* stated in 1969 [16]. This lack was remedied by the well-known manual “A Manual of Standardized Terminology, Techniques and Scoring Systems for Sleep Stages of Human Subjects” of Rechtschaffen and Kales in 1968 [17], the gold standard of sleep scoring for nearly 40 years. Nevertheless, the manual was designed for normal sleep in a non-digital world and “did not take into account important phenomenon including arousals; autonomic nervous system activity, such as cardiac rate and rhythm; respiratory abnormalities; body movement; or behavior in sleep” [13]. This leads to the need of a revised version. Furthermore, researchers starting to implement devices to measure cardiac and respiratory parameters [13] coined the term “polysomnography” in 1974 [18].

Finally, the American Academy of Sleep Medicine (AASM) initiated a new scoring manual, which was published in 2007 “AASM Manual for the Scoring of Sleep and Associated Events: Rules, Terminology, and Technical Specifications” [19]. In 2012 the AASM Scoring Manual Version 2.0 was introduced, which has continuously been updated by then [20], [21].

The term “polysomnography” refers to the setup of several diagnostic tools to observe sleep but is also used to describe a certain type of studies for the examination of sleep.

2.1.2 Modern polysomnography

Today PSG is a standard tool in sleep medicine. Containing several measurements to describe sleep, sleep stages and sleep disorders, it characterizes brain activity, muscle activity, air flow, chest movement, heart rate and oxygen saturation. The following items are part of a PSG measurement:

- **Electroencephalography (EEG)** detects electrical activity of the brain with electrodes attached to the scalp in the 10/20 system. The appearance of different wave patterns in the EEG is the basis for sleep stage scoring [22], [23].
- **Electrooculography (EOG)** measures electrical activity created by the dipole of the eye. It is used to identify rapid-eye-movement sleep (REM) and sleep onset associated with slow-rolling eye movements [23].
- **Electrocardiography (ECG)** records electrical activity of the heart muscles with electrodes attached to the chest wall. On the one hand it monitors heart rate and function, on the other hand it identifies cardiac artifacts in the EEG [23].
- **Electromyography (EMG)** senses electrical activity of muscle cells. Typically it is applied to chin and legs, in order to measure muscle tonus, which decreases during REM. It is also used to detect periodic limb movement disorders and restless legs syndrome [23].
- **Respiratory movements** are detected by thorax and abdomen belts; used for measuring diaphragm and chest breathing. In combination with air flow sensors obstructive apneas (breathing movement, but locked air paths) and central apneas (no breathing movement) can be distinguished.
- **Air flow** is captured by oronasal thermal sensors and pressure sensors at the nostrils [23].
- **Photoplethysmography (PPG)** monitors blood flow and oxygen saturation of the blood at the fingertip. This allows also to calculate PTT.
- **Video** (with infrared illumination) is recorded to visualize the movements during the measurement. It allows to describe the body position, but also sleep related movement disorders and unexpected events during the night.
- **Snoring microphone** attached to the neck will exclusively record snoring sounds.

This greatly developed system is currently the gold standard of sleep assessment. It provides detailed information about sleep architecture, sleep quality and sleep quantity [24]. Sleep architecture is related to the sequence and proportions of the sleep stages. Sleep quality is, on the one hand, a subjective perception of the patient and, on the other hand, sleep quality can be described by objective parameters, such as the number

of nocturnal wakings, sleep latency, sleep efficiency, and sleep-related diseases. Sleep quantity describes the amount of sleep.

A disadvantage of PSG is the necessity of a sleep laboratory, including a lot of cables, technical devices and well-trained personal. This is not only inflexible, cost-intensive and complex but also combined with some side effect for the subjects, as first night effects [25]–[28], caused by a new sleep environment and a lot of attached cables. To avoid this problem mobile devices are upcoming [29]. PSG is furthermore focused on the time in bed, and cannot care for sedentary and more active episodes during day, which could help to understand sleep disorders.

2.1.3 Sleep stages

One of the most important results of a PSG examination is the sleep stage classification. Basically sleep can be divided into non-rapid-eye-movement sleep (NREM) and rapid-eye-movement sleep (REM), which can be identified by rapid eye movements in the EOG. The NREM is further divided into three sleep stages: light sleep, N1 and N2, and deep sleep N3. Wakefulness can be considered as an additional stage, which is mostly short awakenings associated with sleep stage changes or external stimuli like noises. During a normal night, there are 4 to 6 sleep cycles of 90 minutes each, with pronounced variations between subjects and nights. A cycle consists of light sleep, deep sleep and REM. Abnormalities in this sequence can help to identify sleep problems. The following will explain briefly the four sleep stages. Details about the classification can be found in the AASM sleep scoring manuals [20].

N1 is the lightest sleep and the transition between wake and sleep. It is easy to wake up from this stage. Heart and breathing rate decrease and eye movements slow down. The associated EEG typically shows so-called θ waves. The stage typically lasts for several minutes before transition to N2. About 5 % of total sleep is spent in N1 [23], [30], [31].

During **N2** heart and breathing rate decrease and muscles relax while eye movements stop. The body temperature decreases. In the EEG, N2 is characterized by sleep spindles and K-complexes. One episode lasts about 10 to 25 minutes before transition to N3. 45 % of the night is typically spent in N2 [23], [30], [31].

N3 is the deepest sleep, where it is difficult to wake up. Heart and respiration rate reach the lowest frequencies and almost no movements are visible. Typical for N3 are so-called δ waves in the EEG. An episode of N3 lasts about 30 minutes, before mostly transitioning to REM sleep. Typically, N3 accounts for 25 % of the nighttime sleep [23], [30], [31].

In **REM** sleep, as the name says, eyes move rapidly from one side to the other while the lids are closed. Heart and respiration rates increase, accompanied by more movements. One episode lasts for about 10 to 50 minutes before transition back to

N1 or N2. 25 % of the night is typically spent in REM sleep [23], [30], [31].

2.2 Accelerometry

This section will cover the development and technical details of accelerometers (Subsection 2.2.1 and 2.2.2) focused on the area of sleep research. Two accelerometry devices from which we used data, are described in Subsection 2.2.3. Furthermore, modern problems and solutions in the use of accelerometers will be discussed in Subsection 2.2.4.

2.2.1 Historic development

After Rechtschaffen and Kales [17] laid the foundation for modern sleep assessment based on EEG, so-called telemetric mobility recorders were introduced and tested at the wrist to add information about motoric activity. These tests showed a high correlation between activity and wakefulness [32], [33]. In 1978, Kripke *et al.* [34] introduced the term actigraphy and used a piezoceramic element attached to a moving mass to measure movements via displacement of the mass. With this approach, sleep and wakefulness could be estimated [34], [35].

The first automated sleep-wake scoring algorithm based on actigraphy was developed by Webster *et al.* in 1982 [36] and improved by Cole *et al.* in 1992 [37] with a reported accuracy of 88 % compared to PSG. Unfortunately, such algorithms score sleep much better than wake episodes, a problem which still exists [38]. If we score all episodes as sleep, we would get an agreement rate as high as sleep efficiency, which is for most subjects above 80 % [39], [40]. For this reason actigraphy sleep-wake scoring algorithms may fail for subjects with sleep issues such as insomnia [40], [41] or a disturbed sleep-wake cycle like jet lag or shift work [38]. Therefore it is crucial to improve the detection of wakefulness episodes.

The next improvement was the piezoelectric accelerometer. Attached to the wrist, it measured accelerations along the radius-to-ulna axis¹ [42]. However, with each new device available, new algorithms and device specifications came such as pre-filter and amplifier setting, sampling rate and acceleration resolution. Basically, the devices reported epochwise so-called “counts”, calculated by one of three operation modes: time above threshold, numbers of zero crossings or cumulative sum [42]. These counts were then used to score sleep-wake. As a consequence the results of different devices were not comparable.

Terrill *et al.* [43] improved actigraphy by using a triaxial accelerometer (3D, three accelerometers orthogonal to each other) and storing the raw sensor data instead of counts. This allows to use detailed analysis of the signals, like spectral analysis, to score sleep-wake [44], [45]. Furthermore, machine learning can be used to estimate not only sleep and wake but also sleep stages [4], [JZ5].

¹Radius-to-ulna axis is the axis parallel to the forearm.

But as this work will show, a lot of more information can be found in acceleration data.

Modern accelerometer devices still use proprietary software and algorithms to calculate counts and other metrics, but it is becoming increasingly possible to download and to use the raw acceleration data.

2.2.2 Technical details

Basically, acceleration sensors use the inertia of a mass in relation to the sensor housing. Therefore, three sensor types should be mentioned:

Capacitive accelerometers consist of two capacitor plates, one connected to the housing and one to the internal mass. The capacity of this capacitor is modulated by the acceleration acting on the mass [46], [47].

Piezoresistive accelerometers use the piezoresistive effect of metals or semiconductors, which is basically a change of their electrical resistance due to strain. Therefore, the electrical resistance from the mass-carrying spring or strips can be measured as a function of acceleration [46], [47].

Piezoelectric accelerometers use the piezoelectric effect of crystals that generate an electrical potential when mechanically compressed or stretched. Therefore acceleration can be measured as function of the crystal's voltage [46], [47].

2.2.3 Accelerometer devices

In this work the data of two accelerometer brands has been used, SOMNOwatch and ActiGraph.

SOMNOwatch™ plus

The SOMNOwatch™ plus (SOMNOmedics, Randersacker, Germany) is a watch-like device, which can record 3D accelerometry up to 128 Hz. In addition, attached via cable an ECG (up to 256 Hz) and nasal air flow can be measured. The used accelerometer sensor type is unfortunately a trade secret, but it measures in the range of -6 to 6 g. The unit g is the gravitational acceleration of 9.81 m/s^2 , for small movements $1 \text{ mg} = 0.001 \text{ g}$ is commonly used. The device records with 12-bit resolution, which leads to a theoretical resolution of $12 \text{ g}/2^{12} = 2.9 \text{ mg}$, but noise levels reduce the resolution to 5 mg [JZ1].

ActiGraph™

ActiGraph™ GT3X+ and ActiGraph™ wGT3X-BT (ActiGraph, Pensacola, USA) are similar devices, which measure 3D acceleration in range of -6 to 6 g and -8 to 8 g, respectively, with a piezoelectric sensor and up to 100 Hz. As both models

2. METHODOLOGY

have the same bit number of 12 bit, the resolutions are $12 \text{ g}/2^{12} = 2.9 \text{ mg}$ and $16 \text{ g}/2^{12} = 3.9 \text{ mg}$, respectively. Our findings indicate a higher noise level in this sensors compared with the SOMNOwatch sensor.

In this work SOMNOwatch was exclusively worn at the wrist and the ActiGraph models exclusively at the hip.

2.2.4 Advantages of accelerometry

Accelerometers are usually very small devices in the size of a watch and are very easy to handle, which means subjects can put them on and take them off themselves. In addition, accelerometer sensors, though usually with lower precision and no calibration, are already implemented in smartphones and smartwatches, which will make the transition from resulting algorithms of scientific research to costumers applications a bit easier.

Another advantage is the long operational time, depending on the device, but often more than 7 days. This allows not only to measure physical activity, sedentary behavior and sleep times on one day but also to compare the parameters for several consecutive days and week versus weekend.

Furthermore, large epidemiological studies, e.g. “NAKO Gesundheitsstudie” [1], “SHIP studies” [2] and “UK-biobank” [3], are increasingly often using accelerometer devices with data accessible for researches.

The problem of black-box algorithms and incomprehensible counts based on company secrets is resolved in access to the raw data and open scientific algorithms, metrics and software. Examples are mean amplitude deviation (MAD) [48], euclidian norm minus one (ENMO) [49] and the GGIR package [50]. MAD and ENMO are metrics to estimate physical activity from 3D accelerometer data. As an open source package, GGIR includes both and further metrics and algorithms.

Especially the MAD metric is already well-established for physical activity, as MAD is strongly correlated with oxygen consumption [51], and is defined as the mean derivation of the amplitude over a certain interval. It can be calculated in the following steps [48]:

First, the magnitude r_i of the 3D accelerometer signal (x, y, z) is calculated,

$$r_i = \sqrt{x^2 + y^2 + z^2}. \quad (2.1)$$

In a second step, this magnitude is averaged in epochs of length N , e.g. in a 128 Hz signal with N equals to 128, an epoch has a duration of one second.

$$R_{ave} = \frac{1}{N} \sum_{i=j}^{j+N-1} r_i \quad (2.2)$$

Finally, the MAD values of the epoch length N can be calculated as

$$\text{MAD} = \frac{1}{N} \sum_{i=j}^{j+N-1} |r_i - R_{ave}|. \quad (2.3)$$

As mentioned above, basic sleep parameters can be estimated on a good level. Nevertheless, there is a difference between PSG and actigraphy, which is not random, and can therefore be partially corrected [52]. However, it cannot be expected that the agreement between actigraphy and PSG will be better than between two PSG scorings [52], which means that e.g. sleep stage scoring of the same data differs between the scorers [53].

2.3 Data acquisition studies

The heart of data analysis is the data itself. Poor quality in data collection cannot lead to meaningful results. Therefore a valid, systematic and high quality acquisition of biosignals is crucial.

This section presents two important studies for this work. The first study is the “NAKO Gesundheitsstudie”, also known as German National Cohort (Subsection 2.3.1).

Accompanying the NAKO Gesundheitsstudie a smaller observatory study (Subsection 2.3.2) has been conducted. This study has the advantage of a fast data availability and the special characteristic of measuring PSG and accelerometry at the same time. The latter one allows to investigate motion behavior during the night, develop algorithms for biosignal reconstruction and sleep stage detection via accelerometry. The gained knowledge and algorithms can be transferred to the NAKO study.

2.3.1 NAKO Gesundheitsstudie

The NAKO Gesundheitsstudie (German National Cohort) is one of the largest German population-based prospective cohort studies².

Organized in 18 study centers spread all over Germany, the study includes over 205.000 participants, which were randomly drawn from general population of the area of the study centers with strata of age and sex [1], [54], [JZ6]. At the recruitment, the age of the participants ranged from 20 to 69 years.

The longitudinal study contains a baseline examination of all participants, written follow up questionnaires every two to three years and several follow up examinations every five years. At the moment³ the first follow up examination is in progress and the second follow up examination is in planning.

2014 till 2019 the baseline examination of all participants was performed. The examination program was split in Level 1 for all participants and Level 2 for only 25 % of the participants with additional measurements.

Level 1. Level 1 includes several questionnaires (e.g. socio-economic status, medical history, drugs, life quality, mental health, physical activity, diet), several examinations (e.g. blood pressure, 12 leads ECG, spirometry, tooth count, olfactory test, hand grip strength, anthropometric measurements) and the collection of biosamples (blood, saliva, nasal swab, stool, urine). In addition, a subgroup of about 80.000 subjects wore a accelerometer device (ActiGraph™ GT3X+ or wGT3X-BT) for 7 days at the

²The NAKO study was funded by the Federal Ministry of Education and Research (BMBF) (project funding reference numbers: 01ER1301A/B/C and 01ER1511D) and the federal states and the Helmholtz Association, with additional financial support by the participating universities and the institutes of the Leibniz Association.

³December 2022

hip.

Level 2. The Level 2 examination contained a 24 hour accelerometry measurement recorded by a SOMNOwatch™ plus. Only 30.9 % of Level 2 participants (8.3 % of all participants) got a SOMNOwatch measurement, which equals to approximately 17.000 records, due to problems with the SOMNOwatch device itself (e.g. battery failure, shortages of devices in the study centers) and rejection of wearing the device. The SOMNOwatch™ plus device was worn at the non-dominant arm, recording simultaneously 3D wrist acceleration with a sampling rate of 128 Hz and in addition a one channel ECG at 256 Hz. Three electrode patches, placed at the chest wall, were connected to the SOMNOwatch with a small wire to measure the one channel ECG in parallel with the accelerometer data.

2.3.2 Detection of the sleep-wake structure at night from actimetry and ECG recordings

The results of this thesis are mainly based on this additional study. In the project “Dynamical and causal relationships in the coupling of heartbeat, respiration and motion activity”⁴, a clinical trial “Detection of the sleep-wake structure at night from actimetry and ECG recordings” was performed.

The study includes 450 subjects, who spent a diagnostic night in a clinical sleep laboratory of the Charité-Universitätsmedizin Berlin, Germany, between April 2017 and March 2019. All subjects wore a SOMNOwatch™ plus device, recording simultaneously 3D wrist acceleration of the non-dominant arm at 128 Hz sampling rate and a one channel ECG at 256 Hz, in accordance to the NAKO standard operating procedures for SOMNOwatch. In addition, full PSG was recorded using either an ALICE (Philips, Amsterdam, Netherlands), an Embla® (Natus, Pleasanton, USA), or a SOMNOscreen™ PSG system (SOMNOmedics, Randersacker, Germany). Sleep stages based on 30 second epochs have been determined from the PSG data by trained experts following standard guidelines of the AASM manuals [21]. R peak detection was applied for the SOMNOwatch ECG data and for the PSG ECG data. Since both measurements have been performed independently, time shifts and offsets had to be corrected. To do this, the R peak positions of both systems were synchronized.

⁴This project was funded by the German-Israeli Foundation for Scientific Research and Development, GIF Grant No: I-1372-303.7/2016.

3 | PART I: HIDDEN SIGNALS IN ACCELEROMETER DATA

The present chapter addresses the possibility of reconstructing biosignals from 3D wrist accelerometry during sleep. First, in Section 3.1, basic ideas and mechanisms behind the reconstruction are introduced (Subsection 3.1.1) together with a metric to compare reconstructed and measured signals (Subsection 3.1.2). This introduction is followed by the presentation of the published results. A first publication (Section 3.2) is concerned with an algorithm to reconstruct pulse waves. The second publication (Section 3.3) deals with the extraction of respiration activity and rate. The third publication (Section 3.4) compares both with respect to sleep stages and apnea events.

3.1 Introduction to signal reconstruction

3.1.1 A first hint - power spectra of accelerometry data

Simple frequency spectra of nightly accelerometer data are presented in Fig. 3.1. The periodogram is calculated for different sleep stages (Fig. 3.1, blue colors), wake episodes (green colors) and for the whole night measurement (black). During sleep, two interesting peaks can be seen, one around 0.25 Hz and one around 8 Hz.

The peak around 0.25 Hz is clearly in the range of the respiration frequency during rest of 0.2 Hz (5 seconds per breath or 12 breaths per minute) till 0.3 Hz (3.3 seconds per breath or 18 breaths per minute). Accelerometers worn at the wrist are coupled to the upper body and its respiration movements. Especially during sleep, the wrist could lie on the chest or the respiration movements are transferred via the mattress to the wrist lying on it, which is why respiration frequency can be seen in accelerometry data.

The origin of the 8 Hz peak has no trivial explanation. The phenomena has already been discovered in the 19th century [55] and has been labeled as tremor [56], [57]. A lot of publications stayed with the term “tremor” while the origin remained subjected to speculations. Some suggested oscillations in reflex loops [58], [59] or a central oscillatory process [60]. In a later work, Lakie *et al.* showed in 2012 that the tremor peak was not a result of EMG modulations and therefore is not neuronally regulated [61]. Also it has been shown that the tremor frequency is only a mechanical property of oscillating limbs [62]. In 1969, Marsden *et al.* [63] could not find any coherence of the tremor between two hands and furthermore assumed as origin cardiac thrust.

3. PART I: HIDDEN SIGNALS IN ACCELEROMETER DATA

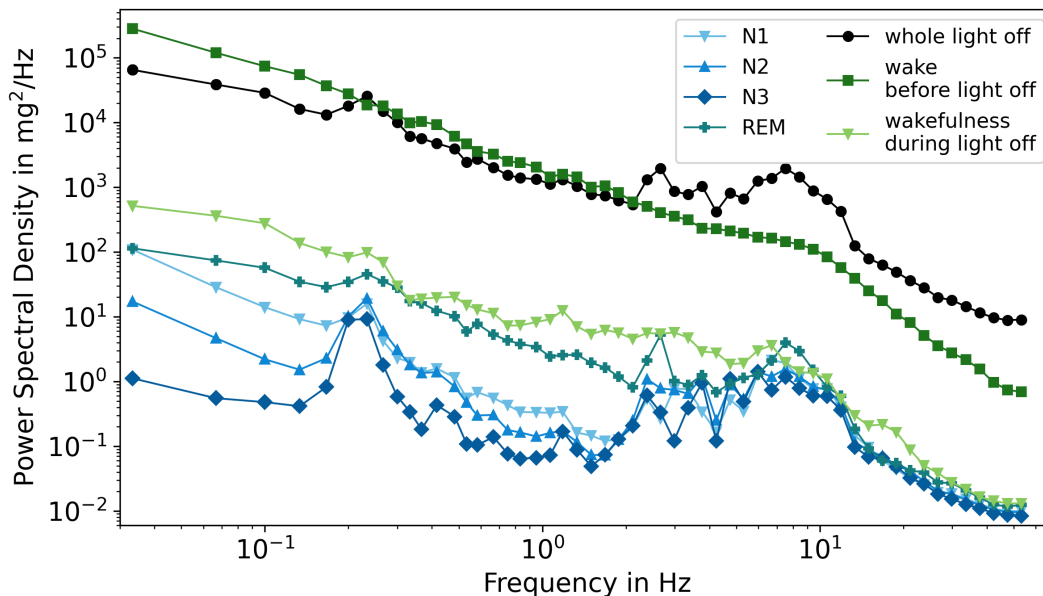


Figure 3.1: **Periodogram.** Periodogram of the y axis of accelerometry data during different sleep stages (blue colors), wake before the light off time, i.e. before bed time, (dark green), time of wakefulness during the light off, i.e. during bed time, (light green), and the whole night (black) on a double logarithmic plot. Data is averaged over 30 second episodes, in which the MAD value (see Eq. 2.3) does not exceed a threshold of 5 mg, indicating movements [JZ1]. The data was taken from one subject of the study described in Subsection 2.3.2.

Rohracher [64] introduced the term “microvibration”, as small rhythmic vibrations of warm-blooded organisms, and suggested its origin in muscle contractions. In 1997, Gallasch and Kenner [65] identified ballistocardiac forces as mechanism behind the microvibrations, as the motion is transferred via bone tissue and is finally damped to a 7 to 13 Hz resonant response over muscle tissue. Nevertheless all reported tremor frequencies or microvibration frequencies lay between 7 and 14 Hz.

As we will show in the first publication [JZ1] we support strongly that this tremor or microvibrations are of cardiac origin. We suggest that the pulse wave triggers the 8 Hz peak, as the peak occurs around 200 to 300 ms after the R peak, typical for PTT. This enables the measurements of the pulse rate via accelerometry.

Wohlfahrt *et al.* 2013 [44] used both peaks of the accelerometry periodogram in episodes of 30 seconds to distinguish between sleep, wake and non-wear time. A problem in accelerometry data analysis is the detection of non-wear time, because sleep and non-wear time are very similar on timescales of minutes. But in high-resolution accelerometers, the respiration peak or the 8 Hz peak will be visible only during sleep, which would solve the problem [45].

Following this idea, we inspected a spectrogram, see Fig. 3.2. Both peaks at 0.25 and 8 Hz can seen over the whole night, only interrupted by movement artifacts or

3.1. Introduction to signal reconstruction

wake episodes. As we see in Fig. 3.2 a-c, the peaks are not permanently visible in all three axis, which depends on the orientation of the wrist. Artifacts, indicated by a high intensity of all frequencies (Fig. 3.2 a-c, red vertical lines), are correlated with sleep stage changes (Fig. 3.2, d) or movements, which can be seen in Fig. 3.2 e, when the activity value (MAD, see Eq. 2.3) crossed the 5 mg limit (horizontal black line).

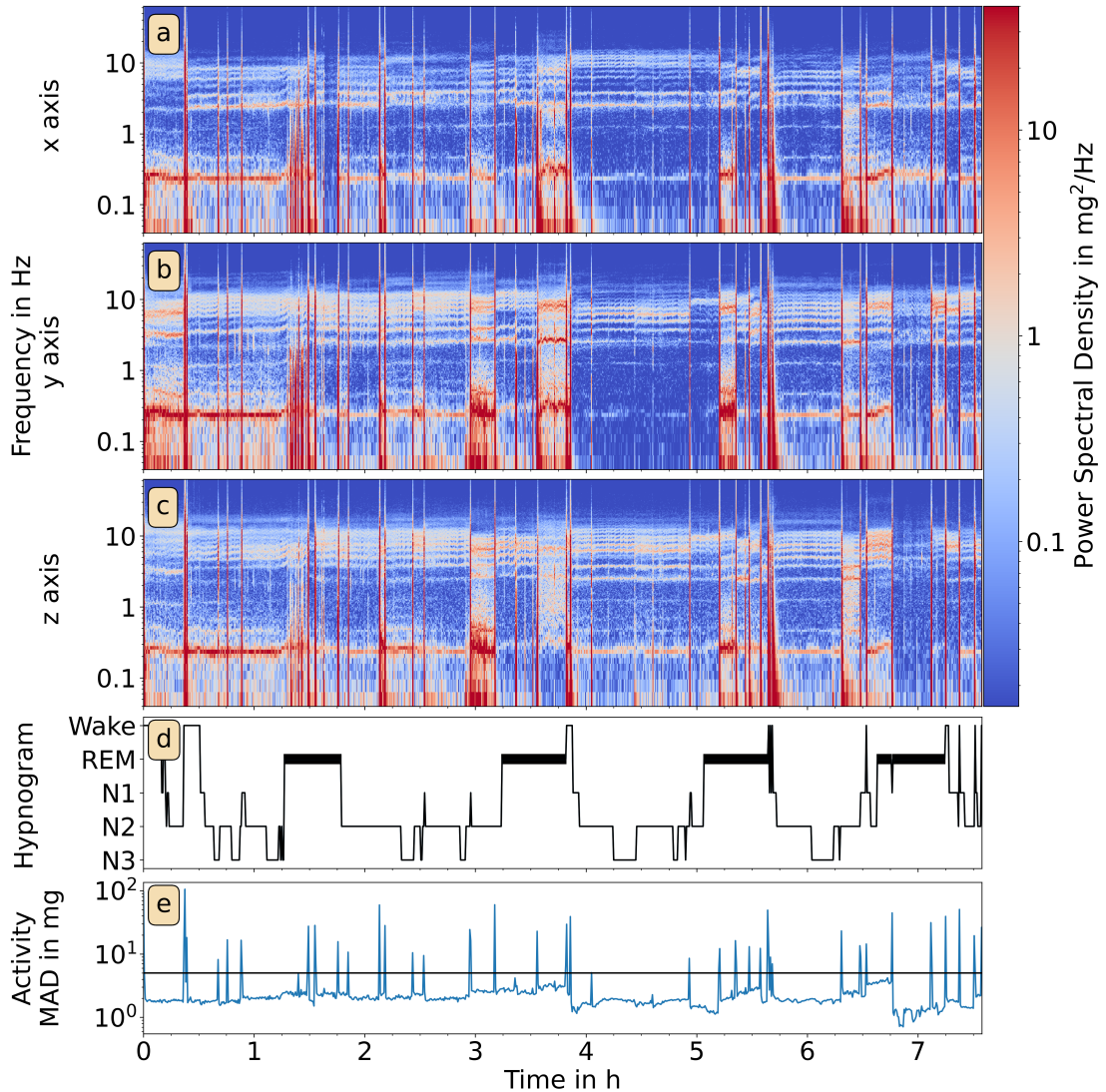


Figure 3.2: **Spectrogram.** Spectrogram of wrist accelerometry data during sleep. The upper three plots (a-c) show the spectrograms of each axis, while (d) contains a hypnogram, showing the sleep stages. Plot (e) shows the movement activity (MAD, see Eq. 2.3) of the subject, the black horizontal line indicates the 5 mg threshold. The data was taken from one subject of the study described in Subsection 2.3.2.

The analysis of both peaks during the night is the topic of the following three Publications: pulse wave peaks extraction via accelerometry [JZ1], the estimation of respiration activity [JZ2] and both compared for different sleep stages [JZ3].

3.1.2 How to compare signals

Event-to-event comparison. There are several approaches to compare two time series. In the first publication Section 3.2 [JZ1] we used an event to event comparison to match R peaks and pulse wave peaks. In our case this has the disadvantage that time shifts between events, like PTT, lead to a certain degree of uncertainty.

Another problem arises when comparing respiration signals. Respiration can measured via flow sensors but also via chest belts. While the flow is maximal during inhalation, the chest belt signal (stretching) is maximal during the change between inhalation and exhalation. If we want to discern a derived signal from the wrist movement, we cannot determine the actual phase of respiration, which leads to an unknown time shift between the maxima of the signals.

Cross-correlation between reconstructed and measured signals could determine the shift, but changes in wrist position during sleep could change the shift and the amplitude of the signal. Therefore, this approach is not best suited.

Phase synchronization index (PSI). To avoid these problems we used phase synchronization in the second and third publication (Section 3.3 [JZ2] and 3.4 [JZ3]). Specifically, we focused on analyzing and comparing phases. To extract the phase of a signal, we used some pre-filters (details can be found in the publications [JZ2], [JZ3]), a Hilbert transform [66] to gain a complex signal, and applied $\arctan2$ to the complex signal to get a phase oscillating from $-\pi$ to $+\pi$ in a sawtooth curve. The PSI γ , to compare two phases, is defined as followed [67]:

$$\gamma(t_0) = \left| \frac{1}{T} \int_{t_0}^{t_0+T} \exp\{i \cdot Phase_{signal_1}(t) - i \cdot Phase_{signal_2}(t)\} dt \right|, \quad (3.1)$$

where i is the imaginary unit, T is the epoch length over which we want to average (30 seconds in the publications, according to scoring of sleep stages in 30 seconds), and t_0 is the actual time point as multiple of T , running till the end of the signals.

This definition, to compare signals, has two advantages. First, a constant phase difference (in the 30 second epoch) between both phases (signals) can be disregarded, which solves the described problem due to PTT in R peaks and pulse wave peaks, and the unknown phase of the reconstructed respiration signal. Second, the signals' amplitude has no effect on the phase signal.

By definition, the PSI γ runs from 0, no synchronization between the signals, to 1, matching signals, and can be used to determine the accordance between reconstructed signals and measured signals. To compare the PSI between subjects, it was averaged over the whole night of each subject, and then compared subject wise (see Section 3.3 [JZ2]). In addition, synchronization indices are averaged sleep stage wise and compared (see Section 3.4 [JZ3]).

3.2 Publication: Pulse wave reconstruction

About this publication. The following publication “Detection and analysis of pulse waves during sleep via wrist-worn actigraphy” [JZ1] introduces a method for measuring pulse rate via wrist accelerometry and identifying single pulse wave peaks at the wrist. Using 3D accelerometry data, the algorithm provides pulse wave peaks for each of the three axes, from which a best axis selection for 30 second epochs was implemented. In addition, the comparison of tachograms¹ shows a higher influence of respiration on pulse-to-pulse intervals than on heart beat-to-beat intervals. This leads to the assumption that respiration influences the PTT by blood pressure or arterial stiffness regulation paths, or that the respiration motion influences the accelerometry measurement at the wrist. Furthermore, pulse rate variability parameters, derived from reconstructed pulse wave peaks, are larger than the heart rate variability (HRV) parameters, which indicates a higher modulation of other origin, maybe resulting from blood pressure and arterial stiffness changes. Over all the developed algorithm is sensitive to movement artifacts, which are therefore detected and excluded, and it seems to depend on subjects, which may be related to the tightening strength of the wrist accelerometer.

Copyright statement

©2019 Zschocke *et al.* This publication is licensed under a Creative Commons Attribution 4.0 International (CC BY 4.0) license .

J. Zschocke, M. Kluge, L. Pelikan, A. Graf, M. Glos, A. Müller, R. Mikolajczyk, R. P. Bartsch, T. Penzel, and J. W. Kantelhardt, „Detection and analysis of pulse waves during sleep via wrist-worn actigraphy“, *PloS one*, vol. 14, no. 12, e0226843, 2019. DOI: 10.1371/journal.pone.0226843. Reference [JZ1]

¹The tachogram is a plot of heart beat intervals versus time and provides therefore time-resolved information of heart rate variability. See Fig. 6 in publication [JZ1], Section 3.2.

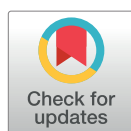
RESEARCH ARTICLE

Detection and analysis of pulse waves during sleep via wrist-worn actigraphy

Johannes Zschocke^{1,2}, Maria Kluge³, Luise Pelikan³, Antonia Graf³, Martin Glos³, Alexander Müller⁴, Rafael Mikolajczyk¹, Ronny P. Bartsch⁵, Thomas Penzel³, Jan W. Kantelhardt^{2*}

1 Institute of Medical Epidemiology, Biostatistics and Informatics, Faculty of Medicine, Martin-Luther-University Halle-Wittenberg, Halle, Germany, **2** Institute of Physics, Martin-Luther-University Halle-Wittenberg, Halle, Germany, **3** Interdisziplinäres Schlafmedizinisches Zentrum, Charite - Universitätsmedizin Berlin, Berlin, Germany, **4** Klinik und Poliklinik für Innere Medizin I, Technische Universität München, Munich, Germany, **5** Department of Physics, Bar-Ilan University, Ramat Gan, Israel

* jan.kantelhardt@physik.uni-halle.de



OPEN ACCESS

Citation: Zschocke J, Kluge M, Pelikan L, Graf A, Glos M, Müller A, et al. (2019) Detection and analysis of pulse waves during sleep via wrist-worn actigraphy. PLoS ONE 14(12): e0226843. <https://doi.org/10.1371/journal.pone.0226843>

Editor: Tomohiko Ai, Indiana University, UNITED STATES

Received: July 24, 2019

Accepted: December 4, 2019

Published: December 31, 2019

Peer Review History: PLOS recognizes the benefits of transparency in the peer review process; therefore, we enable the publication of all of the content of peer review and author responses alongside final, published articles. The editorial history of this article is available here: <https://doi.org/10.1371/journal.pone.0226843>

Copyright: © 2019 Zschocke et al. This is an open access article distributed under the terms of the [Creative Commons Attribution License](https://creativecommons.org/licenses/by/4.0/), which permits unrestricted use, distribution, and reproduction in any medium, provided the original author and source are credited.

Data Availability Statement: The data are available from the project "Detection and analysis of pulse waves via wrist-worn actigraphy during sleep" at OSFHOME (osf.io; location Frankfurt, Germany) under the DOI [10.17605/OSF.IO/XSBHW](https://doi.org/10.17605/OSF.IO/XSBHW).

Abstract

The high temporal and intensity resolution of modern accelerometers gives the opportunity of detecting even tiny body movements via motion-based sensors. In this paper, we demonstrate and evaluate an approach to identify pulse waves and heartbeats from acceleration data of the human wrist during sleep. Specifically, we have recorded simultaneously full-night polysomnography and 3d wrist actigraphy data of 363 subjects during one night in a clinical sleep laboratory. The acceleration data was segmented and cleaned, excluding body movements and separating episodes with different sleep positions. Then, we applied a bandpass filter and a Hilbert transform to uncover the pulse wave signal, which worked well for an average duration of 1.7 h per subject. We found that 81 percent of the detected pulse wave intervals could be correctly associated with the R peak intervals from independently recorded ECGs and obtained a median Pearson cross-correlation of 0.94. While the low-frequency components of both signals were practically identical, the high-frequency component of the pulse wave interval time series was increased, indicating a respiratory modulation of pulse transit times, probably as an additional contribution to respiratory sinus arrhythmia. Our approach could be used to obtain long-term nocturnal heartbeat interval time series and pulse wave signals from wrist-worn accelerometers without the need of recording ECG or photoplethysmography. This is particularly useful for an ambulatory monitoring of high-risk cardiac patients as well as for assessing cardiac dynamics in large cohort studies solely with accelerometer devices that are already used for activity tracking and sleep pattern analysis.

1 Introduction

Full-night polysomnography (PSG) has been regarded as the reference standard in sleep medicine since 1968 [1, 2]. Besides signals used for sleep stage classification, respiratory activity and an electrocardiogram (ECG) are usually recorded and analyzed [3]. However, the applicability

Funding: This study was supported by the German Israel Foundation (GIF, <http://www.gif.org.il>) grants I-1298-415.13/2015 (for JZ and JK) and I-1372-303.7/2016 (for MG, RB, and TP) and the German National Cohort study (www.nako.de), funded by the Federal Ministry of Education and Research (BMBF) and the Helmholtz Association (for JZ, AM and RM). JZ acknowledges support from a Minerva Short-Term Research Grant. We acknowledge the financial support within the funding programme Open Access Publishing by the German Research Foundation (DFG). The funders had no role in study design, data collection and analysis, decision to publish, or preparation of the manuscript.

Competing interests: The authors have declared that no competing interests exist.

of PSG for the assessment of sleep characteristics in large prospective studies is limited due to its costs and its intricacy, requiring many electrodes and cables attached to the subject's head and chest.

Alternatively to PSGs, actigraphy (or accelerometry) is commonly used to monitor human sleep/wake cycles [4–8]. Usually, the accelerometer is placed on the subjects' wrist of the non-dominant arm. Advantages of accelerometry are low costs, higher availability, easy recording of multiple nights, and a less disturbed natural sleep [9, 10]. However, its accuracy varies between different sleep variables and depends on population-specific characteristics [7, 9, 11]. Yet, recent technological progress has led to advanced recording devices with high temporal resolution (above 100 Hz), high acceleration resolution (down to $3 \text{ mg} \approx 0.03 \text{ m/s}^2$), and separate recording of all three spatial directions (see e.g., [12] for a review).

First investigations that demonstrated physiological relevance in the distribution and auto-correlations of wrist activity fluctuations independent of level of physical activity were published by Hu et al. [13, 14]. In later studies it has been shown that wrist activity fluctuations are also related to the circadian rhythm and to the role of the suprachiasmatic nucleus in the brain [15, 16] that is responsible for regulating many different body functions on a 24-hour cycle.

In this paper, we present an approach for exploiting nocturnal wrist accelerometry recordings to identify pulse waves and heartbeats, and assess detection accuracy of individual heartbeats. By comparing with simultaneously recorded ECGs (as part of clinical PSG), we demonstrate that accelerometry could help assessing sleep-related changes not only in heart rate but also in heart rate variability (HRV), including measures that rely on changes between neighboring inter-beat intervals. In Section 2, we summarize previous efforts to derive heart activity without electrodes. In Section 3, we describe our database and present the methods and data processing approaches. Section 4 reports our results including the achieved heartbeat detection reliability, statistics for pulse transit times, and influences of respiration on pulse wave intervals, including age dependences. We conclude in Section 5.

2 Alternative approaches for assessing heart activity

Besides the ECG as gold standard for heart rate and HRV measurements [17], there are several other methods to detect heartbeats not requiring electrodes attached to the body.

Plethysmography

A common approach for measuring pulse waves is photoplethysmography. It relies on the propagation of pulse waves throughout the body. During heart contraction, blood is pumped into the arteries, creating a pressure ("pulse") wave. The velocity and shape of the pulse wave depend mainly on arterial stiffness that is affected by age, physical fitness, heart rate, body height, and gender [18]. According to O'Rourke et al. [18], the ideal aortic pulse wave profile is described as "sharp upstroke, straight rise to the first systolic peak, a definite sharp incisura, and near exponential pressure decay in late diastole". With the pulse waves' propagation to the periphery, the systolic pressure increases, while diastolic and mean pressures decrease due to increased arterial stiffness and incoming reflected pulse waves [19]. Pulse wave measurements on the wrist typically show wave profiles that are a superposition of three waves: an incident wave due to blood flow as well as two reflected waves from the hand and from the lower body, respectively [19, 20]. In plethysmography the pulse wave is recorded by light reflexion and light absorption [21]. We refer to [22] for an early application of using pulse wave intervals from plethysmography to study cardiac dynamics and investigate HRV during rest and exercise without ECG electrodes.

Seismocardiography

Recording chest wall motion via radar-facilitated distance measurements is a possible but rather intricate approach [23]. Another not frequently used method is seismocardiography, where acceleration sensors placed on the chest wall measure the vibrations caused by heartbeats [24]. With higher resolution of acceleration sensors this technique became more interesting in the last years [25–27]. Seismocardiography is closely related to ballistocardiography, a method which measures whole body motions (or vibrations) caused by the heartbeat. Sensors are commonly placed on the chair or bed of the subject [26]. Seismocardiography and ballistocardiography are often used as synonyms.

Measurements of seismocardiography not only detect heartbeats but also respiratory activity. Beside respiration (< 1 Hz), low frequency (0.6 to 5 Hz) chest wall motions related with heart muscle contraction and high frequency (> 5 Hz) chest wall vibrations related with acoustic waves of the valve closing are measured [25, 28]. Both signals can be used to detect respiration and heartbeats [29].

Accelerometry

In spectral analysis of nocturnal wrist-worn acceleration measurements also two distinct peaks have been identified [6]. As shown in Fig 1, there is a rather narrow peak at ≈ 0.3 Hz reflecting respiratory activity and a much broader peak around 10 Hz, which we somewhat incorrectly coined “tremor peak” in the original publication. Both peaks are most pronounced if the variations of acceleration are at an intermediate level for the nocturnal recording, i.e., there is neither strong motion activity (often corresponding to wakefulness episodes or turns, Fig 1

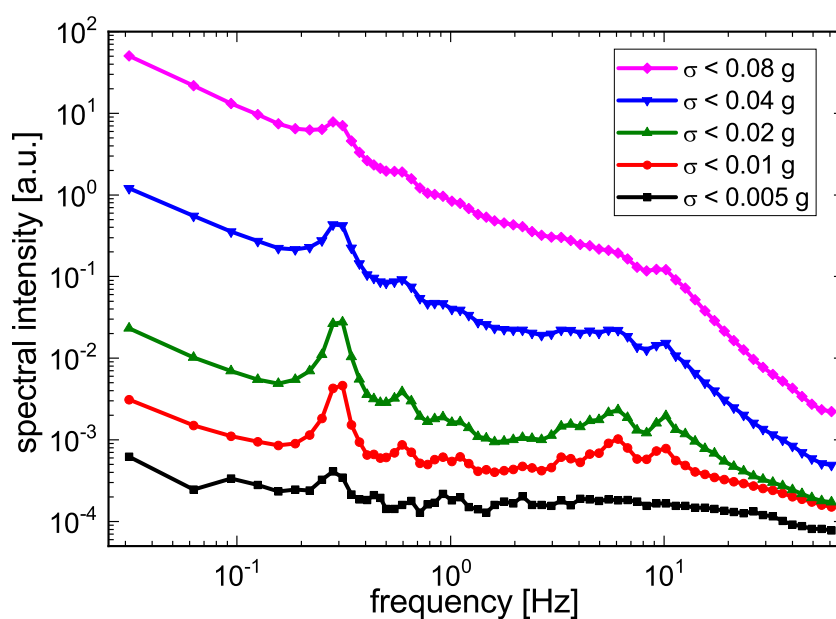


Fig 1. Spectral intensity of wrist acceleration during different levels of motion activity. Periodograms are shown for five exponentially increasing acceleration variance thresholds (black: smallest threshold; magenta: largest threshold). Peaks related with respiratory motion (at ≈ 0.3 Hz) and pulse waves (at $\approx 6 - 10$ Hz) are most clearly visible for intermediate acceleration variance levels (red and green curves) (after [6]).

<https://doi.org/10.1371/journal.pone.0226843.g001>

magenta curve), nor hardly any motion at all (probably corresponding to time intervals when the arm is practically fixed between other body parts and the bed; Fig 1 black curve). Hence, when exploiting these peaks, we cannot expect to get reliable data at all times, but only when there is an intermediate level of total acceleration variations.

Looking closer at the high-frequency (≈ 10 Hz) peak, we have recently identified the main reason for its broadness—the corresponding oscillation is strongly damped, being triggered approximately each second, but then decaying within ≈ 0.2 s. By comparing with a simultaneously recorded ECG, the origin of this “tremor peak” finally became clear to us—it is caused by the pulse wave transversing the subject’s wrist shortly after the heartbeat and probably triggering a short wiggling of the wrist and/or the recording device attached to it. These high frequency vibrations in the wrist caused by the arrival of the pulse wave have some analogy to the above mentioned high frequency chest wall vibrations (> 5 Hz) as detected by seismocardiography.

3 Materials and methods

Measurements

All sleep recordings were performed at the clinical sleep laboratory of the Charité-Universitätsmedizin Berlin, Germany, between April 2017 and December 2018. The study was approved by the ethics committee of the Charité-Universitätsmedizin Berlin and registered at the German Clinical Trial Register (DRKS) with ID DRKS00016908. In total, 392 subjects were included and signed informed consent. During their first diagnostic night at the sleep laboratory, all subjects wore a SOMNOWatch™ plus device, recording simultaneously 3d wrist acceleration of the non-dominant arm at 128 Hz sampling rate and a one channel ECG at 256 Hz. Furthermore, full PSG (including electroencephalography (EEG), electrooculography (EOG), electromyography (EMG), ECG, respiratory effort, etc.) was recorded using either an ALICE, an Embla®[®], or a SOMNOscreen™ PSG system.

Due to noisy or low quality ECG recordings, 29 subjects were excluded from further analysis. The final 363 subjects (180 females, 183 males), aged between 18 and 80 years (mean 50.1 ± 13.7 years) with average body mass index 28.0 ± 5.8 kg/m², had an average time in bed (TiB) of 7.6 ± 0.8 h. All subjects were referred to the sleep laboratory with complaints and an indication to test for sleep disorders. In Table 1 we list the frequency of sleep disorders classified by ICSD-3.

Table 1. Overview of all subjects included in the analysis. Subjects with multiple diagnoses are counted in each appropriate diagnosis line, i.e., multiple times. The last line reports data for all subjects irrespective of diagnosis. The column “duration” reports the median total duration (per subject) of all pulse wave intervals (PWI) correctly associated with corresponding heartbeat intervals from the ECG at an accuracy limit of 0.1 s (see Methods and also Table 2). It is followed by the median fraction of correctly associated PWI and the corresponding median Pearson cross correlation *r* in the subsequent columns (see Results section for details).

Diagnosis	females	males	duration	cor. PWI	r
No sleep disorders	19	18	1.2 h	0.82	0.89
Sleep-related breathing disorders	67	115	1.2 h	0.79	0.93
Insomnia	65	25	1.3 h	0.84	0.93
Central disorders of hypersomnolence	36	20	1.3 h	0.78	0.95
Sleep-related movement disorder	35	26	1.0 h	0.80	0.94
Parasomnias	9	7	1.0 h	0.74	0.95
Circadian rhythm sleep-wake disorders	1	9	1.7 h	0.86	0.95
Other sleep disorders	8	7	1.3 h	0.83	0.95
All subjects	180	183	1.3 h	0.81	0.94

<https://doi.org/10.1371/journal.pone.0226843.t001>

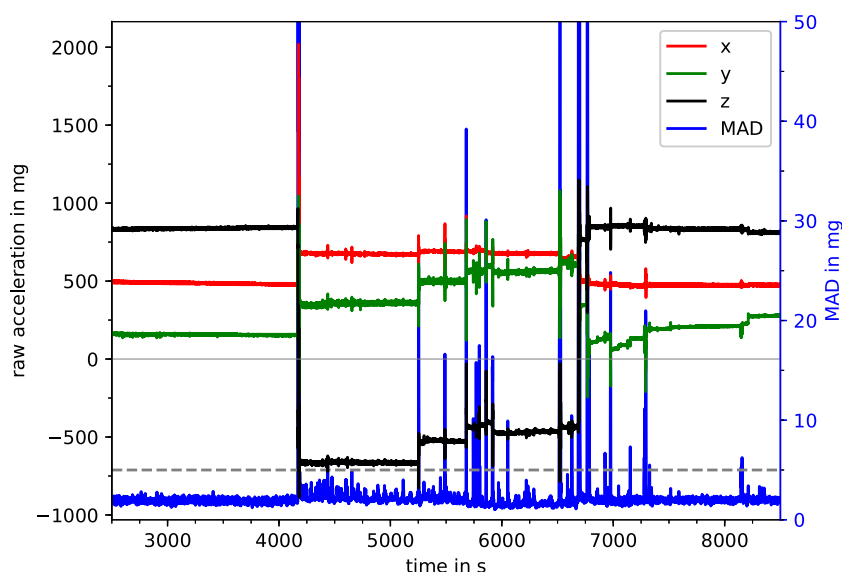


Fig 2. Raw acceleration signals and MAD. A typical nocturnal 100 minute part of the raw data is shown with all three directions (\ddot{x} —red, \ddot{y} —green, \ddot{z} —black) of the acceleration signal according to the left vertical axis. Furthermore, one-second mean amplitude deviation (MAD) values are plotted in blue with the MAD threshold of 5 mg shown as dashed gray line according to the right vertical axis. Time periods in which the MAD_{1s} values are above this threshold were labeled as a position change (i.e., change in wrist orientation, see for example the peak at 4150 s).

<https://doi.org/10.1371/journal.pone.0226843.g002>

Data segmentation and stationarity transform

Fig 2 shows a section of a typical nocturnal recording of a three-axis wrist accelerometer. There are segments of nearly constant acceleration, e.g., from $t = 2500$ s to $t \approx 4100$ s, from $t \approx 4200$ s to $t \approx 5250$ s, etc. During such segments, the broad orientation of the wrist with respect to the gravitational field (i.e., the vertical direction) is constant, so that all three components of acceleration (\ddot{x} , \ddot{y} , and \ddot{z}) represent mainly the constant projections of the gravitational acceleration $g_0 = 9.81$ m/s² on each axis of the device. Specifically, the x axis points towards the hand, while y and z are orthogonal to x and to each other with directions possibly changing between the subjects and throughout the night.

Segments of nearly constant acceleration components (due to gravitational force only) are interrupted by obvious changes of the wrist orientation with respect to the gravitational field. In order to automatically identify such broad orientation changes, we calculated a mean amplitude deviation (MAD) very similar to MAD_{5s} introduced by Vähä-Ypyä et al. [30],

$$MAD_{1s}(t) = \frac{1}{128} \sum_{i=t \times 128Hz-63}^{t \times 128Hz+64} |a_i - \langle a_i \rangle|, \tag{1}$$

with $a_i = \sqrt{\ddot{x}_i^2 + \ddot{y}_i^2 + \ddot{z}_i^2}$ and $\langle a_i \rangle = \frac{1}{128} \sum_{i=t \times 128Hz-63}^{t \times 128Hz+64} a_i$, considering non-overlapping windows of one second here. In our cleaning procedure, all acceleration data are set to zero, if their corresponding $MAD_{1s}(t)$ values exceed the ad-hoc threshold of 5 mg ($= 0.005 g_0$).

In the following, we refer to continuous time segments not interrupted by MAD_{1s} values above the 5 mg threshold as sleeping position segments (SPS). We assume that the subjects did not change their sleeping positions without increased motion activity. In each SPS and for each acceleration component (\ddot{x}_i , \ddot{y}_i , and \ddot{z}_i), we eliminated the offsets (caused by gravity) by

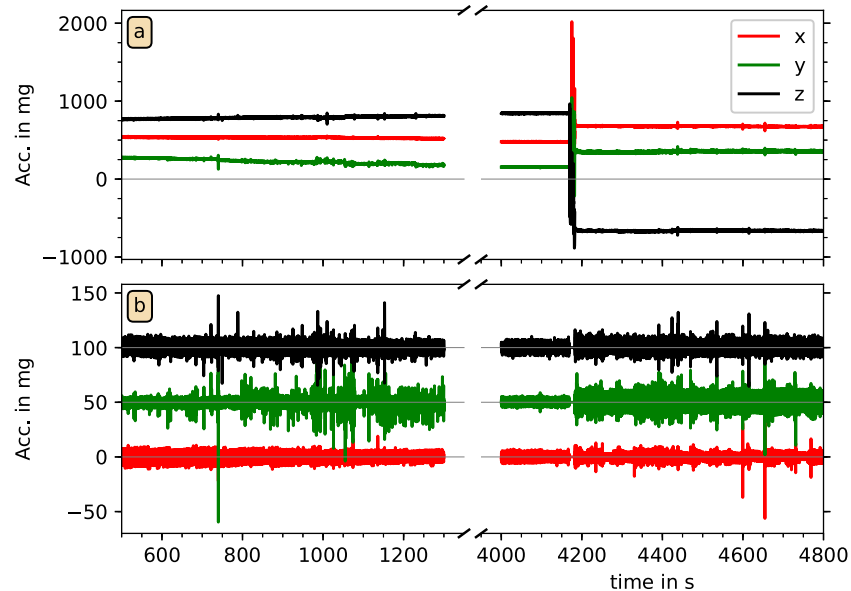


Fig 3. Raw and cleaned acceleration data. The upper panel shows raw acceleration data (\ddot{x} —red, \ddot{y} —green, \ddot{z} —black) during two parts of a recording. A weak steady trend appears in the \ddot{y} component on the left hand side, and a wrist position change appears at time 4150 s on the right hand side (as already mentioned in Fig 2). The lower panel shows a magnification of the cleaned data in both parts, with constant offsets and slow trends removed. All acceleration data with their corresponding MAD_{1s} values above the MAD threshold were set to zero. The data for \ddot{y} and \ddot{z} have been shifted upwards by multiples of 50 mg for visibility.

<https://doi.org/10.1371/journal.pone.0226843.g003>

subtracting the mean values of each second. Fig 3 shows two examples for this acceleration data preprocessing procedure. We note that a subtraction of mean values of each second turned out to be sufficient, since—besides the stronger motions exceeding the threshold—there are only very slowly drifting wrist orientation changes with respect to the gravitational axis, see, e.g., Fig 2 in the range from $t = 6800$ s to 7200 s. The subtraction of one-second averages also turned out to be sufficient for an elimination of the slow (≈ 0.3 Hz) respiratory signal often superimposed on the acceleration recordings via tiny turns of the wrist, see also Fig 4(a) and 4(b). Approximately stationary acceleration data with zero means and only short interruptions have thus been obtained in the data cleaning procedure.

Pulse wave peak (PWP) and pulse wave interval (PWI) detection

Fig 3 shows that amplitude variations of typically 10 – 40 mg remain after the acceleration data have been cleaned. These signals often exhibit a rather periodic behavior, see Fig 4(a) and 4(b) for details at a high temporal resolution. Note that the corresponding variations of measured acceleration are quite small and in fact close to the resolution of the recording device, which digitizes measurements between $-6 g_0$ and $+6 g_0$ at 12 bits, yielding a resolution of 2.9 mg. The small spikes at an approximate periodicity somewhat below one second already look like indications of heartbeats. Most probably, pulse wave propagations through the wrist lead to tiny turns of the wrist with respect to the vertical (gravitational) axis, resulting in changes of the gravitation vector projections on the axes of the acceleration recording device.

In the next step, for a better identification of the pulse wave events, we applied a fast Fourier transform (FFT) based band pass filter with a lower cutoff at 5 Hz and an upper cutoff at 14 Hz

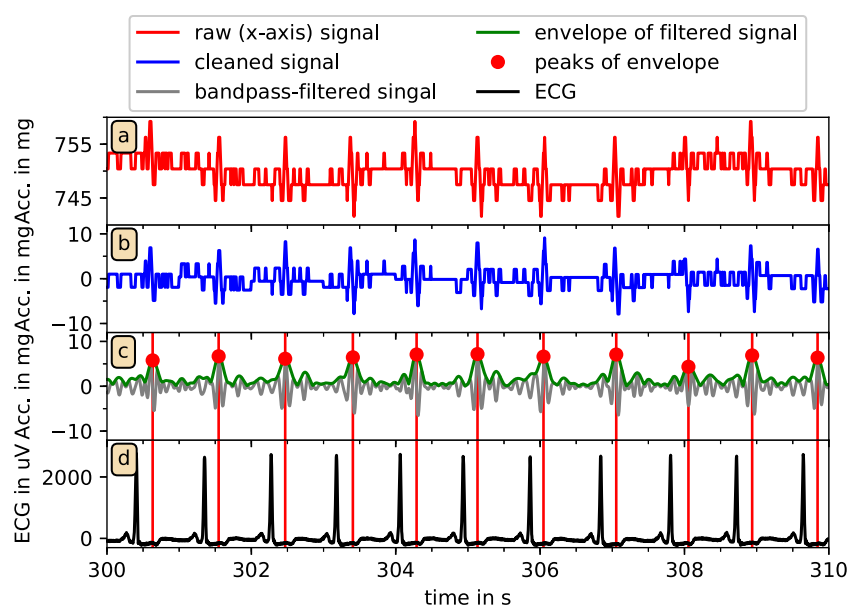


Fig 4. Reconstruction of pulse waves from acceleration data. In (a) and (b) the raw (red) and cleaned (blue) *x*-axis acceleration data from a typical recording is shown for ten seconds. Panel (c) shows the signal after the 5–14 Hz FFT-bandpass-filtering (gray), the absolute of the Hilbert transform (green), and the results of the peak detection (red dots). In (d) the ECG-signal (black) is presented and compared to the pulse wave peak (red vertical lines). Please also note the impact of respiration in panel (a) leading to a modulation of the acceleration data with a period of about 4 s. These modulations are removed in panel (b) by subtracting one-second averages.

<https://doi.org/10.1371/journal.pone.0226843.g004>

to the data of each axis. We have empirically optimized these cutoff frequencies by studying acceleration data of many subjects. A typical result is shown in Fig 4(c), gray line. For a reliable identification of the pulse wave-related peaks we then applied a Hilbert transform [31] to the cleaned and band-pass filtered acceleration data \tilde{a}_i of each axis to supplement the original signal with an imaginary part and calculate the instantaneous amplitudes $A(t)$ in an analytic signal approach,

$$\tilde{a}(t) + i\text{HT}[\tilde{a}(t)] = A(t) \exp[i\varphi(t)], \quad (2)$$

(Fig 4(c), green line). Among the first applications of this approach to physiological dynamics are the works of Ivanov et al. who used Hilbert transform to detect the amplitude of heart rate variability fluctuations [32, 33].

Finally, a peak detection algorithm was used to identify candidate peaks in these pseudo pulse wave time series (Fig 4(c) red dots). Specifically, a local maximum of the time series was accepted as the next pulse wave peak candidate if it exceeded an ad-hoc threshold of 2.9 mg and has a minimum distance to the previous accepted peak of 0.5 s. Note that, in analogy to R peak detection from ECGs, we refer to the peaks as pulse wave peaks (PWP) and to the time intervals between them as pulse wave intervals (PWI). We also note that PWP are not real pulse (pressure) wave peaks, but closely related to them. Fig 4(d) shows that each detected PWP is clearly associated with an R peak of the simultaneously recorded ECG. The Figure also demonstrates the delay of the PWP with respect to the R peaks caused by pulse wave transit time (PTT) from the heart to the wrist.

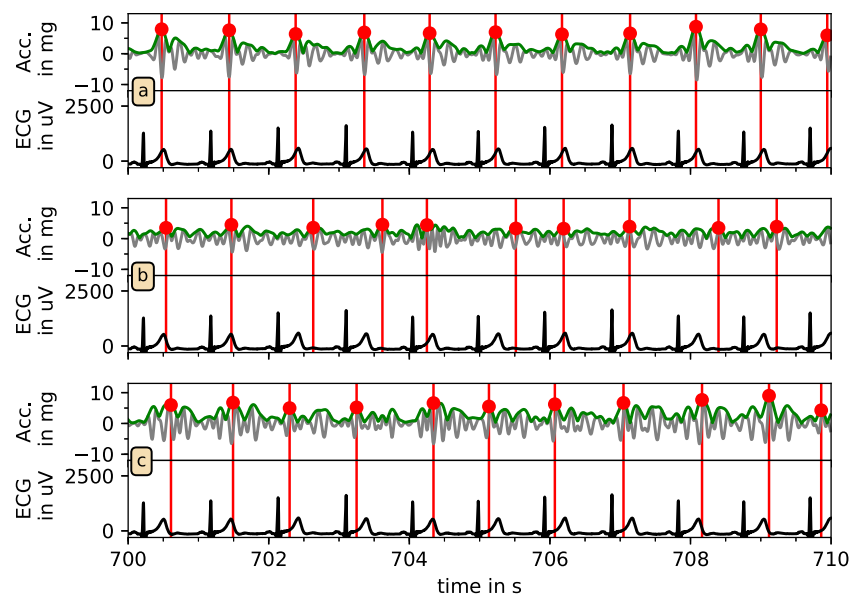


Fig 5. Selection of best axis for pulse wave reconstruction. The bandpass-filtered acceleration signals (gray), the corresponding Hilbert amplitudes (green) and the automatically identified candidate pulse wave peaks (red) are compared with the ECG (black) for all three axes of acceleration for another typical ten-second section of the recordings. Clearly, the detection reliability differs between the axes; in this case the best choice for beat detection is the x axis shown in panel (a).

<https://doi.org/10.1371/journal.pone.0226843.g005>

Having three time series of candidate PWP (from each accelerometer axis) we have to select the best position estimate for each pulse wave. Fig 5 shows that—in this case—the x axis (part (a)) yields the most consistent PWP positions with respect to the R peaks in the ECG. However, in order to select candidate PWP without assessing ECG signals, we defined two criteria to choose—for each SPS—the best acceleration axis. Firstly, the plausibility of the candidate PWP was checked by calculating average pulse rate, requiring a value of at least 40 beats per minute for a plausible signal. If no signal was plausible, the considered SPS has not been used for further analysis. Secondly, if two or all three signals passed the first test, we applied a self-consistency check. Specifically, we calculated auto-correlation functions for the Hilbert amplitude signals and chose the axis with the highest auto-correlation peak in the range from 0.4 s to 1.5 s (40 beats/min to 150 beats/min).

In the final step, we calculated the PWI. In analogy with similar approaches for checking the validity of detected R peaks in an ECG, the duration of each PWI must either be between 0.7 s and 1.5 s (corresponding to instantaneous values of 40 beats/min to 86 beats/min) or in the range of ± 30 percent of the previous PWI. Furthermore, we accepted only uninterrupted sequences of at least 20 PWI, thereby excluding very short SPS. This way we obtained time series of PWI comparable to RR-interval (RRI) time series. For comparing the two types of time series, we have calculated mean heart rate and the following two standard parameters of HRV [17]: standard deviation of normal-normal intervals (SDNN) and root mean square of successive differences (RMSSD).

To derive RRI time series from ECG, these data were processed with the software LibRasch [34]. We visually verified and manually checked QRS classifications (normal, ventricular

Table 2. PWI reconstruction correctness for different accuracy limits. Results are shown for five different maximally accepted differences between RRI and PWI (accuracy limits). The column “time” reports the median total duration of all PWI that are correctly associated with RRI (per subject). As in Table 1, it is followed by the fraction of correctly associated PWI and the corresponding Pearson cross correlation r . Values are median [0.25 quantile; 0.75 quantile].

accuracy limit	time	correct PWI	r
0.05 s	1.2 [0.4; 2.1] h	0.73 [0.61; 0.83]	0.96 [0.93; 0.98]
0.10 s	1.3 [0.5; 2.3] h	0.81 [0.69; 0.89]	0.94 [0.88; 0.96]
0.15 s	1.4 [0.5; 2.4] h	0.84 [0.74; 0.91]	0.89 [0.82; 0.94]
0.20 s	1.4 [0.5; 2.4] h	0.88 [0.77; 0.94]	0.85 [0.77; 0.91]
0.25 s	1.4 [0.5; 2.4] h	0.88 [0.77; 0.94]	0.83 [0.74; 0.90]

<https://doi.org/10.1371/journal.pone.0226843.t002>

ectopic, and supra-ventricular ectopic) and corrected them if necessary. Noisy parts where no QRS detection was possible were manually marked and excluded from further analysis.

Comparison of PWI and RRI

Due to the transition time between each heartbeat and the arrival of the pulse wave at the wrist, a direct comparison of R peaks and PWP is not appropriate. Hence, we compared RRI and PWI, defining their temporal positions as the middle of each interval. A PWI matches an RRI if its position is within 0.0 to 0.3 s after the RRI’s position. Note that the empirical value of this threshold is post-hoc justified by the distribution of PTT we observe in Fig 9. A matching PWI is considered as correct, if its value is less than 0.1 s smaller or larger than the corresponding RRI (accuracy limit). This accuracy limit has been varied to check for its effects on the results (see Table 2 below).

4 Results and discussion

Reliability of reconstructed pulse wave intervals (PWI)

As described in the method section, we have reconstructed PWI from wrist accelerometry time series independent of the ECG. In our 363 datasets we were able to reconstruct PWI during 25.7 percent of the total recording time (in the sleep laboratory), which corresponds to an average duration of 1.7 h per subject.

Fig 6 shows a direct comparison of tachograms of PWI and RRI derived from the simultaneous acceleration and ECG recordings of two subjects. A very close match between the two curves can be seen, although one ventricular heartbeat in (a) is not correctly identified by the pulse wave analysis, and there seems to be an increased high-frequency (HF) component in the PWI data.

In total, 80.9 percent of the detected PWI could be correctly associated with RRI at an accuracy limit of 0.1 s. In terms of time, 1.3 hours of correct PWI were detected per night. Table 2 reports median values and inter-quartile ranges regarding the achieved levels of correctness for the reconstructed PWI also for smaller and larger accuracy limits (see Methods subsection on Comparison of PWI and RRI above). We find that the results do not strongly depend on this accuracy limit, since the fraction of correctly reconstructed and associated PWI varies only between 0.73 and 0.88 for a broad variation of the limit from 0.05 s to 0.25 s (Table 2). In particular, increasing the limit from 0.2 s to 0.25 s does not change this fraction. Since most correctly detected PWI differ from the RRI by less than 0.05 s (1.2 h total time per subject) and doubling or tripling the limit increases this total time only by 0.1 h and 0.2 h, respectively, we conclude that an accuracy limit of 0.1 s is appropriate for a fair comparison.

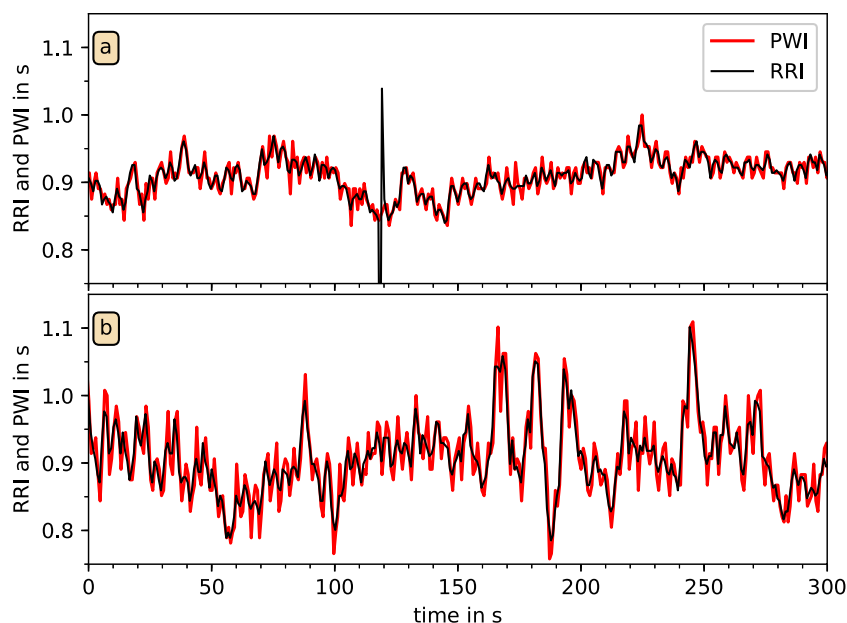


Fig 6. Comparison of tachograms from RRI and PWI. In these two examples from different subjects, RRI derived from the ECG (black) and PWI independently derived from wrist accelerometry (red) are plotted versus time. All detected PWP and all R peaks were used; the PWI are strongly correlated with RRI. However, unexpected heartbeat events, as for example the premature beat at $t = 120$ s in (a), are not present in the PWI signal.

<https://doi.org/10.1371/journal.pone.0226843.g006>

At the 0.1 s accuracy limit, the Pearson cross-correlation coefficient r between the values of reconstructed PWI and correctly associated RRI is quite large, $r = 0.94$. Note, that r can only be calculated with respect to the PWI correctly associated with RRI. As expected, it decreases somewhat with larger accuracy limits as more and more PWI are included. However, $r = 0.85$ at the 0.2 s limit is still very good. Note that r is based on only 351 datasets (instead of 363), since no correct PWI were detected in 12 datasets. In addition, the different ICSD-3 diagnoses of the subjects have little effect upon our results as shown in the last two columns of [Table 1](#).

Next we want to check the variation of the PWI detection performance of our algorithm across all 363 subjects. [Fig 7](#) shows histograms for the total time of detected PWI in each subject and the fraction of correctly reconstructed and associated PWI. Although we have 74 datasets with less than 30 minutes of usable acceleration signals, most recordings—233 datasets—yield reconstructed PWI totaling between 30 minutes and 3.5 hours. In five datasets, we could detect PWI for more than 5.5 hours. The histogram for the fraction of correctly reconstructed and associated PWI ([Fig 7\(b\)](#)) has a small peak at 0 to 10 percent (15 datasets), which includes 12 recordings without any correctly detected PWI, and rises to a maximum at 80 to 90 percent correct detection. In 216 datasets more than 80 percent of the detected PWI were correct.

These percentages hardly depend on the age of the subjects. No systematic differences between three age groups of approximately equal size (see [Table 3](#)) can be observed when comparing the corresponding histograms for each color in [Fig 7](#). This indicates that the reconstruction of pulse waves from wrist actigraphy as presented in this paper does not depend on age. Furthermore, the results in [Table 3](#) show that there is no systematic age dependence in the PWI algorithm selection of particular orientation axes. Across all age groups, the y axis

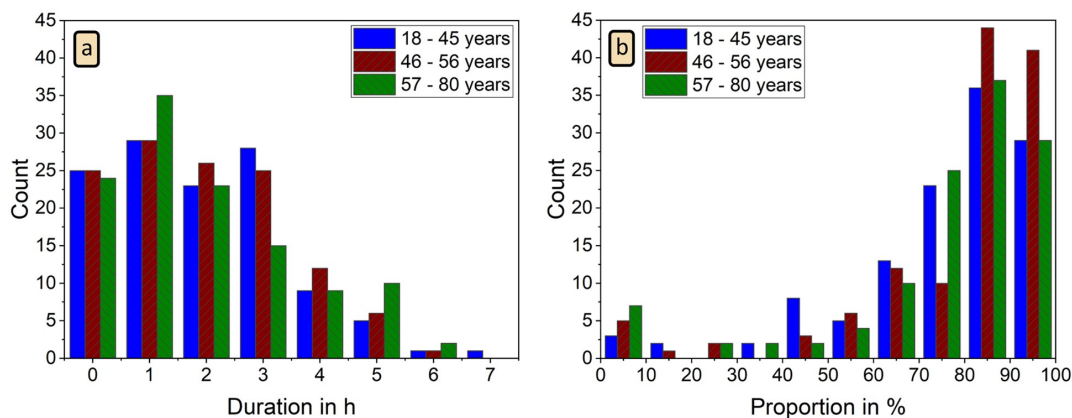


Fig 7. Histograms for total PWI duration and correctness of PWI identification. (a) Histogram of total duration of all detected PWI for each night; (b) histogram of fraction of correctly reconstructed and associated PWI (as compared to RRI from ECG) for each night. No clear differences between the three age groups (see Table 3) can be seen.

<https://doi.org/10.1371/journal.pone.0226843.g007>

acceleration data is selected most frequently for the PWI detection, followed by the *z* axis data. The *x* axis, pointing towards the hand, is only quite rarely selected.

Estimation of heart rate and HRV parameters from PWI

Table 4 compares heart rates and two standard HRV parameters [17] across all three steps of our PWI-RRI matching procedure. Clearly, the effect on resulting mean heart rate is minimal. In addition, there seems to be only little selection bias regarding correctly reconstructed and not reconstructed heartbeats, since the SDNN and RMSSD values for the matched RRI subset are close to the values for the whole (nocturnal) RRI time series. Furthermore, the results for

Table 3. Age dependence of SDNN and RMSSD and origin of matched PWI. For three similarly sized age groups the fractions of matched PWI derived from each of the three accelerometer axes are reported, showing the *y* axis data is used for more than half of all PWI correctly associated with RRI. The mean values of the HRV parameters SDNN and RMSSD and the mean PTT as derived from matched RRI and PWI are shown for comparison with literature [35, 39]. Regarding SDNN and RMSSD, all differences between the young age group and the other two groups are highly significant ($p \leq 0.002$), while no significant differences occur between the intermediate and the elderly group. The results indicate that the reduction in SDNN and RMSSD with age is similar in RRI (as derived from the ECG) and PWI (as reconstructed through wrist actigraphy). The differences between the mean PPT values of the young group and the other two groups are weak but still highly significant ($p = 0.004$ and $p < 0.001$, respectively), but also not significant between the intermediate and the elderly group.

age range	18-45 y	46-56 y	57-80 y
number of subjects	117	114	120
fraction for <i>x</i> axis	0.13	0.15	0.09
fraction for <i>y</i> axis	0.51	0.53	0.52
fraction for <i>z</i> axis	0.35	0.32	0.39
SDNN from RRI	78.5 ms	65.9 ms	65.7 ms
SDNN from PWI	83.5 ms	72.6 ms	72.3 ms
RMSSD from RRI	54.5 ms	39.8 ms	39.5 ms
RMSSD from PWI	71.9 ms	61.6 ms	61.7 ms
mean PTT	216.9 ms	206.7 ms	200.7 ms

<https://doi.org/10.1371/journal.pone.0226843.t003>

Table 4. Comparison of heart rate and HRV parameters from RRI and PWI. We calculated mean heart rate, SDNN, and RMSSD for (i) all RRI detected in the ECGs, (ii) all RRI associated with PWI (at an accuracy limit of 0.1 s, see Table 2), (iii) all PWI associated with RRI, and (iv) the total set of all detected PWI. Group averages over 351 subjects with detected PWIs are presented.

	mean heart rate	SDNN	RMSSD
all RRI	65.1 1/min	93 ms	52 ms
matched RRI	64.4 1/min	70 ms	45 ms
matched PWI	64.4 1/min	76 ms	65 ms
all PWI	64.4 1/min	115 ms	138 ms

<https://doi.org/10.1371/journal.pone.0226843.t004>

the matched PWI closely resemble those for the whole RRI time series. On the other hand, SDNN and in particular RMSSD would be a bit overestimated if no ECGs were available for comparison and these parameters were calculated from all accelerometer-detected PWI (bottom row in Table 4). However, as will be shown below in the results section on the influence of respiration, this cannot be regarded as a problem of our approach, since indeed SDNN and RMSSD are increased by influences of respiratory activity on pulse transit times.

Fig 8 shows Bland-Altman plots as a detailed comparison between the SDNN and RMSSD values derived from RRI and PWI for each subject. Except for six outliers $SDNN_{PWI}$ is larger than $SDNN_{RRI}$ (Fig 8(a)). We can see a slight linear trend in the Bland-Altman plot with a Pearson correlation coefficient of 0.53, since the difference between $SDNN_{PWI}$ and $SDNN_{RRI}$ decreases with higher SDNN. In Fig 8(b) and 8(c) we compared the values of RMSSD, which is a common HRV parameter to estimate parasympatic activity [17]. Furthermore, RMSSD is independent of sleep stages [35]. In nearly all subjects $RMSSD_{PWI}$ is clearly larger than $RMSSD_{RRI}$; the average difference is approximately equal to two standard deviations. This relation holds for both, associated RRI and PWI (Fig 8(b)) and all RRI and PWI (Fig 8(c)), although the difference is much larger in the second case (see also Table 4). The subjects of the three outliers in panel (b) are a subgroup of the six outliers in the SDNN plot (Fig 8(a)). We also see a slight linear trend in the Bland-Altman plot of RMSSD for associated RRI and PWI with a Pearson correlation coefficient of 0.46 (Fig 8(b)), but no clear trend for all RRI and PWI with a Pearson correlation coefficient 0.005 (Fig 8(c)).

The colored symbols in Fig 8, corresponding to the results of the three age groups (see Table 3), show no systematic dependence on age, supporting the conclusion from Fig 7 that our reconstruction of PWI from wrist actigraphy does not depend on age. Furthermore, the mean SDNN and RMSSD values listed in Table 3 for each of the three groups show that the reduction of SDNN and RMSSD with age reported by Schmitt et al. [35] similarly occurs for the HRV parameters derived from RRI and PWI, although their absolute values are different. Apparently, the decrease occurs before the age of approximately 40–50 years, since our results for the last two age groups (46–56 and 57–80 years, respectively) are practically identical.

We note that a recent work also used wrist accelerometry in the frequency range from 4 to 11 Hz to estimate heart rates [36]. However, the study focused on average heart rate (and breathing rate) in intervals of 20 s as determined via spectral analysis, not trying to identify individual heartbeats or beat-to-beat intervals. Besides that, it was limited to 32 h of sleep data from three subjects and 72 minutes of daytime data from twelve subjects. Another recent study determined the average heart rates in 15 subjects using wrist accelerometry [37], reporting an average deviation of 1.6 percent with respect to heart rate from a pulse-oximeter attached to the index finger. This deviation is comparable to the deviation of 0.9 percent we observe between the mean heart rate for all RRI and the PWI-based estimate (Table 4). Another paper from the same group reported that heart rate can be most reliably estimated

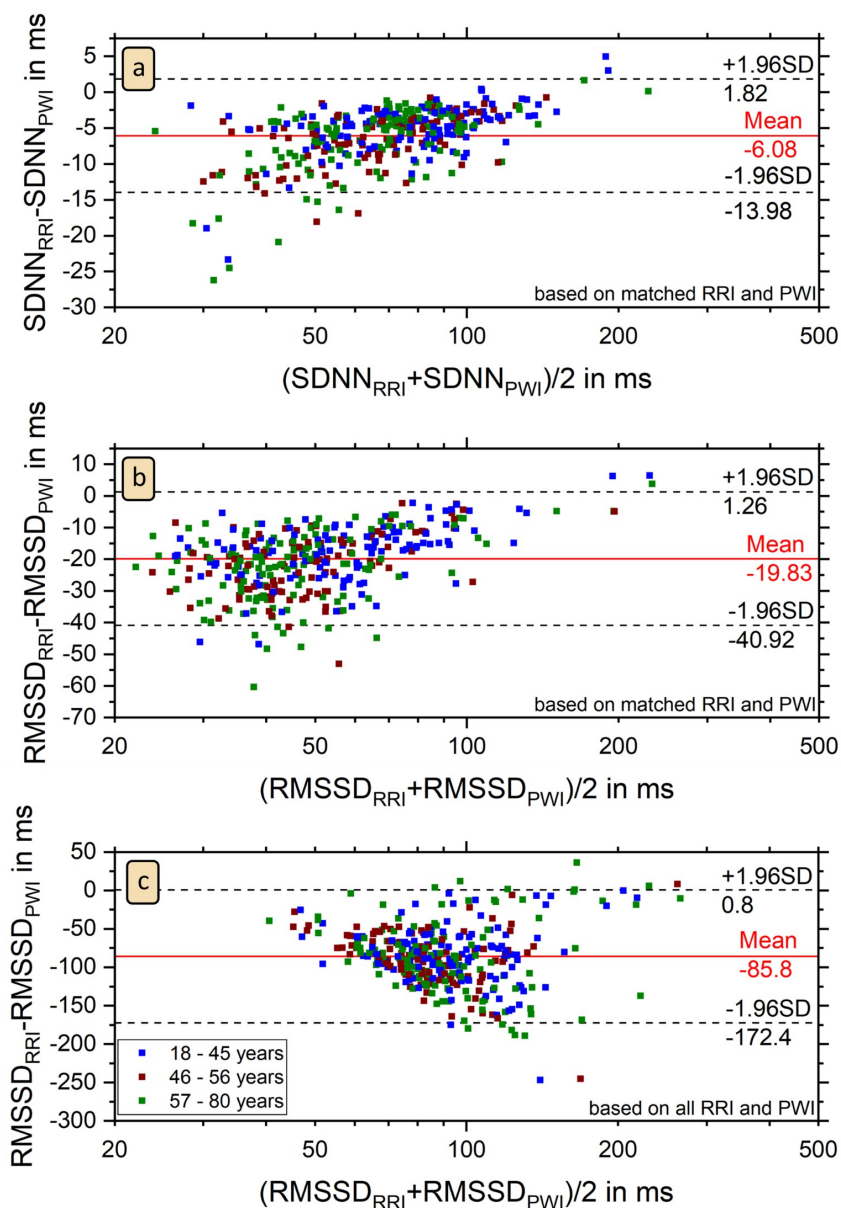


Fig 8. Bland-Altman plots of SDNN and RMSSD. The plots show that SDNN and RMSSD values derived from PWI are larger than those derived in the standard way from RRI for nearly all 351 subjects. There are only six outliers for (a) SDNN comparing associated RRI and PWI, three for (b) RMSSD comparing associated RRI and PWI, and eight for (c) RMSSD comparing all RRI and all PWI. In panel (c), one extreme outlier for a subject with 16 percent of ectopic beats and $RMSSD_{all\ RRI} = 377$ ms, $RMSSD_{all\ PWI} = 163$ ms does not appear in the plot. No clear differences between the three age groups (see Table 3) can be seen.

<https://doi.org/10.1371/journal.pone.0226843.g008>

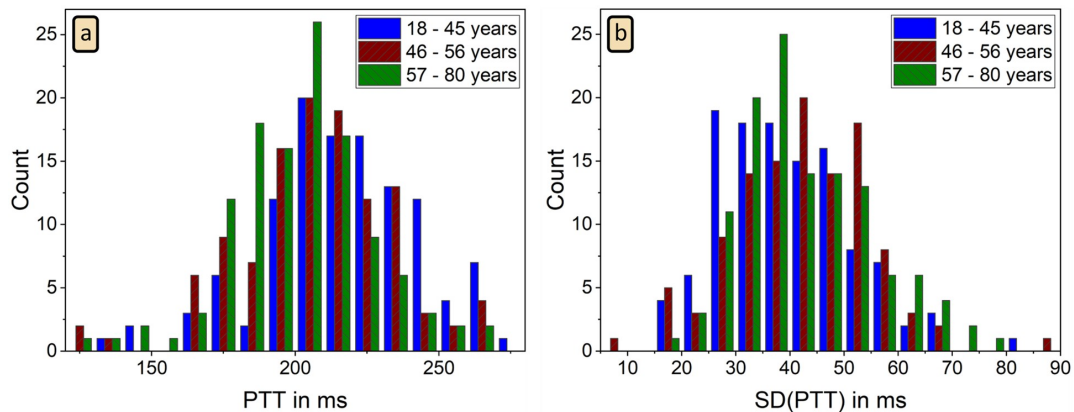


Fig 9. Histograms of mean PTT and its standard deviation. Histograms of average PTT defined as the time delay between ECG R peak and the associated PWP, as well as the corresponding standard deviations of the reconstructed PTT intervals. Data of 351 subjects is presented distinguishing three age groups (see Table 3); no PWP were detected in 12 subjects.

<https://doi.org/10.1371/journal.pone.0226843.g009>

via accelerometry, if the sensor is attached to the subjects' upper forearm or the subjects' belly [38].

Pulse transit times (PTT)

In addition to heartbeat estimation, accelerometer-detected PWP can be used to calculate the time delay between heart beats and PWP, better known as pulse transit time (PTT), if an ECG is simultaneously recorded. The histogram of the mean PTT values in all subjects is shown in Fig 9(a). On average we estimated a PTT of 207 ± 26 ms. This result as well as its range agree with literature [39]. However, PTT values in young subjects seem to be a bit longer than those in the elderly, since a slight difference between the young group and the other two groups can be seen in Fig 9(a) and leads to significantly different means as reported in Table 3. Fig 9(b) shows that the standard deviation of PTT values in each subject (the temporal PTT variation) is distributed around 42 ms and thus comparable with the inter-subject PTT variation.

We think that time series of PTT derived this way could be used in a similar way as ECG-derived RRI are used for studies of HRV, see, e.g., [40]. However, further research will be needed to identify useful PTT-based parameters comparable to the standard HRV parameters. Besides, PTT measurements were suggested to be used as an estimate for continuous blood pressure recording during sleep [41].

Influence of respiration on PWI

In this subsection, we want to address the reason for the increased values of SDNN and particularly RMSSD as observed when calculating these HRV parameters from acceleration-derived PWI instead of ECG-derived RRI (Tables 3 and 4). It has been known since 1860 that respiration modulates heartbeat frequency, a phenomenon called respiratory sinus arrhythmia (RSA) [42]. A closer look at the tachograms of both RRI and PWI data (Fig 10) clearly shows these periodic oscillations due to RSA. It can also be seen that PWI yield larger variations than RRI suggesting a stronger respiration related modulation.

In order to investigate this observation in greater detail, we compared the power spectra of RRI and PWI time series. We selected all uninterrupted episodes of detected PWI of at least

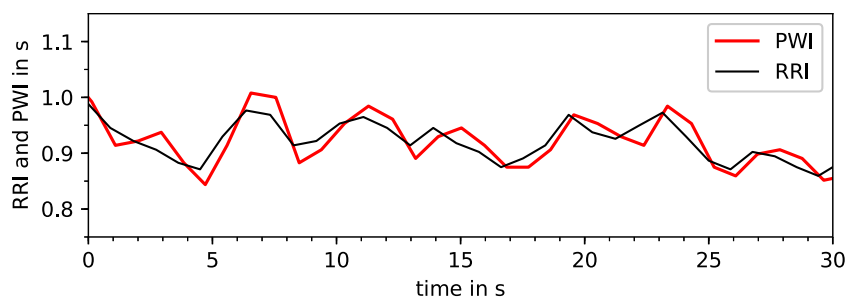


Fig 10. Tachogram of respiratory sinus arrhythmia. This plot shows how RRI (black) and PWI (red) follow oscillations due to respiratory sinus arrhythmia.

<https://doi.org/10.1371/journal.pone.0226843.g010>

five minutes duration and calculated the spectra via FFT. Fig 11 shows average power spectra of at least ten five-minute intervals for six typical subjects. Respiration frequency normally lies in the LF band of HRV, between 0.15 and 0.4 Hz [17], see also [43]. The spectra in Fig 11(a) and 11(b) exhibit a high and broad respiratory peak in both, RRI and PWI. The amplitude of the respiratory peak is considerably higher for PWI than for RRI especially in Fig 11(a). But also in Fig 11(c) to 11(e) higher respiratory peaks appear for PWI compared with RRI. Besides this difference the spectra are very similar for both types of intervals. In Fig 11(f) data from a subject with low RSA is presented. We conclude that respiration tends to modulate PWI stronger than RRI.

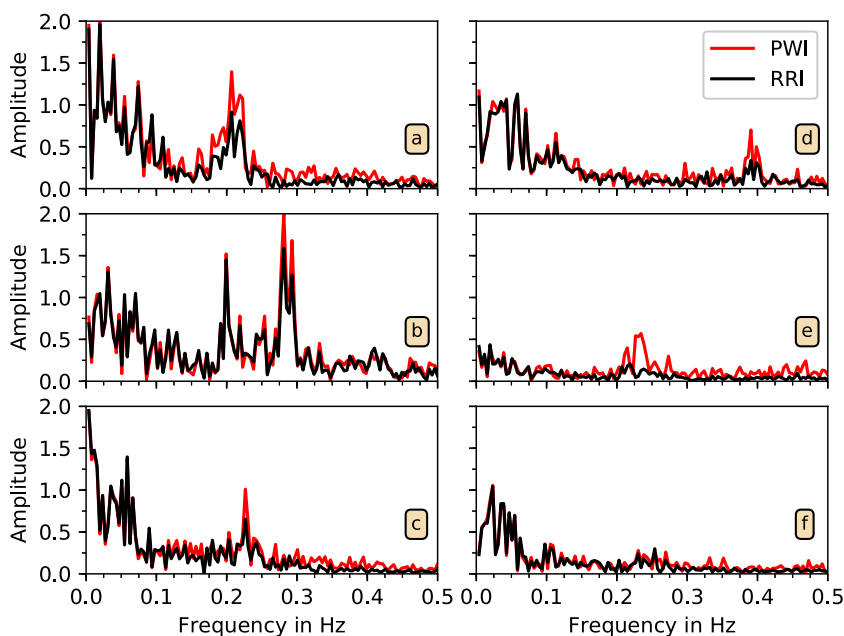


Fig 11. Spectral analysis of PWI and RRI time series. The spectra of PWI data (red) and RRI data (black) are shown for six subjects. In all cases except for (f), the peak in the (respiratory) HF band (0.15 to 0.4 Hz) is increased in the PWI-based spectra.

<https://doi.org/10.1371/journal.pone.0226843.g011>

Conclusion

Although further development, optimization, and validation is necessary, our work represents a novel approach for obtaining long-term nocturnal heartbeat interval time series without the need of ECG recordings (involving electrodes). This could create the possibility to reliably assess heart rate and HRV in large cohort studies solely through accelerometers already used for actigraphy measurements (to characterize activity and sleep patterns). Moreover, our approach could be used to improve plethysmogram-based techniques for measuring heartbeats at the wrist, as currently done in smart watches.

In physiological terms, we show that respiration affects pulse wave velocity in such a way that the respiratory sinus arrhythmia of pulse wave intervals is increased compared with the modulation of RR intervals. However, further research is needed to identify whether the underlying mechanism of increased RSA in PWI is more related to blood pressure modulations or to arterial stiffness modulations.

Acknowledgments

This study was supported by the German Israel Foundation (GIF) grants I-1298-415.13/2015 and I-1372-303.7/2016 and the German National Cohort study (www.nako.de), funded by the Federal Ministry of Education and Research (BMBF) and the Helmholtz Association. JZ acknowledges support from a Minerva Short-Term Research Grant. We acknowledge the financial support within the funding programme Open Access Publishing by the German Research Foundation (DFG).

Author Contributions

Conceptualization: Jan W. Kantelhardt.

Data curation: Alexander Müller.

Funding acquisition: Rafael Mikolajczyk, Ronny P. Bartsch, Thomas Penzel.

Investigation: Maria Kluge, Luise Pelikan, Antonia Graf.

Methodology: Johannes Zschocke.

Project administration: Martin Glos.

Resources: Martin Glos.

Software: Johannes Zschocke.

Supervision: Thomas Penzel, Jan W. Kantelhardt.

Visualization: Johannes Zschocke.

Writing – original draft: Johannes Zschocke, Jan W. Kantelhardt.

Writing – review & editing: Ronny P. Bartsch, Jan W. Kantelhardt.

References

1. Rechtschaffen A, Kales A. A Manual of standardized terminology, techniques and scoring system for sleep stages of human subjects. vol. 204 of National Institutes of Health Publication. Bethesda, MD; 1968.
2. Berry RB, Albartario CL, Harding SM, Lloyd R M, Plante DT, Quan SF, et al. The AASM manual for the scoring of sleep and associated events: rules, terminology and technical specifications, version 2.5. American Academy of Sleep Medicine, Darien, IL. 2018.

3. Penzel T, Kantelhardt JW, Bartsch RP, Riedl M, Kraemer JF, Wessel N, et al. Modulations of Heart Rate, ECG, and Cardio-Respiratory Coupling Observed in Polysomnography. *Frontiers in Physiology*. 2016; 7:460. <https://doi.org/10.3389/fphys.2016.00460> PMID: 27826247
4. Kupfer DJ, Weiss BL, Foster FG, Detre TP, Delgado J, McPartland R. Psychomotor activity in affective states. *Archives of General Psychiatry*. 1974; 30(6):765–768. <https://doi.org/10.1001/archpsyc.1974.01760120029005> PMID: 4832184
5. Koenig SM, Mack D, Alwan M. Sleep and sleep assessment technologies. In: *Eldercare technology for clinical practitioners*. Springer; 2008. p. 77–120.
6. Wohlfahrt P, Kantelhardt JW, Zinkhan M, Schumann AY, Penzel T, Fietze I, et al. Transitions in effective scaling behavior of accelerometric time series across sleep and wake. *EPL (Europhysics Letters)*. 2013; 103(6):68002. <https://doi.org/10.1209/0295-5075/103/68002>
7. Zinkhan M, Berger K, Hense S, Nagel M, Obst A, Koch B, et al. Agreement of different methods for assessing sleep characteristics: a comparison of two actigraphs, wrist and hip placement, and self-report with polysomnography. *Sleep Medicine*. 2014; 15(9):1107–1114. <https://doi.org/10.1016/j.sleep.2014.04.015> PMID: 25018025
8. van Hees VT, Sabia S, Jones SE, Wood AR, Anderson KN, Kivimäki M, et al. Estimating sleep parameters using an accelerometer without sleep diary. *Scientific Reports*. 2018; 8(1):12975. <https://doi.org/10.1038/s41598-018-31266-z> PMID: 30154500
9. Ancoli-Israel S, Cole R, Alessi C, Chambers M, Moorcroft W, Pollak CP. The role of actigraphy in the study of sleep and circadian rhythms. *Sleep*. 2003; 26(3):342–392. <https://doi.org/10.1093/sleep/26.3.342> PMID: 12749557
10. Godfrey A, Conway R, Meagher D, ÓLaighin G. Direct measurement of human movement by accelerometry. *Medical Engineering & Physics*. 2008; 30(10):1364–1386.
11. Sadeh A, Acebo C. The role of actigraphy in sleep medicine. *Sleep Medicine Reviews*. 2002; 6(2):113–124. <https://doi.org/10.1053/smr.2001.0182> PMID: 12531147
12. Zinkhan M, Kantelhardt JW. Sleep assessment in large cohort studies with high-resolution accelerometers. *Sleep Medicine Clinics*. 2016; 11(4):469–488. <https://doi.org/10.1016/j.jsmc.2016.08.006> PMID: 28118871
13. Hu K, Ivanov PC, Chen Z, Hilton MF, Stanley HE, Shea SA. Novel multiscale regulation in human motor activity. In: Bezrukov SM, Frauenfelder H, Moss F, editors. *Fluctuations and Noise in Biological, Biophysical, and Biomedical Systems*. SPIE Proceedings. SPIE; 2003. p. 235.
14. Hu K, Ivanov PC, Chen Z, Hilton MF, Stanley HE, Shea SA. Non-random fluctuations and multi-scale dynamics regulation of human activity. *Physica A*. 2004; 337(1-2):307–318. <https://doi.org/10.1016/j.physa.2004.01.042> PMID: 15759365
15. Ivanov PC, Hu K, Hilton MF, Shea SA, Stanley HE. Endogenous circadian rhythm in human motor activity uncoupled from circadian influences on cardiac dynamics. *Proceedings of the National Academy of Sciences of the United States of America*. 2007; 104(52):20702–20707. <https://doi.org/10.1073/pnas.0709957104> PMID: 18093917
16. Hu K, Scheer FAJL, Ivanov PC, Buijs RM, Shea SA. The suprachiasmatic nucleus functions beyond circadian rhythm generation. *Neuroscience*. 2007; 149(3):508–517. <https://doi.org/10.1016/j.neuroscience.2007.03.058> PMID: 17920204
17. Malik M, Bigger JT, Camm AJ, Kleiger RE, Malliani A, Moss AJ, et al. Heart rate variability: Standards of measurement, physiological interpretation, and clinical use. *European Heart Journal*. 1996; 17(3):354–381. <https://doi.org/10.1093/oxfordjournals.eurheartj.a014868>
18. O'Rourke MF, Pauca A, Jiang XJ. Pulse wave analysis. *British Journal of Clinical Pharmacology*. 2001; 51(6):507–522. <https://doi.org/10.1046/j.0306-5251.2001.01400.x> PMID: 11422010
19. Nichols WW. Clinical measurement of arterial stiffness obtained from noninvasive pressure waveforms. *American Journal of Hypertension*. 2005; 18:3S–10S. <https://doi.org/10.1016/j.amjhyper.2004.10.009> PMID: 15683725
20. Gong S, Schwalb W, Wang Y, Chen Y, Tang Y, Si J, et al. A wearable and highly sensitive pressure sensor with ultrathin gold nanowires. *Nature Communications*. 2014; 5:3132. <https://doi.org/10.1038/ncomms4132> PMID: 24495897
21. Allen J. Photoplethysmography and its application in clinical physiological measurement. *Physiological Measurement*. 2007; 28(3):R1–39. <https://doi.org/10.1088/0967-3334/28/3/R01> PMID: 17322588
22. Karasik R, Sapir N, Ashkenazy Y, Ivanov PC, Dvir I, Lavie P, et al. Correlation differences in heartbeat fluctuations during rest and exercise. *Physical Review E, Statistical, Nonlinear, and Soft Matter Physics*. 2002; 66(6 Pt 1):062902. <https://doi.org/10.1103/PhysRevE.66.062902> PMID: 12513330
23. Will C, Shi K, Schellenberger S, Steigleder T, Michler F, Fuchs J, et al. Radar-Based Heart Sound Detection. *Scientific Reports*. 2018; 8(1):11551. <https://doi.org/10.1038/s41598-018-29984-5> PMID: 30068983

24. Zanetti JM, Salerno DM. Seismocardiography: a technique for recording precordial acceleration. In: Bankman IN, Tsitlik JE, editors. Computer-based medical systems. Los Alamitos, CA: IEEE Computer Society Press; 1991. p. 4–9.
25. Pandia K, Inan OT, Kovacs GTA, Giovangrandi L. Extracting respiratory information from seismocardiogram signals acquired on the chest using a miniature accelerometer. *Physiological Measurement*. 2012; 33(10):1643–1660. <https://doi.org/10.1088/0967-3334/33/10/1643> PMID: 22986375
26. Inan OT, Migeotte PF, Park KS, Etemadi M, Tavakolian K, Casanella R, et al. Ballistocardiography and seismocardiography: a review of recent advances. *IEEE Journal of Biomedical and Health Informatics*. 2015; 19(4):1414–1427. <https://doi.org/10.1109/JBHI.2014.2361732> PMID: 25312966
27. Jafari Tadi M, Lehtonen E, Hurnanen T, Koskinen J, Eriksson J, Pänkäälä M, et al. A real-time approach for heart rate monitoring using a Hilbert transform in seismocardiograms. *Physiological Measurement*. 2016; 37(11):1885–1909. <https://doi.org/10.1088/0967-3334/37/11/1885> PMID: 27681033
28. Paolo Castiglioni, Andrea Faini, Gianfranco Parati, Marco Di Rienzo. 2007 Annual International Conference of the IEEE Engineering in Medicine and Biology Society. Piscataway, NJ: IEEE Service Center; 2007.
29. Jafari Tadi M, Koivisto T, Pänkäälä M, Paasio A. Accelerometer-based method for extracting respiratory and cardiac gating information for dual gating during nuclear medicine imaging. *International Journal of Biomedical Imaging*. 2014; 2014:690124. <https://doi.org/10.1155/2014/690124> PMID: 25120563
30. Vähä-Ypyä H, Vasankari T, Husu P, Suni J, Sievänen H. A universal, accurate intensity-based classification of different physical activities using raw data of accelerometer. *Clinical Physiology and Functional Imaging*. 2015; 35(1):64–70. <https://doi.org/10.1111/cpf.12127> PMID: 24393233
31. Gabor D. Theory of communication. The analysis of information. *Journal of the Institution of Electrical Engineers-Part III: Radio and Communication Engineering*. 1946; 93(26):429–441.
32. Ivanov PC, Rosenblum MG, Peng CK, Mietus J, Havlin S, Stanley HE, et al. Scaling behaviour of heart-beat intervals obtained by wavelet-based time-series analysis. *Nature*. 1996; 383(6598):323–327. <https://doi.org/10.1038/383323a0> PMID: 8848043
33. Ivanov PC, Rosenblum MG, Peng CK, Mietus JE, Havlin S, Stanley HE, et al. Scaling and universality in heart rate variability distributions. *Physica A: Statistical Mechanics and its Applications*. 1998; 249(1-4):587–593. [https://doi.org/10.1016/s0378-4371\(97\)00522-0](https://doi.org/10.1016/s0378-4371(97)00522-0) PMID: 11541514
34. Schneider R, Bauer A, Barthel P, Schmidt G. LibRasch: a programming framework for signal handling. In: Institute of Electrical and Electronics Engineers 2004 – Computers in Cardiology; p. 53–56.
35. Schmitt DT, Stein PK, Ivanov PC. Stratification pattern of static and scale-invariant dynamic measures of heartbeat fluctuations across sleep stages in young and elderly. *IEEE Transactions on Bio-Medical Engineering*. 2009; 56(5):1564–1573. <https://doi.org/10.1109/TBME.2009.2014819> PMID: 19203874
36. Hernandez J, McDuff D, Picard R. BioWatch: Estimation of heart and breathing rates from wrist motions. In: Arnrich B, Ersoy C, Dey A, Kunze K, Berthouze N, editors. Proceedings of the 9th International Conference on Pervasive Computing Technologies for Healthcare. ICST; 20.05.2015–23.05.2015.
37. Haescher M, Matthies DJC, Trimpop J, Urban B. A study on measuring heart- and respiration-rate via wrist-worn accelerometer-based seismocardiography (SCG) in comparison to commonly applied technologies. In: Urban B, Kirste T, editors. Proceedings of the 2nd International Workshop on Sensor-based Activity Recognition and Interaction. New York: ACM Press; 2015. p. 1–6.
38. Haescher M, Matthies DJC, Trimpop J, Urban B. SeismoTracker: Upgrade any smart wearable to enable a sensing of heart rate, respiration rate, and microvibrations. In: Kaye J, Druin A, Lampe C, Morris D, Hourcade JP, editors. Proceedings of the 2016 CHI Conference Extended Abstracts on Human Factors in Computing Systems. New York, USA: ACM Press; 2016. p. 2209–2216.
39. Nitzan M, Khanokh B, Slovik Y. The difference in pulse transit time to the toe and finger measured by photoplethysmography. *Physiological Measurement*. 2002; 23(1):85–93. <https://doi.org/10.1088/0967-3334/23/1/308> PMID: 11876244
40. Schumann AY, Bartsch RP, Penzel T, Ivanov PC, Kantelhardt JW. Aging effects on cardiac and respiratory dynamics in healthy subjects across sleep stages. *Sleep*. 2010; 33(7):943–955. <https://doi.org/10.1093/sleep/33.7.943> PMID: 20614854
41. Gesche H, Grosskurth D, Küchler G, Patzak A. Continuous blood pressure measurement by using the pulse transit time: comparison to a cuff-based method. *European Journal of Applied Physiology*. 2012; 112(1):309–315. <https://doi.org/10.1007/s00421-011-1983-3> PMID: 21556814
42. Einbrodt P. Über den Einfluss der Athembewegungen auf Herzschlag und Blutdruck. –: Abhandlungen und Mittheilungen. Sitzungsberichte der Akademie der Wissenschaften mathematisch-naturwissenschaftliche Klasse. 1860;(40):361–418.
43. Hamann C, Bartsch RP, Schumann AY, Penzel T, Havlin S, Kantelhardt JW. Automated synchrogram analysis applied to heartbeat and reconstructed respiration. *Chaos (Woodbury, NY)*. 2009; 19(1):015106. <https://doi.org/10.1063/1.3096415>

3.3 Publication: Respiration reconstruction

About this publication. The publication “Reconstruction of the respiratory signal through ECG and wrist accelerometer data” compares several methods to estimate respiration during sleep. As reference signal for respiration the nasal flow was used. The comparison was mainly based on PSI [67], but also breaths per minute in epochs of 30 seconds were calculated and compared.

First, established ECG features (ECG baseline, amplitude and frequency change) to derive respiration were analyzed, which have been used successfully in the past [68]. Second, respiration movements, extracted from accelerometry data, are investigated. In detail, we used each axis of the accelerometer separately (x , y and z), and derived two angles, ϕ and θ , as combination of the three axis. ϕ corresponds to a rotation of the wrist around the radius-to-ulna axis² and θ represents a turning angle with respect to the elbow. All five channels are pre-filtered to extract the respiration motion and its phase, as indicated in Fig. 3.1 and 3.2.

It can be shown that accelerometry data are more reliable in reconstructing respiration, than the ECG features, with respect to the PSI.

In addition, to see differences between the reconstructions, the PSIs between reconstructed signals were analyzed. The acceleration channels show more similarity between each other than the ECG features.

Comparing the influence of the nocturnal hours, e.g. 1 am to 2 am with 3 am to 4 am, an influence on the reconstruction is barely seen.

In general, the reconstruction of respiration via wrist accelerometry yields promising results and opens new possibilities, while movement artifacts and the restriction to sleep are still limiting factors.

Copyright statement

©2020 Leube *et al.* This publication is licensed under a Creative Commons Attribution 4.0 International (CC BY 4.0) license .

J. Leube, J. Zschocke, M. Kluge, L. Pelikan, A. Graf, M. Glos, A. Müller, R. P. Bartsch, T. Penzel, and J. W. Kantelhardt, „Reconstruction of the respiratory signal through ECG and wrist accelerometer data“, *Scientific Reports*, vol. 10, no. 1, p. 14 530, 2020. DOI: 10.1038/s41598-020-71539-0. Reference [JZ2]

²Rotation around the axis of the forearm.



OPEN

Reconstruction of the respiratory signal through ECG and wrist accelerometer data

Julian Leube¹, Johannes Zschocke^{1,2}, Maria Kluge³, Luise Pelikan³, Antonia Graf³, Martin Glos³, Alexander Müller⁴, Ronny P. Bartsch⁵, Thomas Penzel^{3,6} & Jan W. Kantelhardt¹✉

Respiratory rate and changes in respiratory activity provide important markers of health and fitness. Assessing the breathing signal without direct respiratory sensors can be very helpful in large cohort studies and for screening purposes. In this paper, we demonstrate that long-term nocturnal acceleration measurements from the wrist yield significantly better respiration proxies than four standard approaches of ECG (electrocardiogram) derived respiration. We validate our approach by comparison with flow-derived respiration as standard reference signal, studying the full-night data of 223 subjects in a clinical sleep laboratory. Specifically, we find that phase synchronization indices between respiration proxies and the flow signal are large for five suggested acceleration-derived proxies with $\gamma = 0.55 \pm 0.13$ for males and 0.58 ± 0.14 for females (means \pm standard deviations), while ECG-derived proxies yield only $\gamma = 0.36 \pm 0.16$ for males and 0.39 ± 0.14 for females. Similarly, respiratory rates can be determined more precisely by wrist-worn acceleration devices compared with a derivation from the ECG. As limitation we must mention that acceleration-derived respiration proxies are only available during episodes of non-physical activity (especially during sleep).

There is substantial evidence that deviations of the respiratory rate from its normal behavior can be used as a predictor of clinically relevant and potentially fatal events and conditions (see, e.g., the very recent review paper by Liu et al.¹ and references therein), although the relevance of respiratory rate has long been overlooked in clinical setting² and other fields³. For example, spontaneous breathing rates below six breath per minute (bpm) was prospectively shown to be a stronger predictor of subsequent in-hospital mortality than abnormal heart rate, hypertension or the decrease (or loss) of consciousness⁴. In a very recent study of non-invasive risk assessment for cardiac patients, abnormally high respiratory rate (> 18.6 bpm) and low expiration-triggered sinus arrhythmia turned out to be among the three most sensitive early risk indicators as components of the Polyscore index⁵; previous work also demonstrated the importance of respiratory rate for cardiac patients^{6,7}. Therefore, it is appropriate to include measurements of respiratory rate and the influence of respiration activity on the heart in large cohort studies that aim at identifying early indicators for health risks and to study effects of healthy aging^{8,9}.

Although many methods and technologies for the measurement of respiratory rate and the identification of breathing intervals have been suggested over the past decades^{1,10,11}, there is still a need for inexpensive, reliable, and non-obtrusive sensors. In order to assess respiratory behavior in large epidemiological cohort studies with many thousands of participants from the general population, the handling of the measurement technology should be as easy as possible with a minimum of additional costs. The derivation of respiration proxies from the recordings of devices already used in such studies are thus particularly valuable. An important approach in this regard is exploiting the respiratory modulation of other physiological signals, such as the electrocardiogram (ECG) often registered in long-term (Holter) recordings for 24 h^{1,12–14} or during sleep studies¹⁵. ECG amplitude and baseline as well as frequency are modulated by respiration via motions of the heart axis and respiratory sinus arrhythmia (RSA), respectively, leading to more than a dozen of respiration proxies¹².

¹Institute of Physics, Martin-Luther-University Halle-Wittenberg, 06099 Halle, Germany. ²Institute of Medical Epidemiology, Biostatistics and Informatics, Faculty of Medicine, Martin-Luther-University Halle-Wittenberg, 06099 Halle, Germany. ³Interdisziplinäres Schlafmedizinisches Zentrum, Charité - Universitätsmedizin Berlin, 10117 Berlin, Germany. ⁴Klinik und Poliklinik für Innere Medizin I, Technische Universität München, 81675 Munich, Germany. ⁵Department of Physics, Bar-Ilan University, Ramat Gan 5290002, Israel. ⁶Saratov State University, Saratov, Russia. ✉email: jan.kantelhardt@physik.uni-halle.de

Measure	Description
Acc _x	Wrist acceleration in longitudinal direction (in mg)
Acc _y	Wrist acceleration in lateral direction (in mg)
Acc _z	Wrist acceleration in lateral direction (in mg)
ϑ	rotational angle of the wrist (in rad)
φ	rotational angle of the wrist (in rad)
B1	Average of maximum and minimum of QRS complex (in μV)
B2 (EDR)	Difference of maximum and minimum of QRS complex (in μV)
B3	Duration of RR interval (in ms)
B5	Maximum of QRS complex (in μV)

Table 1. List of respiration proxies considered in this work; see “Methods” section below for the description of the signals and particularly Fig. 6 for wrist acceleration measurements.

Diagnosis	Females	Males
No diagnosed sleep disorder	5	6
Sleep-related breathing disorders (SRBD)	42	69
Insomnia	29	15
Central disorders of hypersomnolence	25	16
Sleep-related movement disorder	20	11
Parasomnias	6	5
Circadian rhythm sleep-wake disorders	0	6
Other sleep disorders	5	7
All subjects	110	113

Table 2. Overview of all subjects included in the analysis. Subjects with multiple diagnoses are counted in each appropriate diagnosis line, i.e., multiple times. The last line reports data for all subjects irrespective of diagnosis.

In addition, similar proxies can be derived from the photoplethysmogram (PPG)^{16,17}, with best signals recorded at the forehead and the finger for normal and deep breathing pattern, respectively¹⁸. In a systematic comparison study, feature-based techniques in the time domain turned out to be generally superior to filter-based techniques and techniques in the frequency domain^{1,12}. In addition, feature-based time-domain techniques facilitate the determination of the individual breathing intervals (instead of a mere breathing rate), and they are more useful for studying the data of patients with possibly irregular breathing (e.g., due to apneas) or extremely low or high breathing rates.

A few approaches tried a fusion of ECG or PPG derived respiration with respiration proxies from accelerometer and gyroscope data^{19–21}. Accelerometer-based methods for measuring breathing-related movements have been roughly validated^{22–24}. However, mainly accelerometers and gyroscopes, appropriately positioned over the diaphragm¹, the dome-shaped skeletal muscle of the thoracic cavity²⁵ (or the chest wall¹¹), as well as the forehead²⁶ have been considered, so that an additional sensor is needed in these efforts.

In this paper we propose and validate an approach for extracting proxy signals for respiratory events from wrist accelerometer data. Wrist accelerometers are often employed in large cohort studies for the purpose of activity/inactivity tracking as well as sleep/wake identification of the subjects. No cables nor obtrusive sensors are needed, since a wrist accelerometer is worn like a common wrist watch. There are a few previous studies on wrist accelerometer data^{10,26,27} that focus on estimating mean respiratory rate using spectral techniques.

Results

Here, we present our results for respiratory proxies derived from wrist accelerometer data. Specifically, we consider the instantaneous respiratory phases and respiratory rates derived from acceleration recorded for all three perpendicular axes (x , y , and z) on the non-dominant arm of 223 subjects. For details, we refer to the “Methods” section and Tables 1 and 2, in particular. In addition to the proxies Acc_x, Acc_y, and Acc_z for the normal axes, we have studied data for the corresponding rotational angles ϑ and φ of the wrists.

In order to relate with previous literature, we compare our results with respiratory proxies derived from ECG recordings. Specifically, we have considered the following four previously established ECG-derived proxies of respiration: averages of maximum and minimum of QRS complex (B1), differences of maximum and minimum of QRS complex [B2, also commonly referred to as ECG-derived respiration (EDR)], duration of RR intervals (B3), and maxima of QRS complex (B5), see also Table 1 and “Methods” section. We have selected these four proxies based on their superior performance in a previous study¹³.

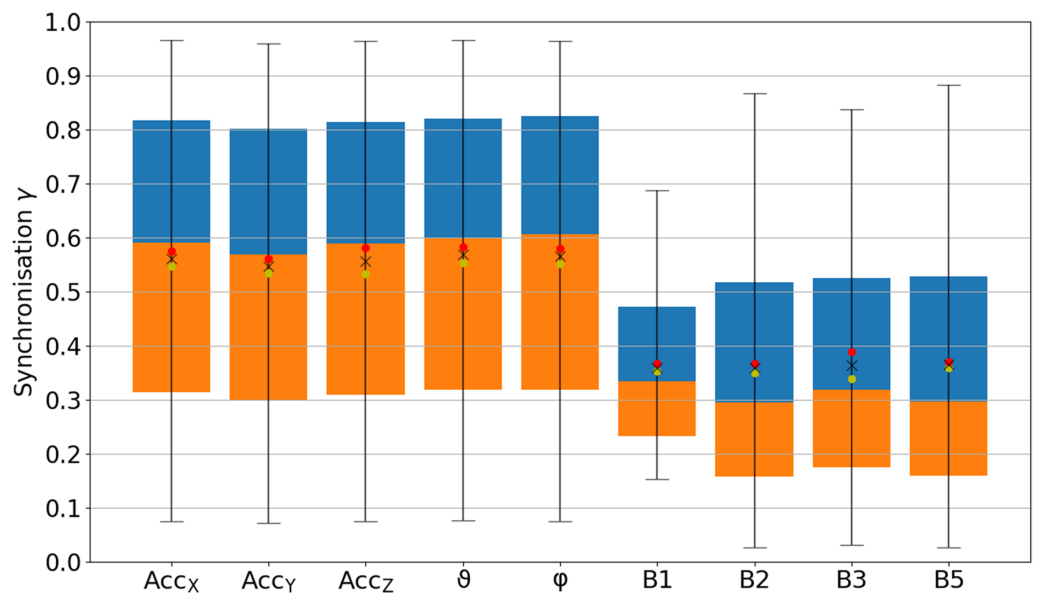


Figure 1. Boxplot of the average synchronization between proxies and measured respiration. Phase synchronization indices γ according to Eq. (5) between all respiration proxies (see Table 1) and the recorded flow signal have been averaged over the complete sleeping period and all 223 subjects (see Table 2). The orange part of each box represents the values between the lower quartile and the median, and the blue part represents the values between the median and the upper quartile. The ends of the whiskers mark the 2.5% quantile and the 97.5% quantile, respectively. The total average values appear as black crosses in the boxplot along with the averages for male (yellow dots) and female (red dots) subjects. According to t-tests, the results for Acc_x , Acc_y , Acc_z , ϑ , and φ were significantly different from all other results ($p < 0.001$), but not significantly different from each other. The same holds for the results regarding the ECG-derived proxies B1, B2, B3 and B5. Differences between males and females were marginally significant ($0.05 > p \geq 0.01$) for Acc_x , Acc_y , φ , ϑ , and B2, and significant ($p < 0.01$) for Acc_z and B3.

Phase synchronization. Figure 1 shows a boxplot of the phase synchronization indices γ [Eq. (5)] for all considered respiration proxies (see Table 1) compared to flow as the respiration standard signal, including the results for all 223 subjects (see Table 2). Although many previous works focused on EDR proxies (see “Methods”), we found that all wrist acceleration proxies perform significantly better (t-tests: $p < 0.001$). The rotational angles φ and ϑ performed best with averages $\gamma = 0.55 \pm 0.13$ (0.58 ± 0.14) and 0.55 ± 0.13 (0.58 ± 0.15) for males (females), respectively (mean \pm standard deviation). Acc_x ($\gamma = 0.55 \pm 0.13$ and 0.58 ± 0.15 for males and females, respectively), Acc_y ($\gamma = 0.53 \pm 0.13$ and 0.56 ± 0.13), and Acc_z ($\gamma = 0.53 \pm 0.13$ and 0.58 ± 0.15) also achieved significantly larger average synchronization indices than each of the ECG-derived proxies. The best ECG proxies were B3 (based on RSA) with $\gamma = 0.34 \pm 0.12$ (0.39 ± 0.14) and B5 with $\gamma = 0.36 \pm 0.12$ (0.37 ± 0.18) for males (females). Differences between males and females were significant for Acc_z ($p < 0.05$) and B3 ($p < 0.01$).

A direct comparison of all subjects with sleep-related breathing disorders (SRBD) and all other subjects yielded similar results for both subgroups, although, in the SRBD subgroup, the γ values were significantly ($p < 0.05$) smaller for all acceleration-derived proxies and even reached $p < 0.01$ for ϑ and Acc_z . ECG-derived proxies B1 and B5 yielded slightly larger γ values in the SRBD subgroup ($p < 0.05$), while differences were not significant for B2 and B3.

Figure 2 shows the mean values of all pairwise synchronization indices γ between the proxies and the flow. Clearly, all acceleration-derived proxies are quite well synchronized to each other. ϑ is very similar to Acc_x , while φ is similar to Acc_y and Acc_z , for example [cp. Eq. (2)]. Many ECG-derived proxies (particularly B1, B2 and B5) are well synchronized with each other, but not so well synchronized with the recorded respiratory flow.

In Fig. 3 the phase synchronization of all proxies to the recorded flow signal is traced for several nocturnal hours with least wakefulness (1:00 am to 5:00 am). Overall, φ and Acc_x yielded the best synchronization, but the differences compared with ϑ , Acc_y , and Acc_z are tiny. It seems that the synchronization of B3 slightly increases with time.

Figure 4 shows the distributions of synchronization indices for all 30 s segments of all recordings. If only ECG-derived proxies were available for the selection, synchronization indices between 0.2 and 0.3 would be most common, and values above 0.9 could rarely be achieved. However, for accelerometer data derived proxies, synchronization indices above 0.9 turned out to be the most frequent. In fact, the distributions of γ values reached if all proxies are considered is not much different from the distribution achieved for acceleration-derived proxies only, except in the regime of $\gamma < 0.2$.

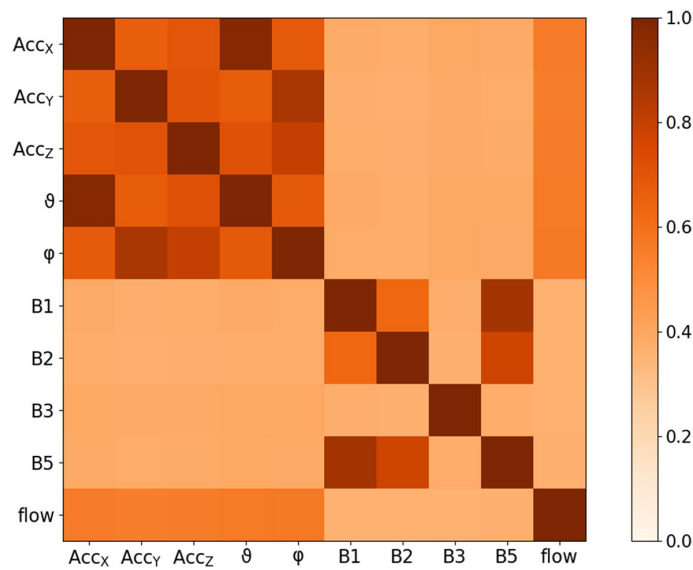


Figure 2. Synchronization matrix. Phase synchronization indices γ according to Eq. (5) between all pairs of respiration proxies (see Table 1) and the flow have been averaged over the complete sleeping period and all 223 subjects. They are presented in a symmetrical color-coded matrix with brown indicating full synchronization and white indicating no synchronization—see color bar on the right.

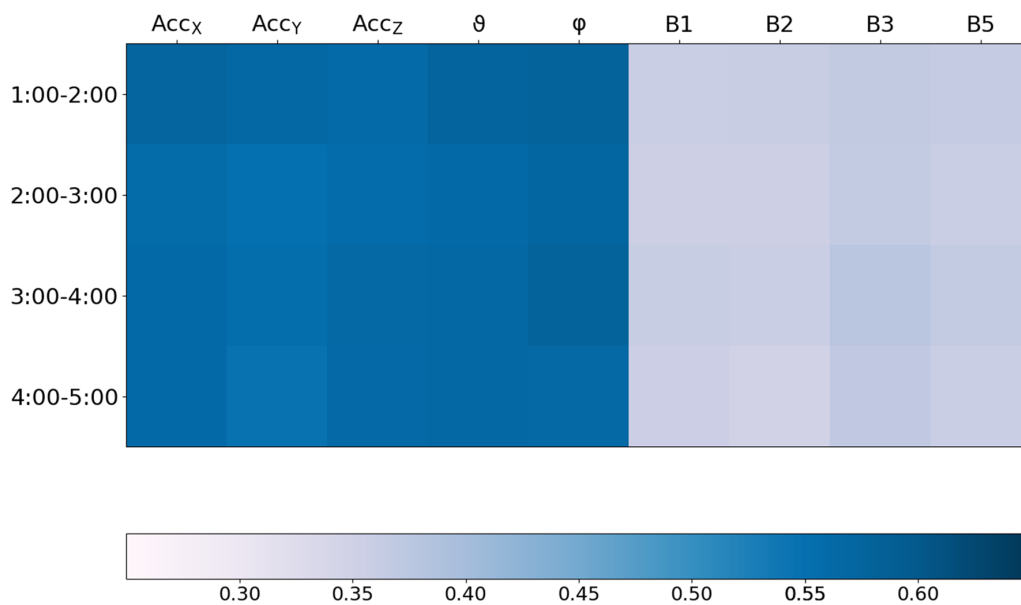


Figure 3. Best synchronization with flow during nocturnal hours. For each respiration proxy (see Table 1), this matrix shows the average phase synchronization index γ with respect to the flow signal (see color bar on the bottom) during the considered nocturnal hour.

Respiratory rates. Figure 5 shows the differences of average respiratory rates derived from all proxies and the recorded flow signal. The acceleration-derived respiratory rates closely agreed with the real respiratory rate with average deviations between -0.38 breaths per minute (bpm, -2.6%) for ϕ and up to $+0.32$ bpm ($+2.1\%$) for the other acceleration-derived proxies. The ECG-derived proxies generally underestimated respiratory rates with average deviations between -3.1 bpm and -1.5 bpm (-21.2 to -10.4%). However, we would like to stress that the estimation of mean respiratory rates is not the main goal of our medically oriented approach, which shall also capture interruptions of respiration (apneas) as well as times with very low and high respiratory rates,

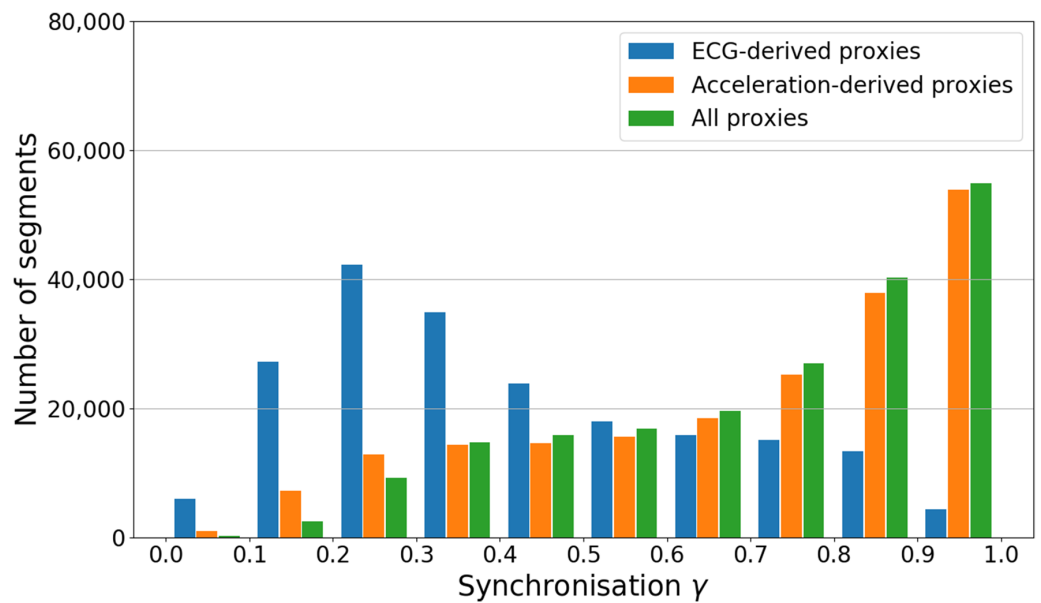


Figure 4. Histogram of best achievable proxy synchronization. The histograms show the numbers of 30 s segments of the total data (all 223 subjects) for which a γ value in the particular interval (0.0 to 0.1, 0.1 to 0.2, etc.) could be achieved taking into account all proxies (green), only acceleration-derived proxies (orange), and only ECG-derived proxies (blue).

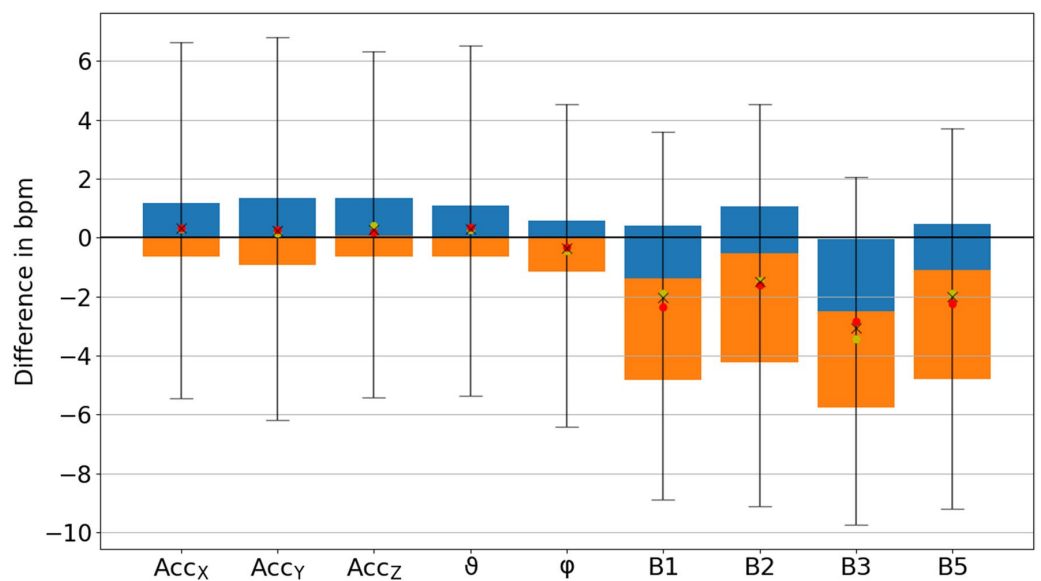


Figure 5. Boxplot of average difference of respiratory rate. The differences of respiratory rates calculated from each respiration proxy and the measured flow signal has been averaged over all 30 s segments and all 223 subjects. The boxes and markers correspond to those in Fig. 1. Note that ϕ yielded a slightly lower respiratory rate (negative difference) than the other acceleration-derived proxies. The results regarding the ECG-derived proxies B1, B2, and B5 were also lower. Differences between males and females were not significant.

i.e., extreme events and respiratory variability. In this respect, we would like to note that significant differences between subjects with and without SRBD (present in the flow signal) could be identified in most acceleration-based proxies (Acc_x, Acc_y, θ , and ϕ) and in B1, but not in B2, B3, or B5.

Discussion

In this paper, we have introduced and validated an approach for obtaining respiration proxies from nocturnal long-term wrist acceleration measurements from 223 clinical subjects including (but not restricted to) patients with various sleep-related disorders. We have shown that each of the suggested five acceleration-derived proxies is significantly ($p < 0.001$) more reliable than each of the four known standard ECG-derived respiration proxies, exploiting ECG baseline, amplitude, and frequency changes.

For comparison, we have considered four established ECG-derived proxies of respiration, B1, B2, B3, and B5, selected because of their superior performance in the study by Charlton et al.¹³, where 15 proxies for a reconstruction of respiratory activity from one-channel ECGs were compared in healthy subjects. Measures B1, B2, and B5 are based on the varying direction of the heart axis during the respiratory cycle, leading to ECG baseline wander (exploited in B1 and B5) and ECG amplitude modulation (exploited in B2 and B5). B2 is also known as ECG-derived respiration (EDR) method and considered in many other studies, see e.g.²⁸ B3 is based on the effects of RSA²⁹ leading to ECG frequency modulation and thus also known as RSA method³⁰. Specifically, in the study of Charlton et al., B2 yielded the highest median subject-specific correlation coefficients (CC) with respiratory activity in both, young and elderly subjects (CC = 0.76 and 0.77, respectively), B5 performed similarly well (CC = 0.74 and 0.76, respectively), and B1 was at the third rank for elderly subjects (CC = 0.72, versus 0.66 in the young). We also included the best frequency modulation based proxy B3 for comparison, although it performed well in young subjects only (CC = 0.66, versus 0.44 in the elderly)¹³.

The variation of phase synchronization values among the subjects was large for the acceleration-derived γ values as indicated by the widths of the box plots and their whiskers in Fig. 1. This is most probably due to multiple possibilities of arm placement of the subjects during sleep. While an arm lying on the chest will lead to an improved respiration proxy, a widely extended arm leads to weaker respiratory movements at the wrist. As expected, the length of the acceleration vector, r , reached a drastically lower phase synchronization index (not shown in Fig. 1), since the magnitude of the gravitational force does not change with respiration. Nevertheless, the directions of this vector in the reference frame of the wrist-fixed recording device change as respiration causes slight repetitive turns of the wrist¹, as exploited in our other accelerometer-derived proxies. While B2 was the best proxy in earlier studies¹³, in our study all ECG-derived respiration proxies yielded similar (not significantly different) results.

The respiratory rate can be determined more exactly by wrist worn acceleration devices. Respiration proxies obtained from the data of all three accelerometer axes using a simple moving average smoothing (Acc_x , Acc_y , Acc_z) as well as the derived rotation angle ϑ turned out to be similarly reliable. Since the derived rotation angle φ yielded a significant deviation in the respiratory rate, we suggest not using it although the approach seemed very promising initially. Based on our data, our recommendation goes to Acc_x and ϑ .

We note that recent work on a BioWatch²⁶ used single-axis wrist accelerometer data in the frequency domain from 0.13 to 0.66 Hz (corresponding to 8 and 40 breaths per minute) to estimate respiratory rates. The technique focused on average breathing rate in intervals of 20 s as determined via spectral analysis, not trying to identify individual breaths, breathing interruptions, or breath-to-breath intervals. Besides that, it was limited to 32 h of sleep data from three subjects and 72 mins of daytime data (sitting, standing and lying without motion) from twelve subjects. Another recent study determined the average respiratory rates in 15 subjects using wrist accelerometer data²⁷, reporting an average deviation of 16.6% with respect to respiratory rate from a chest band. Another paper from the same group reported that respiratory rate can be most reliably estimated via accelerometry, if the sensor is attached to the subjects' torso or shoulders³¹.

As an improvement compared to BioWatch, the recently introduced SleepMonitor¹⁰ exploited wrist accelerometer data recorded at 16 Hz in 30-s windows, fusing the spectrally determined respiratory rates from all three axes and this way obtaining results with errors about half as large as those of BioWatch. Mean absolute errors for the wrist-motion determined respiratory rate as compared with the chest-motion determined rate were 0.72 and 1.08 breaths per minute for normally and disorderedly (either sleep apnea or intentional strong breathing variations) breathing subjects, respectively. The technique, validated with data from 70 nights of 16 subjects (including two subjects with sleep-disordered breathing), included a Kalman filter working with predictions of respiratory rate in addition to FFT filtering and did not try to capture interruptions of respiration (apneas) nor extreme variations of respiratory rates.

Since our approach fully works in the time domain, not involving spectral analysis, it is rather insensitive to non-stationarities of the recorded data and not limited to certain ranges of respiratory rate or requiring smooth changes of respiratory activity. Therefore, not only respiratory rate but also possibly clinically relevant extreme events and interruptions of respiratory activity can be assessed. Although further development, optimization, and validation is necessary before our approach could be clinically applied, we think our method can be used in its current form to derive the respiratory signal from nocturnal accelerometer recordings obtained in large cohort studies. Such cohorts are currently recorded in the framework of, e.g., the UK Biobank study and the German National Cohort (GNC) study.

Limitations. We must certainly mention that acceleration-derived respiration proxies are available during episodes of non-physical activity (especially during sleep) only, while ECG-derived respiration is not limited in this way. We also remark that our approach for using accelerometer data as a respiratory proxy will fail in a zero-gravity environment, e.g. in a space station, since it requires the vertical gravitational direction as reference.

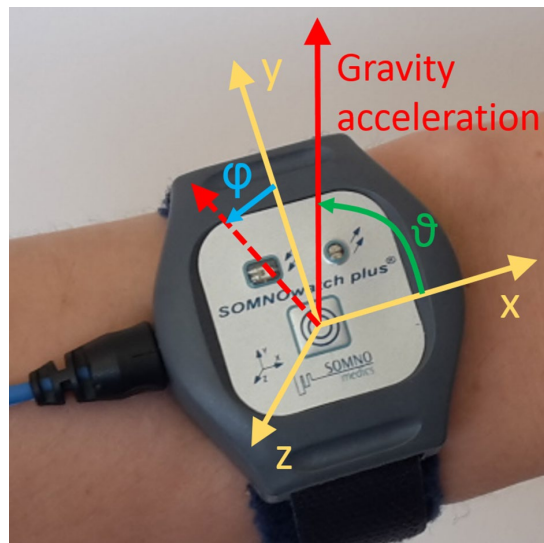


Figure 6. Acceleration recording at the wrist. The photo shows the placement of the SOMNOWatch plus device (Somnomedics GmbH, Randersacker, Germany) at the wrist with the coordinate axes (x , y , and z ; yellow) according to the device's orientation as well as the gravity acceleration vector (red) pointing vertically upwards from the center of the earth. The device measures the three components of the gravity acceleration with respect to its coordinate axes. From this data the two orientational angles, ϑ = angle between x axis and gravity acceleration and φ = angle between y axis and projection of the gravity acceleration into the $y - z$ plane (dashed red vector), can be calculated according to Eq. (3).

Methods

Measurements. All measurements took place in the sleep laboratory of the Charité-Universitätsmedizin Berlin, Germany, between April 2017 and December 2018. The study was approved by the ethics committee of the Charité-Universitätsmedizin Berlin and registered at the German Clinical Trial Register (DRKS) with ID DRKS00016908. All methods were performed in accordance with the relevant guidelines and regulations. In total, 392 subjects were included in the study after signing informed consent. During their first diagnostic night at the sleep laboratory, all subjects wore a SOMNOWatch plus device (Somnomedics GmbH, Randersacker, Germany), recording simultaneously 3d wrist acceleration of the non-dominant arm at 128 Hz sampling rate (see Fig. 6) and a one channel ECG at 256 Hz. Furthermore, full polysomnography (PSG), including recordings of electroencephalography (EEG), electrooculography (EOG), electromyography (EMG), ECG, respiratory flow, etc.) was recorded using either the system Alice (Löwenstein Medical, Bad Ems, Germany), Embla (Embla systems, Broomfield, CO, United States), or SOMNOScreen (Somnomedics GmbH, Randersacker, Germany). For our analysis we used the acceleration and ECG data recorded by SOMNOWatch and the respiratory flow signal recorded by the PSG system.

The measurements of the SOMNOWatch device and the PSG system were synchronized after recording by matching the R peaks of the ECGs recorded by both of them. 145 subjects had to be excluded from further analysis, since reliable synchronization could not be established this way because of poor ECG quality in either of the two recordings. We note that this synchronization method required matching R peaks from the simultaneously recorded ECGs during each 20 minutes of the recordings, since we identified jumps (i.e. unmarked time gaps) in more than 15% of all PSG recordings across all three recording systems; no such gaps occurred in the Somnowatch recordings. In addition, we had to determine and take into account drifts of the recorded time cumulating to typically 1–2 s per night. Another 24 subjects had to be excluded because their respiratory recordings from the SOMNOScreen system could not be successfully exported into the European data format (EDF+) leading to completely or substantially (for more than half of the recording time) missing flow signals. The final 223 subjects, aged between 18 and 78 years (mean 47.9 ± 13.7 years) with average body mass index 27.7 ± 5.7 kg/m², had an average time in bed (TiB) of 7.6 ± 0.8 h. Only data recorded during the lights-off period were considered. All subjects were regular patients of the sleep laboratory with confirmed sleep disorders. In Table 2 we list the frequency of sleep disorders classified by ICSD-3 (International Classification of Sleep Disorders).

Reconstruction of respiratory signals from accelerometry. Our initial observation of a peak in the 0.3 Hz range (corresponding to ≈ 18 breaths per minute) in nocturnal three-axis accelerometry data recorded at the wrist³² was the starting point for our approach towards respiration proxies. After we had found that the high amplitude resolution of modern accelerometers (down to 3 mg ≈ 0.03 m/s²) can resolve tiny motions caused

by respiratory activity^{10,32,33}, we have systematically studied if this effect can be used for a practical derivation of respiration proxies.

The data processing consists of several steps and starts by smoothing the recorded 128 Hz raw acceleration data $\ddot{x}(t)$ by calculating a moving average. Specifically, we calculated a moving average with a window width of ± 0.5 s (i.e., ± 64 data points),

$$\text{Acc}_x(t) = \frac{1}{129} \sum_{j=-64}^{+64} \ddot{x}(t + (j/128\text{Hz})) \quad (1)$$

to obtain smoothened longitudinal acceleration (with the x axis in the direction towards the elbow and the hand, see Fig. 6) as first respiration proxy. Similarly, we obtained smoothened lateral accelerations for the y and z axes oriented perpendicular to x , Acc_y and Acc_z , see Table 1. The window size of 1 s in Eq. (1) was chosen such that there is typically one heartbeat in each window so that effects of heartbeats and pulse wave propagation through the wrist (see also³⁴) are systematically dampened in this moving average procedure. Finally, a resampling to a rate of 4 Hz is applied, since respiration proxies do not need temporal resolutions beyond that.

The red curve in Fig. 7a shows an example for the final respiration proxy determined from y axis accelerometry during sleep. The respiratory cycles can clearly be identified.

We note however, that wrist accelerations caused by respiratory activity are relatively small. In fact, what the acceleration measurement device registers is not an respiration-caused acceleration per se, but instead a slight turning of the wrist in synchrony with the respiratory activity (see also¹). This turning leads to slightly modified projections of the (vertical) gravitational force onto the axes of the coordinate system of the sensor device and thus to slight variations of the x , y and z components of the registered gravitational vector, see Fig. 6. Therefore, one can expect that one or both of the two angles representing the direction of the gravitational vector are even better proxies for respiration than the components in particular directions. Hence, in addition to Acc_x , Acc_y and Acc_z , we consider their angles in spherical coordinates, ϑ (angle between gravity vector and x axis), and φ (angle between projection of gravity vector into the $y-z$ plane and y axis) as shown in gravity vector Fig. 6:

$$\text{Acc}_x = r \cos \vartheta, \text{Acc}_y = r \cos \varphi \sin \vartheta, \text{Acc}_z = r \sin \varphi \sin \vartheta, \quad (2)$$

corresponding to

$$r = \sqrt{\text{Acc}_x^2 + \text{Acc}_y^2 + \text{Acc}_z^2}, \varphi = \arctan_2(\text{Acc}_z, \text{Acc}_y), \vartheta = \arccos(\text{Acc}_x/r), \quad (3)$$

see also Table 1. We have applied the same smoothening [Eq. (1)] and resampling procedure to r , φ , and ϑ as to the acceleration components above. We expect that φ and/or ϑ are much better respiration proxies than r if our assumption regarding changing directional projections of the (constant) gravitational vector holds. Hence, the suggested transformation can facilitate the selection of an optimal proxy.

Finally, instantaneous respiratory phases have been calculated from all respiration proxies as well as the directly registered respiratory signal flow(t) (blue curve in Fig. 7a). The first step in this procedure was the normalization of the time series via (i) subtraction of a moving average similar as in Eq. (1) and (ii) division by a moving standard deviation. Both of these moving quantities have been calculated for windows of ± 5 s duration around the center point, so that effectively frequencies between 0.1 Hz (cutoff by moving average with 10 s window size) and 1 Hz (cutoff by moving average with 1 s window size) remain in the respiration proxies. The resulting narrow-banded signals oscillating around zero can easily be transformed into instantaneous respiratory phases $\phi(t)$ via a Hilbert transform³⁵,

$$x(t) + i\text{HT}[x(t)] = A(t) \exp[i\phi_x(t)], \quad (4)$$

using $\phi_x(t) = \arctan_2(\text{HT}[x(t)], x(t))$ for $x = \text{Acc}_x, \text{Acc}_y, \dots, \text{flow}(t)$. Fig. 7b shows these reconstructed respiratory phases for all signals of Fig. 7a.

In this study we focus on analyzing and comparing instantaneous respiratory phases (instead of respiratory rates or breathing cycles), because the phases comprise all information without the need to define certain points in the breathing cycle, e.g., beginning or ending, transition from inspiration to expiration, etc. Respiratory phases increase continuously from $-\pi \approx -3.14$ to $+\pi$ and then jump back to $-\pi$ in a sawtooth-like pattern, see Fig. 7b. However, since phases are actually defined on a circle, the values of $-\pi$ and $+\pi$ refer to identical phase angles, the selection of the jump point is arbitrary, and constant phase shifts (possibly including multiples of 2π) have no relevance. Therefore, when comparing instantaneous phase signals, their differences are always taken modulo 2π , and constant differences are disregarded. This is advantageous, since proxies derived, e.g., from inverted flow or acceleration (or ECG) signals, leading to phases differing by $+\pi$ or $-\pi$ exactly, will be considered as equivalent. Nevertheless, pauses and flow variations within the respiratory cycle are well reproduced by instantaneous phases as can be seen by the deviations from a straight sawtooth pattern for the flow phases in the bottom panel of Fig. 7b.

Reconstruction of respiratory signals from ECG. To derive measures B1, B2, B3, and B5, the ECG data were processed with the software LibRasch³⁶ to identify QRS complexes. We visually verified and manually checked QRS classifications (normal, ventricular ectopic, and supra-ventricular ectopic) and corrected them if necessary. Noisy parts where no QRS detection was possible were manually marked and excluded from further analysis. All normal QRS complexes were used for B1, B2, and B5, while only time intervals between two successive normal QRS complexes were used for B3. The resulting time series were homogeneously resampled at a rate

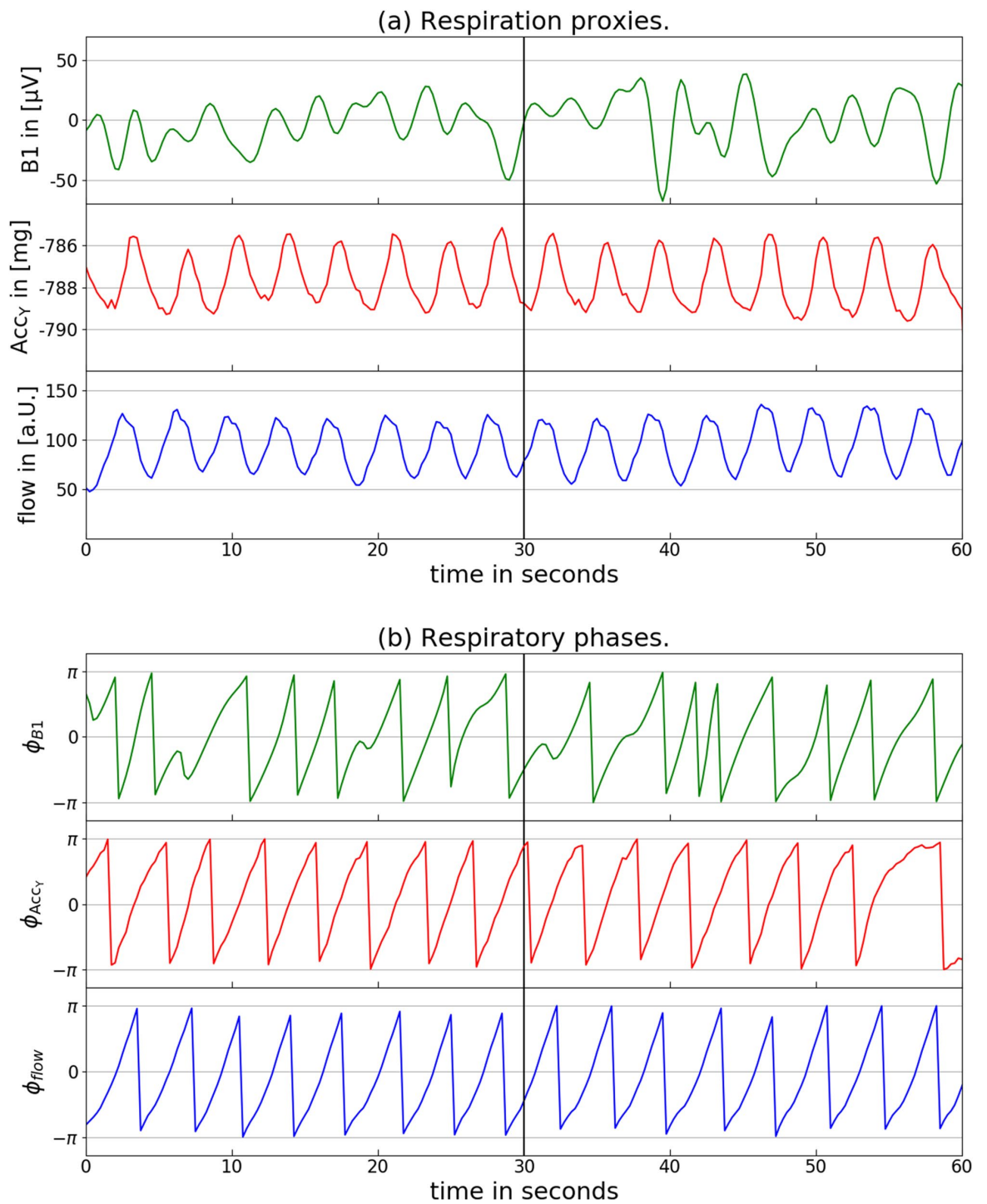


Figure 7. Proxy data and reconstructed respiratory phases. **(a)** Respiration proxies determined from the averages of maximum and minimum of each QRS complex (proxy B1, green) and smoothed lateral y axis acceleration Acc_y (red) recorded at the subjects wrist during sleep. For comparison, the respiratory flow recorded by a separate sensor placed at the subject's nose is also shown (blue). The vertical line at $t = 30$ s marks the window size we have used for our comparisons. **(b)** Corresponding respiratory phases $\phi(t)$ derived from each of the signals shown in part **(a)** via Hilbert transform and Eq. (4).

of 4 Hz by cubic spline interpolation. Subsequently, a FFT band pass filter with limit frequencies 0.01 Hz and 0.5 Hz was applied to eliminate variations clearly outside the respiratory band. As an example, the green curve in Fig. 7a shows the B1 proxy for a typical subject during sleep.

Phase synchronization and comparison of respiratory rates. In order to compare and test two reconstructed respiratory phases $\phi_x(t)$ and $\phi_y(t)$ (for $x, y = \text{Acc}_x, \text{Acc}_y, \dots, \text{flow}(t)$), we calculate the phase synchronization index γ by³⁷

$$\gamma(k) = \left| \langle \exp[i(\phi_x(t) - \phi_y(t))] \rangle \right|, \quad (5)$$

where the average $\langle \dots \rangle$ runs over all times from $t - 15\text{s}$ to $t + 15\text{s}$ with $t = k \cdot 30\text{s}$ and k is the index of the 30 s windows. This definition has the advantage that constant phase differences between the two proxies (and differences by multiples of 2π) as well as changing proxy amplitudes are disregarded. A γ value close to one indicates strong phase synchronization, i.e., a close similarity of the two phase signals, while a γ value close to zero indicates dissimilarity. The approach will be used for comparisons of two proxies as well as comparisons of proxies with the flow signal considered as a reference for real respiration. As examples for the typical values of γ , we note that the first (second) 30-s window of the signals presented in Fig. 7b yields $\gamma = 0.35$ (0.57) for the comparison of EDR (the B1 proxy, green) with the flow (blue), and $\gamma = 0.98$ (0.90) for the comparison of the Acc_y proxy (red) with the flow.

We note that we used respiratory phases derived from the PSG-recorded flow signal as reference without a validation in this study. However, this approach does not lead to any bias regarding the comparison with different respiration proxies, since a corrupted flow signal will not be synchronized with any respiration proxy. Excluding subjects with partly unreliable flow recordings would probably have led to somewhat larger group averages of the phase synchronization index γ for all proxies. But since it would also have led to excluding subjects with nocturnal breathing disorders, we have decided against this. Nevertheless, for a subset of 118 PSG recordings, we compared the flow-derived respiratory phase signal with respiratory phases derived from thorax and abdomen inductive plethysmography by calculating the average synchronization indices according to Eq. (5) for each of the three pairs. Our results of $\gamma = 0.68 \pm 0.19$ (comparison flow versus thorax plethysmography), 0.42 ± 0.33 (flow versus abdomen plethysmography), and 0.45 ± 0.34 (thorax versus abdomen plethysmography) indicate that (i) phase synchronization indices γ in the range from 0.4 to 0.7 indicate good phase synchronization and (ii) flow and thorax inductive plethysmography recordings are probably more reliable than abdomen recordings.

In another approach to compare the respiration proxy signals, we calculated and compared respiratory rates. A breathing interval was defined by jumps of the instantaneous respiratory phase $\phi_x(t)$ from a value above +1 to a value below -1 one time step (0.25 s) later, see Fig. 7b (for $x = \text{Acc}_x, \text{Acc}_y, \dots, \text{flow}(t)$). We calculated the average respiratory rate for each 30 s window, and finally obtained an average respiratory rate of all windows for each respiration proxy and the flow signal. We note that this approach defines the beginning of a breath by the phase jump, however, since we only count number of breaths in large windows of 30 s, different beginnings for different proxies are not relevant.

Since the distributions of both, γ values and respiratory rates, are close to Gaussian, we applied a two-tailed Student's t-test to check for the significance levels of differences between our results for all proxies. In addition, we checked for the significance of differences between two sets of similarly sized subgroups, (i) males and females and (ii) subjects with and without diagnosed sleep apnea syndrome; see Table 2 for the numbers of subjects in these subgroups.

Received: 24 October 2019; Accepted: 10 August 2020

Published online: 03 September 2020

References

- Liu, H., Allen, J., Zheng, D. & Chen, F. Recent development of respiratory rate measurement technologies. *Physiol. Meas.* **40**, 07TR01. <https://doi.org/10.1088/1361-6579/ab299e> (2019).
- Parkes, R. Rate of respiration: the forgotten vital sign. *Emerg. Nurs.* **19**, 12–17. <https://doi.org/10.7748/en2011.05.19.2.12.c8504> (2011).
- Nicolò, A., Massaroni, C. & Passfield, L. Respiratory frequency during exercise: the neglected physiological measure. *Front. Physiol.* **8**, 922. <https://doi.org/10.3389/fphys.2017.00922> (2017).
- Buist, M., Bernard, S., Nguyen, T. Q. T., Moore, G. E. & Anderson, J. N. Association between clinically abnormal observations and subsequent in-hospital mortality: a prospective study. *Resuscitation* **62**, 137–141 (2004).
- Steger, A. *et al.* Polyscore of non-invasive cardiac risk factors. *Front. Physiol.* **10**, 49. <https://doi.org/10.3389/fphys.2019.00049> (2019).
- Barthel, P. *et al.* Respiratory rate predicts outcome after acute myocardial infarction: a prospective cohort study. *Eur. Heart J.* **34**, 1644–1650. <https://doi.org/10.1093/eurheartj/ehs420> (2013).
- Dommasch, M. *et al.* Nocturnal respiratory rate predicts non-sudden cardiac death in survivors of acute myocardial infarction. *J. Am. Coll. Cardiol.* **63**, 2432–2433. <https://doi.org/10.1016/j.jacc.2014.02.525> (2014).
- Schumann, A. Y. *et al.* Aging effects on cardiac and respiratory dynamics in healthy subjects across sleep stages. *Sleep* **33**, 943–955. <https://doi.org/10.1093/sleep/33.7.943> (2010).
- Penzel, T. *et al.* Modulations of heart rate, ECG, and cardio-respiratory coupling observed in polysomnography. *Front. Physiol.* **7**, 460. <https://doi.org/10.3389/fphys.2016.00460> (2016).
- Sun, X., Qiu, L., Wu, Y., Tang, Y. & Cao, G. Sleepmonitor: monitoring respiratory rate and body position during sleep using smartwatch. *Proc. ACM Interact. Mob. Wearable Ubiquitous Technol.* **1**, 1–22. <https://doi.org/10.1145/3130969> (2017).
- Massaroni, C. *et al.* Contact-based methods for measuring respiratory rate. *Sensors* **19**, 908. <https://doi.org/10.3390/s19040908> (2019).
- Charlton, P. H. *et al.* An assessment of algorithms to estimate respiratory rate from the electrocardiogram and photoplethysmogram. *Physiol. Meas.* **37**, 610–626. <https://doi.org/10.1088/0967-3334/37/4/610> (2016).

13. Charlton, P. H. *et al.* Extraction of respiratory signals from the electrocardiogram and photoplethysmogram: technical and physiological determinants. *Physiol. Meas.* **38**, 669–690. <https://doi.org/10.1088/1361-6579/aa670e> (2017).
14. Patil, P. K. Reconstruction of respiratory signal from ECG. *International Research Journal of Engineering and Technology (IRJET)* **10**, 668–72 (2017).
15. Lyons, M. M. *et al.* Screening for obstructive sleep apnea in commercial drivers using ECG-derived respiratory power index. *J. Clin. Sleep Med.* **15**, 23–32. <https://doi.org/10.5664/jcsm.7562> (2019).
16. Karlen, W., Raman, S., Ansermino, M. & Dumont, G. Multiparameter respiratory rate estimation from the photoplethysmogram. *IEEE Trans. Bio-Med. Eng.* **60**, 1946–1953. <https://doi.org/10.1109/TBME.2013.2246160> (2013).
17. Birrenkott, A. D., Pimentel, M. J., Watkinson, P. & Clifton, D. A robust fusion model for estimating respiratory rate from photoplethysmography and electrocardiography. *IEEE Trans. Biomed. Eng.* **65**, 2033–2041. <https://doi.org/10.1109/TBME.2017.2778265> (2017).
18. Hartmann, V. *et al.* Toward accurate extraction of respiratory frequency from the photoplethysmogram: effect of measurement site. *Front. Physiol.* **10**, 732. <https://doi.org/10.3389/fphys.2019.00732> (2019).
19. Liu, G.-Z., Wu, D., Mei, Z.-Y., Zhu, Q.-S. & Wang, L. Automatic detection of respiratory rate from electrocardiogram, respiration induced plethysmography and 3d acceleration signals. *J. Central South Univ.* **20**, 2423–2431. <https://doi.org/10.1007/s11771-013-1752-z> (2013).
20. Jafari Tadi, M., Koivisto, T., Pänkäälä, M. & Paasio, A. Accelerometer-based method for extracting respiratory and cardiac gating information for dual gating during nuclear medicine imaging. *Int. J. Biomed. Imaging* **2014**, 1–11. <https://doi.org/10.1155/2014/690124> (2014).
21. Shen, C.-L. *et al.* respiratory rate estimation by using ECG, impedance, and motion sensing in smart clothing. *J. Med. Biol. Eng.* **37**, 826–842. <https://doi.org/10.1007/s40846-017-0247-z> (2017).
22. Jin, A., Yin, B., Morren, G., Duric, H. & Aarts, R. Performance evaluation of a tri-axial accelerometry-based respiration monitoring for ambient assisted living. In *Proceedings of the 31st Annual International Conference of the IEEE Engineering in Medicine and Biology Society*, 5677–80. <https://doi.org/10.1109/IEMBS.2009.5333116> (Institute of Electrical and Electronics Engineers, 2009).
23. Bates, A., J. Ling, M., Mann, J. & Arvind, D. Respiratory rate and flow waveform estimation from tri-axial accelerometer data. In *2010 International Conference on Body Sensor Networks, BSN 2010*, 144–150. <https://doi.org/10.1109/BSN.2010.50> (2010).
24. Pandia, K., Inan, O. T., Kovacs, G. T. A. & Giovannardi, L. Extracting respiratory information from seismocardiogram signals acquired on the chest using a miniature accelerometer. *Physiol. Meas.* **33**, 1643–1660. <https://doi.org/10.1088/0967-3334/33/10/1643> (2012).
25. Tortora, G. J. & Derrickson, B. *Principles of Anatomy and Physiology* (Wiley, Hoboken, 2000).
26. Hernandez, J., McDuff, D. & Picard, R. Biowatch: estimation of heart and breathing rates from wrist motions. *EAI Endors. Trans. Pervas. Health Technol.* **1**, 3. <https://doi.org/10.4108/icst.pervasivehealth.2015.259064> (2015).
27. Haescher, M., Matthies, D. J. C., Trimpop, J. & Urban, B. A study on measuring heart- and respiration-rate via wrist-worn accelerometer-based seismocardiography (scg) in comparison to commonly applied technologies. In *Proceedings of the 2nd international Workshop on Sensor-based Activity Recognition and Interaction - WOAR '15*. <https://doi.org/10.1145/2790044.2790054> (ACM Press, 2015).
28. Helfenbein, E., Firoozabadi, R., Chien, S., Carlson, E. & Babaeizadeh, S. Development of three methods for extracting respiration from the surface ECG: A review. *J. Electrocardiol.* **47**, 819–825. <https://doi.org/10.1016/j.jelectrocard.2014.07.020> (2014).
29. Bartsch, R. P., Schumann, A. Y., Kantelhardt, J. W., Penzel, T. & Ivanov, P. C. Phase transitions in physiologic coupling. *Proc. Natl. Acad. Sci.* **109**, 10181–10186 (2012).
30. Hamann, C. *et al.* Automated synchrogram analysis applied to heartbeat and reconstructed respiration. *Chaos* **19**, 015106 (2009).
31. Haescher, M., Matthies, D. J., Trimpop, J. & Urban, B. SeismoTracker: upgrade any smart wearable to enable a sensing of heart rate, respiration rate, and microvibrations. In *Proceedings of the 2016 CHI Conference Extended Abstracts on Human Factors in Computing Systems*, 2209–16 (ACM Press, 2016).
32. Wohlfahrt, P. *et al.* Transitions in effective scaling behavior of accelerometric time series across sleep and wake. *EPL (Europhys. Lett.)* **103**, 68002. <https://doi.org/10.1209/0295-5075/103/68002> (2013).
33. Zinkhan, M. & Kantelhardt, J. W. Sleep assessment in large cohort studies with high-resolution accelerometers. *Sleep Med. Clin.* **11**, 469–488. <https://doi.org/10.1016/j.jsmc.2016.08.006> (2016).
34. Zschocke, J. *et al.* Detection and analysis of pulse waves during sleep via wrist-worn actigraphy. *PLoS ONE* **14**, e0226843. <https://doi.org/10.1371/journal.pone.0226843> (2019).
35. Gabor, D. Theory of communication. part 1: The analysis of information. *J. Inst. Electr. Eng.* **III 93**, 429 (1946).
36. Schneider, R., Bauer, A., Barthel, P. & Schmidt, G. LibRasch: a programming framework for signal handling. *Comput. Cardiol.* **53–6**, 2004. <https://doi.org/10.1109/CIC.2004.1442869> (2004).
37. Rosenblum, M., Pikovsky, A., Kurths, J. & Pikovsky, A. Phase synchronization: from theory to data analysis. In: *Handbook of Biological Physics* **279** (2001).

Acknowledgements

We thank Rafael Mikolajczyk for discussions, Livnat Corelenchein-Rozen and Yaopeng Ma for help with data pre-processing, and Niklas Wallstein for calculating the synchronization between flow and respiration from inductive plethysmography as a reference. This study was supported by the German-Israeli Foundation (GIF) Grants I-1298-415.13/2015 and I-1372-303.7/2016 and the German National Cohort study (www.nationalekohorte.de), funded by the Federal Ministry of Education and Research (BMBF) and the Helmholtz Association. TP was partially supported by Russian Federation Government Grant № 075-15-2019-1885. JZ acknowledges support from a Minerva Short-Term Research Grant.

Author contributions

J.L. developed and implemented the data processing methodology, analyzed the data and prepared most of the figures. J.Z. co-supervised the work of J.L. and participated in discussions. M.K., L.P. and A.G. conducted the experiments and data recordings under supervision of M.G. and T.P. A.M. evaluated the ECGs of all subjects and participated in discussions. R.P.B. participated in discussions and helped in writing the manuscript. J.W.K. devised the data analysis, supervised the work of J.L. and J.Z., participated in discussions, and wrote most parts of the manuscript. All authors reviewed the manuscript.

Competing interests

The authors declare no competing interests.

Additional information

Correspondence and requests for materials should be addressed to J.W.K.

Reprints and permissions information is available at www.nature.com/reprints.

Publisher's note Springer Nature remains neutral with regard to jurisdictional claims in published maps and institutional affiliations.



Open Access This article is licensed under a Creative Commons Attribution 4.0 International License, which permits use, sharing, adaptation, distribution and reproduction in any medium or format, as long as you give appropriate credit to the original author(s) and the source, provide a link to the Creative Commons license, and indicate if changes were made. The images or other third party material in this article are included in the article's Creative Commons license, unless indicated otherwise in a credit line to the material. If material is not included in the article's Creative Commons license and your intended use is not permitted by statutory regulation or exceeds the permitted use, you will need to obtain permission directly from the copyright holder. To view a copy of this license, visit <http://creativecommons.org/licenses/by/4.0/>.

© The Author(s) 2020

3.4 Publication: Reconstruction dependencies on sleep stages

About this publication. The final publication of the first part “Reconstruction of the pulse wave and respiration from wrist accelerometer during sleep” combines the results of the previous two publications, and adds a characterization of sleep-stage dependencies. In here, the PSI was applied to compare heart beats and pulse wave peaks derived from accelerometry data, as already done for respiration and its reconstruction from accelerometry in the previous publication, Section 3.3 [JZ2]. In addition, we compare surrogate pulse wave peaks and respiration reconstructions, which results in a PSI below 0.1, describing the lower limit of the PSI. Furthermore, pulse wave peaks from PPG, the gold standard for pulse wave detection, are compared to heart beats, which revealed a PSI above 0.9, the upper limit of PSI under real conditions. Nevertheless the pulse wave reconstruction compared to heart beats yields better PSI (≈ 0.7) than the respiration reconstruction (PSI ≈ 0.6) based on accelerometry.

The main focus is on the reconstruction quality during different sleep stages. As expected, best results are reached during N3, followed by N2, and REM sleep, while PSI drops during episodes of wakefulness.

The investigation of the influences of apneas on the PSI of respiration indicates lower synchronization in subjects with an higher apnea index³. But also during apnea events, the PSI decreases. However, PSI of pulse wave reconstruction is hardly effected by apnea events.

Additionally, we show, that an internal evaluation process of the accelerometer data can improve the quality of reconstruction by identifying epochs of poor quality, due to noise and weak signal power, at the cost of using less data.

Finally, the results of the previous publications are confirmed, and one way to eliminate movement artifacts is demonstrated.

Copyright statement

©2022 IEEE. Reprinted, with permission, from J. Zschocke, J. Leube, M. Glos, O. Semyachkina-Glushkovskaya, T. Penzel, R. Bartsch, and J. Kantelhardt, „Reconstruction of pulse wave and respiration from wrist accelerometer during sleep“, *IEEE Transactions on Bio-Medical Engineering*, vol. 69, no. 2, pp. 830–839, 2022. DOI: 10.1109/TBME.2021.3107978. Reference [JZ3].

In reference to IEEE copyrighted material which is used with permission in this thesis, the IEEE does not endorse any of Martin-Luther-University Halle-Wittenberg’s products or services. Internal or personal use of this material is permitted. If interested in reprinting/republishing IEEE copyrighted material for advertising or promotional purposes or for creating new collective works for resale or redistribution,

³The apnea index or better apnea-hypopnea-index reports the average numbers of apneas (and hypopneas) per hour.

3. PART I: HIDDEN SIGNALS IN ACCELEROMETER DATA

please go to http://www.ieee.org/publications_standards/publications/rights/rights_link.html to learn how to obtain a License from RightsLink. If applicable, University Microfilms and/or ProQuest Library, or the Archives of Canada may supply single copies of the dissertation.

Comment

The reprinted publication is the accepted version and not the final published version, for copyright reasons. Differences affect only the layout. In addition the supplementary material of this publication was added.

Reconstruction of Pulse Wave and Respiration from Wrist Accelerometer During Sleep

Johannes Zschocke, Julian Leube, Martin Glos, Oxana Semyachkina-Glushkovskaya, Thomas Penzel, Ronny P. Bartsch, and Jan W. Kantelhardt

Abstract—Objective: Nocturnal recordings of heart rate and respiratory rate usually require several separate sensors or electrodes attached to different body parts – a disadvantage for at-home screening tests and for large cohort studies. In this paper, we demonstrate that a state-of-the-art accelerometer placed at subjects' wrists can be used to derive reliable signal reconstructions of heartbeat (pulse wave intervals) and respiration during sleep. **Methods:** Based on 226 full-night recordings, we evaluate the performance of our signal reconstruction methodology with respect to polysomnography. We use a phase synchronization analysis metrics that considers individual heartbeats or breaths. **Results:** The quantitative comparison reveals that pulse-wave signal reconstructions are generally better than respiratory signal reconstructions. The best quality is achieved during deep sleep, followed by light sleep N2 and REM sleep. In addition, a suggested internal evaluation of multiple derived reconstructions can be used to identify time periods with highly reliable signals, particularly for pulse waves. Furthermore, we find that pulse-wave reconstructions are hardly affected by apnea and hypopnea events. **Conclusion:** During sleep, pulse wave and respiration signals can simultaneously be reconstructed from the same accelerometer recording at the wrist without the need for additional sensors. Reliability can be increased by internal evaluation if the reconstructed signals are not needed for the whole sleep duration. **Significance:** The presented methodology can help to determine sleep characteristics and improve diagnostics and treatment of sleep disorders in the subjects' normal sleep environment.

Index Terms—Accelerometers, Biomedical monitoring, Signal reconstruction, Pulse waves, Respiration, Time series analysis, Sleep stages, Sleep apnea

I. INTRODUCTION

SLEEP disturbances are associated with impaired health and well-being, reduced performance and higher risk of adverse events and accidents [1]–[5]. Specifically, there is evidence of a link between insomnia, sleep apnea, or unusually short or long total sleep durations and risk factors for major cardiovascular diseases, morbidity, and mortality [6]–[8]. However, the explanatory value of many such studies is limited because of restrictions in the study designs, or limitations in the methods used for the assessment. Therefore, it is premature to infer causal relationships from the current body of literature. Additional large prospective studies thus have to address sleep characteristics as possible determinants of personal health in more differentiated ways in large subject populations [9].

Although cardiorespiratory polysomnography (PSG) has been regarded as the gold standard in sleep medicine since 1968 [10], [11], its intricacy and costs disallow studying very large subject populations. Beyond that, PSG may produce first-night effects and may lead to a selection bias [12]–[14]. As an alternative to PSG, movement-based methods, such as actigraphy (or accelerometry), have been established since 1974 [15], [16]. Advantages of accelerometry over PSG are described as lower costs, higher availability, easy recording of multiple nights, and lower influence on natural sleep [17]–[20]. However, the full potential of modern accelerometers with long-term three-axis recordings at sampling rates above 100 Hz and acceleration resolutions of just a few milli-g^1 , i.e., a few thousandth of the gravitational acceleration on earth, still needs to be explored [9].

In this paper we describe and evaluate procedures for deriving reconstructions of cardiac dynamics (through the reconstruction of the pulse wave signal) and respiratory activity from wrist accelerometer data. While we have already introduced the overall methodological approaches in two previous publications [21], [22], this study is the first systematic evaluation that takes into account sleep architecture, i.e., different sleep stages and sleep disorders such as sleep apnea. Based on 226 full-night recordings from typical patients of a clinical sleep laboratory, we characterize the reliability of

Submitted: 26.04.2021. This work was supported in part by German Israeli Foundation (GIF) Grant No I-1372-303.7/2016, by the German National Cohort (GNC) (www.nako.de), funded by the Federal Ministry of Education and Research (BMBF) and the Helmholtz Association, and by the Russian Federation Government Grant No 075-15-2019-1885.

J. Zschocke is with the Institute of Medical Epidemiology, Biometrics and Informatics (IMEBI) Interdisciplinary Center for Health Sciences and the Institute of Physics, Martin-Luther University Halle-Wittenberg, Halle (Saale), Germany (johannes.zschocke@physik.uni-halle.de).

L. Leube is with the Department of Nuclear Medicine, University of Würzburg, Würzburg, Germany, and was with the Institute of Physics, Martin-Luther University Halle-Wittenberg, Halle (Saale), Germany (leube.j@ukw.de).

M. Glos is with the Interdisciplinary Sleep Medicine Center, Charité - Universitätsmedizin Berlin, Berlin, Germany (martin.glos@charite.de).

O. Semyachkina-Glushkovskaya is with the Saratov State University, Saratov, Russia (glushkovskaya@mail.ru).

T. Penzel is with the Interdisciplinary Sleep Medicine Center, Charité - Universitätsmedizin Berlin, Berlin, Germany and the Saratov State University, Saratov, Russia (thomas.penzel@charite.de).

R. P. Bartsch is with the Department of Physics, Bar-Ilan University, Ramat Gan, Israel (bartsch.ronny@gmail.com).

J. W. Kantelhardt is with the Institute of Physics, Martin-Luther University Halle-Wittenberg, Halle (Saale), Germany (jan.kantelhardt@physik.uni-halle.de).

¹In this paper we use g as gravitational acceleration of 9.81 m/s^2 .

our pulse wave signal reconstructions and respiration signal reconstructions by means of a phase synchronization analysis that quantifies the similarity of the reconstructed data with reference heartbeat (RR) and respiratory flow data as recorded by PSG.

The paper is organized as follows. In Section II we describe our study population, the data recordings, and the data pre-processing, followed by our techniques for calculating pulse wave reconstructions and respiratory reconstructions from the same wrist acceleration time series. We also describe the phase synchronization analysis technique we use to quantify the similarity of the reconstructed signals with the recorded reference signals as well as our surrogate data analysis for statistical testing. The results are presented in Section III, including an additional suggestion for internal evaluation of the reconstructed data to identify temporal periods and channels with particularly reliable data. The paper concludes with discussion and outlook presented in Section IV. Some technical details regarding the synchronization of time series data from different recording devices and reconstruction techniques are reported in the supplementary material to facilitate other implementations of our ideas.

II. DATA AND METHODS

A. Data

We analyzed single night data from 226 subjects recorded in clinical sleep laboratories at the Charité-Universitätsmedizin Berlin, Germany, between April 2017 and March 2019. The study was approved by the ethics committee of the Charité-Universitätsmedizin Berlin and registered at the German Clinical Trial Register (DRKS) with ID DRKS00016908. All enrolled subjects gave written informed consent prior to the study. During their first diagnostic night at the sleep laboratory, all subjects wore a SOMNOWatch™ plus device (SOMNOmedics, Randersacker, Germany), recording simultaneously 3d wrist acceleration of the nondominant arm at 128 Hz sampling rate as well as one channel electrocardiogram (ECG) at 256 Hz. For this purpose, a thin cable leading to three electrodes placed below each collarbone and above the fifth intercostal space of the left side of the body is attached to the watch-like device worn at the wrist of the non-dominant hand. A picture of the device is shown in the online supplementary material. Furthermore, full polysomnography (PSG) (including electroencephalography (EEG), electrooculography (EOG), electromyography (EMG), ECG, photoplethysmogram (PPG), oxygen saturation, respiratory effort, etc.) was recorded using either an ALICE (Philips, Amsterdam, Netherlands), an Embla® (Natus, Pleasanton, USA), or a SOMNOscreen™ PSG system (SOMNOmedics, Randersacker, Germany).

Since accelerometry was recorded only by SOMNOWatch™, while sleep stages and reference respiratory activity were available only from the PSG systems, as initial step we had to establish synchronization between the recording devices. This turned out more intricate than expected because the clocks of the devices drifted with respect to each other by several seconds throughout the night, and brief interruptions occurred in the PSG recordings. However, since all devices

recorded ECGs, a one-to-one matching of the R-peak positions was used for establishing synchronization, see the supplementary material for details. Due to insufficient ECG quality mainly in the PSG systems' data, this procedure was unsuccessful for 105 subjects (i.e., recording nights), reducing the number of available data correspondingly. Another 108 subjects had to be excluded because of noisy or corrupt respiration recordings. Therefore, only 226 out of the original 439 data sets were available for analysis. To show that no bias was introduced this way, we have compared many clinical and sleep-related parameters for the 226 data sets we used and the 213 we excluded, see Table II in the supplementary material. The final used data set consists of single-night recordings of 109 female and 117 male participants with body mass index 27.9 ± 5.7 [17.0, 51.5] kg/m², age 48.6 ± 13.9 [18.1, 78.4] years, and time in bed 7.6 ± 0.8 [5.4, 10.2] hours (mean \pm standard deviation [minimum, maximum]). Each measurement was cropped to only contain data between the 'lights off' and 'lights on' time stamps, indicating beginning and end of the sleep opportunity period, respectively.

B. Overview of Previous Works for Reconstructing Cardiac and Respiratory Activity from Acceleration Sensor Data

In seismocardiography, acceleration sensors placed on the chest wall measure the vibrations caused by heartbeats [23]. In recent years, this technique became more relevant due to better accelerometers [24], [25]; it has also been used to assess respiratory activity [26], [27]. Besides respiration (< 1 Hz), low frequency (0.6 to 5 Hz) chest wall motions caused by heart muscle contraction and high frequency (> 5 Hz) chest wall vibrations related with acoustic waves of the valve closing are measured [26], [28]. In ballistocardiography whole body motions (or vibrations) caused by the heart (and respiration) are measured. Sensors are commonly placed on the bed [24], [29], [30], a recliner chair [31] or a vehicle seat [32]. Accelerometer-based methods for measuring breathing-related movements have been roughly validated [26], but mainly accelerometers and gyroscopes positioned over the diaphragm [33], the chest wall [34] or the forehead [35], [36] have been considered. The latter two publications also used wrist accelerometry to estimate heart rates and respiratory rates. However, they focused on average rates in 20 s intervals as determined via spectral analysis, not trying to identify individual heartbeats or breaths, and were limited to 32 h of sleep data from three subjects plus daytime data. Another paper reported that heart rate can most reliably be estimated via accelerometry, if the sensor is attached to the subjects' upper forearm or the subjects' belly [37]. A recent study [38] also considered a sensor placement on the upper arm, together with a sensor at the foot and finger plethysmography, studying data recorded during standing and hemodynamic interventions.

C. Reconstruction of Pulse Wave Signals from Wrist Accelerometer Data

Pulse waves transversing the wrist initiate damped vibrations of the tissue at frequencies around 8 Hz [9], [42]. These

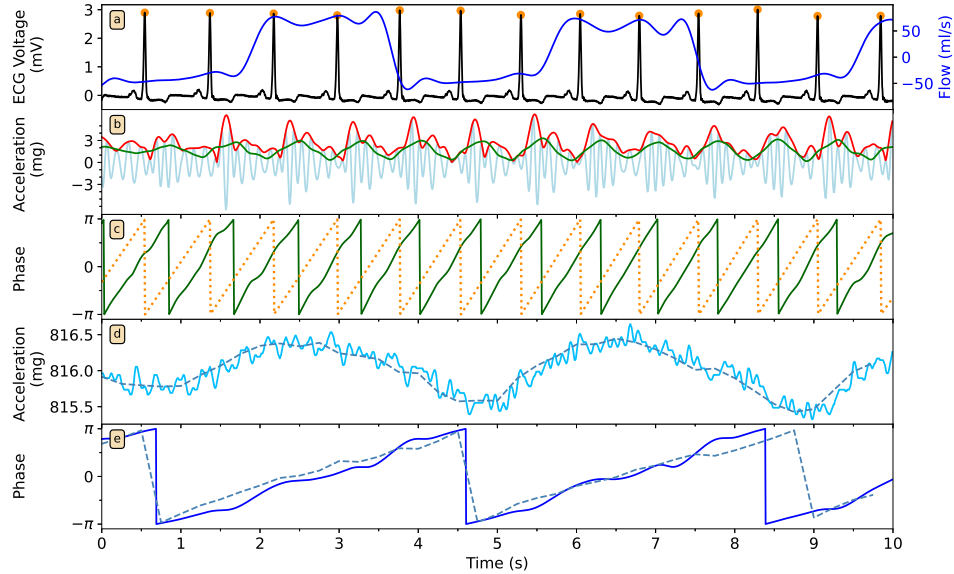


Fig. 1. Signal processing procedure as demonstrated for an epoch of 10 seconds of data for a typical subject. (a) In the ECG signal (black curve) recorded by the SOMNOWatch™ device, R-peaks are marked by orange dots. The respiration flow signal recorded simultaneously by the PSG system is shown in blue. (b) By passing through the wrist, pulse pressure waves cause tiny high frequency vibrations that can be measured by an accelerometer. The light blue curve depicts these vibrations for the y axis after 5-14 Hz bandpass filtering. The envelope of this signal (red curve), as derived by the analytic signal approach [39], [40], shows one high peak and several smaller peaks after each heartbeat, representing the main pulse pressure wave as well as its reflections. These reflections are erased by a smoothing procedure, which results in our pulse wave reconstruction (green curve). (c) The instantaneous phase of the oscillating pulse wave reconstruction (green curve) is plotted together with the ECG phase (dotted orange curve) that is obtained by linear interpolation between the R-peaks (“Poincaré method” [41]). (d) The respiratory activity signal is derived from the same y axis wrist accelerometer recording as used in (b) by applying a one-second moving average filter (light blue curve). The respiration reconstruction (dashed blue curve) is obtained by further smoothing and down sampling. Panel (e) shows the instantaneous respiratory phases derived from the flow signal (from panel (a), solid blue curve) and from the processed accelerometer signal (from panel (d), dashed blue curve).

fast oscillations are slightly but sufficiently above the detection threshold of the wrist accelerometer (at $\approx 3\text{mg} \approx 0.003\text{m/s}^2$; the accelerometer digitizes at a resolution of 12 bit for the range $-6g$ to $+6g$)². In the field of radio telecommunication, the high frequency tissue vibration would represent a carrier frequency, which is amplitude-modulated by the pulse wave. Therefore, after bandpass filtering in the range of 5 to 14 Hz, the registered acceleration signal appears like an amplitude modulated carrier frequency (light blue curve in Fig. 1 (b)). The instantaneous amplitudes of the carrier are obtained by calculating its Hilbert transform, constructing the analytic signal [39], [40] and taking the absolute value (red curve in Fig. 1(b)). This envelope signal is modulated by systolic and diastolic pressure changes as well as reflections of the pulse wave coming back from the hand. After applying a suitable smoothing procedure (see [21] and supplementary material), we obtain a reconstruction for the systolic pulse wave (green curve in Fig. 1 (b)).

We apply the same signal processing procedure to all three recording axes (x , y , z) of the accelerometer to obtain the

acceleration-based pulse wave signal reconstructions A_x^{PW} , A_y^{PW} , and A_z^{PW} . To take into account that combinations of the three acceleration axes could improve our results, we derive two additional pulse wave signal reconstructions A_ϕ^{PW} and A_θ^{PW} for the wrist rotation angles ϕ , rotation around the lower arm, and θ , turning angle with respect to the elbow (see supplementary material for more details).

D. Reconstruction of Respiration Signals from Wrist Accelerometer Data

Respiratory activity causes tiny periodic turns of the wrist, which can be detected via high-resolution accelerometer recordings [9], [22], [42], because the projection of the gravitational (vertical) direction on the recording axes changes periodically with the breathing cycle. Since modulations of the acceleration signal caused by respiratory activity are slower compared to pulse wave modulations, a moving average over intervals of one second is applied to the raw acceleration data for preprocessing (Fig. 1 (d) (light blue curve)), followed by downsampling to 4 Hz (Fig. 1 (d) (blue dotted curve)). The rotational angles ϕ and θ are also derived. Further smooth-

²Corresponding to the technical details of a SOMNOWatch™.

ing procedures lead to the respiration signal reconstructions A_x^{RESP} , A_y^{RESP} , A_z^{RESP} , A_ϕ^{RESP} , and A_θ^{RESP} (see supplementary material for more details).

E. Comparison between Reconstructed Signals and Reference Signals

We evaluate the quality of the five pulse wave signal reconstructions and the five respiration signal reconstructions by systematically comparing them to the ECG and respiratory flow signal, respectively. To this end, we need to take into account that there is a small variable time delay between the contraction of the ventricular muscles (as registered by the R-peak in the ECG) and the pulse wave measured at the wrist. This time delay corresponds to the pulse transit time and is the reason for the few hundred milliseconds long shift between R-peaks in the ECG and the pulse wave signal reconstructions (compare R-peak positions and maxima of A_y^{PW} in Fig. 1 (a) (red curve) and (b) (black curve) and the phase shift in (c)). In addition, respiratory activity derived from wrist motion is also likely to be phase shifted with respect to the respiratory flow, because variations of the wrist angles can either be in synchrony with the maxima or the minima of the lung volume. Hence, the quality of the signal reconstructions can be best evaluated by studying the *stability* of the time or phase delays or differences between reconstructions and their corresponding reference signals. Looking at phases instead of the signals themselves has the additional advantage of independence from the signals' amplitude, which is likely to fluctuate throughout the night due to different arm and wrist positions as well as varying positions of the recording device at the wrist. In addition, a comparison based on phases takes into account the full information in the signals' cycles and not just one data point from each cycle as for an event synchronization [43] or coordination [44] approach. This leads to more reliable statistics.

Instantaneous phases of the signal reconstruction have been obtained by means of a Hilbert transform and the analytic signal approach [39], [40] (see supplementary material for more details) and are shown in Fig. 1 (c) and (e) for pulse waves and respiratory activity, respectively. In order to derive an instantaneous phase from the ECG, we have performed a linear interpolation between the R-peaks ("Poincaré method" [41]). The R-peak-derived reference phase signal φ^{ECG} has thus sawtooth shape with jumps from $+\pi$ to $-\pi$ at the time positions of the R-peaks (orange dotted curve in Fig. 1 (c)). This signal is similar to the phase signal φ_y^{PW} derived from the reconstruction A_y^{PW} (green curve in Fig. 1 (c)), however, φ_y^{PW} does not have a constant slope from $-\pi$ to $+\pi$ and the phase jumps from $+\pi$ to $-\pi$ occur at shifted temporal positions relative to φ^{ECG} (due to the pulse transit time).

The temporal stability of a phase shift is quantified by phase synchronization indices (PSIs) [41]. A particular PSI can be calculated from pairs of phase signals, e.g., φ_y^{PW} and φ^{ECG} , by averaging complex exponentials of the phase difference over time epochs of duration T and taking the absolute value

of the complex result [45],

$$\gamma_y^{PW}(t_0) = \left| \frac{1}{T} \int_{t_0}^{t_0+T} \exp[i\varphi_y^{PW}(t) - i\varphi^{ECG}(t)] dt \right|. \quad (1)$$

Here, i denotes the imaginary unit, and the integration turns into a sum for time series with a specific sampling rate. Equation (1) further shows that the PSI γ is not affected by a constant phase shift $\Delta\varphi$ since the exponential of an imaginary constant, $\exp(i\Delta\varphi)$, has an absolute value of one. Choosing time windows of $T = 30$ seconds duration, we obtain PSI values γ^{PW} for each epoch of 30 seconds and each of the five acceleration-derived pulse wave reconstructions, A_x^{PW} , A_y^{PW} , A_z^{PW} , A_ϕ^{PW} , and A_θ^{PW} .

The same approach is used for comparing the acceleration-derived respiratory reconstructions A_x^{RESP} , A_y^{RESP} , A_z^{RESP} , A_ϕ^{RESP} , and A_θ^{RESP} to the respiratory flow signal (Fig. 1 (a) (blue curve)). Fig. 1 (e) shows an example for the instantaneous respiratory phases φ^{FLOW} derived from the flow signal (solid blue curve) and the processed y axis accelerometer signal φ_y^{RESP} (dashed blue curve). We refer to the supplementary material for more details on reconstruction and phase computation.

F. Surrogate Data Testing

In order to probe the significance of our PSI results, we have performed two types of surrogate data tests. In the first test, the reference phases φ^{ECG} and φ^{FLOW} are replaced by surrogate phases created by inverting the time direction of the corresponding ECG and flow recordings. The results will show the level of PSI for unsynchronized data, i.e., the lower limit for relevant PSI values.

In the second surrogate test, we have replaced the reconstructed phases by phases φ^{PPG} derived from the PSGs PPG measured at the finger tips for a subgroup of 134 subjects. Since the PPG is assumed to represent the real pulse wave activity, this approach will yield an upper limit for PSI values, i.e., the PSI values that could be expected for optimal pulse wave reconstructions. Instantaneous pulse wave phases are derived from the PPG by the same filtering and smoothing procedure as was used for the acceleration-based pulse wave reconstructions.

III. RESULTS

A. Time-Dependent and Average Phase Synchronization Index

Fig. 2 shows examples of PSI results for full nocturnal measurements of two subjects. For each epoch of 30 seconds, the quality of pulse wave reconstructions and respiratory reconstructions is indicated by γ_j^{PW} (Fig. 2 (orange curves)) and γ_j^{RESP} (Fig. 2 (purple curves)), considering different accelerometer axes and angles $j = x, y, z, \theta$ for the reconstructions. While reconstruction of pulse wave signals works very well, as indicated by γ_j^{PW} values close to one (i.e., perfect phase synchronization), respiratory reconstructions exhibit episodes of acceptable ($\gamma_j^{RESP} \geq 0.5$) as well as non-acceptable ($\gamma_j^{RESP} < 0.5$) quality. For example, for the time

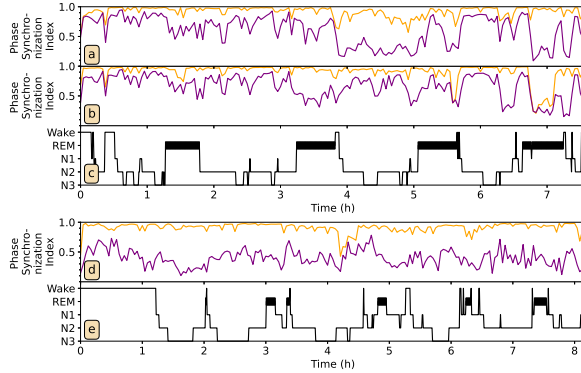


Fig. 2. Phase synchronization indices (PSIs) for whole-night recordings of two subjects. (a-c) For the first subject, PSIs of two pulse wave reconstructions, (a) γ_x^{PW} and (b) γ_z^{PW} (orange curves) show good reconstruction quality except for around 7 h after lights-off for γ_z^{PW} . The quality of the respiratory reconstructions, (a) γ_x^{RESP} , (b) γ_z^{RESP} (purple curves) is mixed, since PSI curves frequently drop to low values in the second half of the night. A complementary behavior of γ_x^{RESP} and γ_z^{RESP} in the period between 3 h and 5 h after lights-off (i.e., low values of γ_z^{RESP} vs. higher values in γ_x^{RESP} between 3 h and 4 h and high values of γ_z^{RESP} vs. low values γ_x^{RESP} between 4 h and 5 h) could indicate rearrangement of the arm or wrist during this period. The hypnogram for this subject with hypersomnolence is shown in (c). (d-e) For the second subject, the quality of the pulse wave reconstruction γ_y^{PW} (orange) is very good for almost the entire night, while the respiratory reconstruction γ_θ^{RESP} yields only low PSI values. Panel (e) shows the hypnogram for this subject with a circadian rhythm sleep-wake disorder.

window from 3 to 5 h after lights-off in Fig. 2 (a), (b) and for long periods of the time in Fig. 2 (d) the respiratory signal can not be sufficiently reconstructed. Sometimes the reconstruction from one axis is clearly superior to the reconstruction from another axis (cp. much larger values of γ_x^{PW} in Fig. 2 (a) than γ_z^{PW} in (b) at around 7 h after lights-off).

There seems to be no obvious relationship between reconstruction quality and sleep stages throughout the night as indicated by the hypnograms in panels Fig. 2 (c) and (e) for each subject. However, as expected, PSI values are dropping during wake episodes, see e.g. Fig. 2 (a) and (b) at times 3.9 h and 5.6 h. Furthermore, arm placement seems to be more important for respiration detection via wrist acceleration than for pulse wave detection.

Fig. 3 summarizes the PSI results for all 226 subjects. Averaging over all 30 second epochs during the night, an average PSI value has been calculated for each subject and each type of reconstruction. The box plots show mean, median, quartiles and 2.5 percent whiskers for the corresponding distributions of 226 PSI values in each case. One can see in Fig. 3 (a) that γ_y^{PW} and γ_ϕ^{PW} yield a slightly better synchronization with the ECG-derived instantaneous phase (mean values ≈ 0.70) as compared to γ_x^{PW} , γ_z^{PW} , and γ_θ^{PW} (mean values ≈ 0.67). The whiskers typically range from PSI values of 0.42 for the subjects with worst reconstruction quality to 0.85 for the subjects with best reconstruction quality. Regarding respiratory reconstructions, Fig. 3 (c) shows that most PSI values are in the range of 0.5 to 0.6. Here, the results derived from the wrist rotation angles are slightly better.

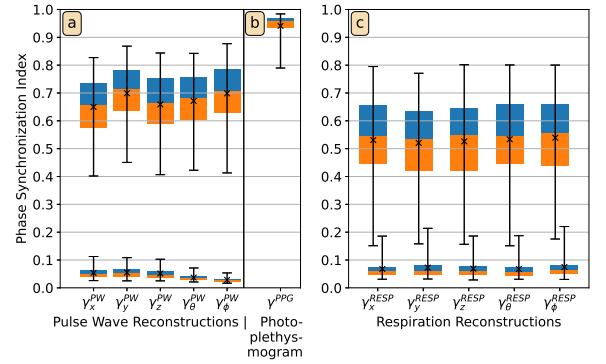


Fig. 3. Box plots of phase synchronization indices between acceleration-based reconstructions and ECG signal or respiration signal averaged across subjects. Results for pulse wave reconstructions and respiratory reconstructions are shown in (a) and (c), respectively. For each reconstruction, the orange part represents the values between the lower quartile and the median, and the blue part represents the values between median and upper quartile. Whiskers mark the 2.5% and the 97.5% quantile of the distributions among the 226 subjects. The average values appear as black crosses within the box plot. Box plots on the bottom of the figure summarize the results of the surrogate analysis utilizing time inverted data (see Section II-F). In addition, the results for optimally synchronized pulse wave data based on the PPG are shown in (b). In general, pulse wave reconstructions yield up to 20% higher PSI values than respiratory reconstructions, and A_y^{PW} and A_θ^{RESP} perform slightly better than other signals to reconstruct pulse wave and respiration signal, respectively.

We note that the existence of different superior channels, i.e., y axis for pulse wave and rotation angle θ for respiration reconstruction is not surprising. While pulse waves crossing the wrist cause small internal wrist vibrations that are most pronounced perpendicular to the axis of wave propagation, respiration leads to changes of wrist orientation (i.e., wrist rotation). In fact, respiratory activity causes wrist movements only 'externally' via the arm or due to wrist placement next to the upper body. In this sense, it becomes clear why the quality of respiratory reconstructions is more variable throughout the night (Fig. 2) and their overall PSI values are lower than for pulse wave reconstructions.

In order to probe the significance of the PSI values calculated for pulse wave and respiratory reconstructions, Fig. 3 also includes PSI values for unsynchronized data (inverted time direction) and optimally synchronized pulse wave data using the PPG (see Section II-F for details). The corresponding box plots indicate that 97.5 percent of the 30-second epochs of surrogate data yield PSI values below 0.11 for pulse waves (Fig. 3 (a)) and 0.21 for respiration (Fig. 3 (c)). In contrast, optimally synchronized pulse waves derived from the PPG yield an average PSI value of 0.94 ± 0.06 (Fig. 3 (b)).

B. Sleep-Stage Dependent Synchronization

As shown in Fig. 2, the quality of pulse wave and respiration reconstructions may drop during nocturnal arousals and brief awakenings due to changes in neuronal characteristics [46]. To investigate systematically the reliability of our pulse wave and respiration reconstructions throughout the night, we calculate PSI values separately for each sleep stage taking into account

TABLE I
AVERAGE PULSE WAVE AND RESPIRATION PHASE SYNCHRONIZATION INDICES SORTED BY RECONSTRUCTION SIGNAL AND SLEEP STAGE

	γ_x^{PW}	γ_y^{PW}	γ_z^{PW}	γ_θ^{PW}	γ_ϕ^{PW}	γ_x^{RESP}	γ_y^{RESP}	γ_z^{RESP}	γ_θ^{RESP}	γ_ϕ^{RESP}	# of epochs
all	0.65	0.70	0.66	0.67	0.70	0.53	0.52	0.53	0.54	0.54	189,635
Wake	0.50	0.53	0.50	0.52	0.54	0.40	0.38	0.39	0.40	0.38	25,849
REM	0.67	0.72	0.67	0.69	0.71	0.49	0.49	0.50	0.49	0.51	28,491
N1	0.63	0.69	0.64	0.66	0.68	0.48	0.46	0.47	0.48	0.48	31,653
N2	0.68	0.74	0.70	0.70	0.74	0.57	0.56	0.56	0.58	0.58	72,637
N3	0.72	0.76	0.73	0.74	0.77	0.65	0.64	0.65	0.66	0.67	31,005

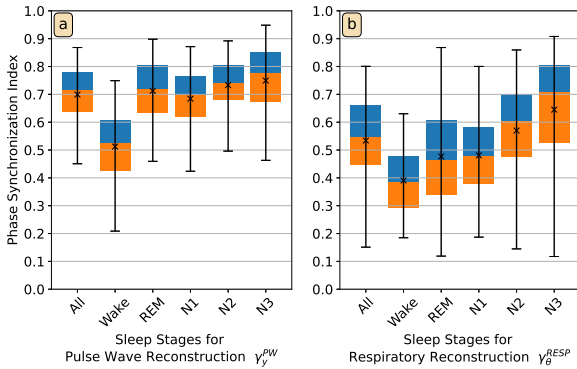


Fig. 4. Box plots of phase synchronization indices during different sleep stages for pulse waves, here γ_y^{PW} in panel (a), and respiration, here γ_θ^{RESP} in (b). Average values for each subject were considered to obtain the box plots. The orange part of each box represents the values between the lower quartile and the median, and the blue part represents the values between the median and the upper quartile. The ends of the whiskers mark the 2.5% quantile and the 97.5% quantile, respectively. The total average values appear as black crosses in the box plot. For both reconstructions, best results are obtained for N2 and N3 sleep, whereas during wake, reconstruction quality is rather low.

all 226 subjects. Sleep stages based on 30-second epochs have been determined from the PSG data by trained experts following standard guidelines [11] to distinguish light sleep (stages N1 and N2), deep sleep (stage N3), and rapid eye movement (REM) sleep. As example, we choose γ_y^{PW} and γ_θ^{RESP} obtained from the pulse wave and respiration reconstruction, respectively and depict results in Fig. 4, see also [22]. The results for all pulse wave and respiration reconstructions for each sleep stage are listed in Table I.

Overall, our results (Table I, Fig. 4) indicate that particularly large PSI values are obtained for both pulse wave and respiration reconstruction during deep sleep N3 followed by light sleep stage N2, while lowest reliability is achieved during wakefulness. For REM sleep, pulse waves can be reconstructed very well (comparable to non-REM sleep), however, respiration reconstructions resemble the real respiratory signal to much lower degree. Again, this can be explained by the different nature of the reconstructions' origins – 'internal' pulse wave vibrations vs. 'external' respiration triggered wrist rotation. A lower reliability is also observed for the respiration reconstruction during N1 sleep with comparable values as for wakefulness and REM sleep. No particular advantage of certain axes or angles can be observed for any sleep stage (Table I). Fig. 4 also shows that the inter-quartile range is

generally larger for respiration reconstructions, in particular during REM and N3 sleep. Although the averages of γ_θ^{RESP} are larger during N2 and N3, there are still outliers with nearly unsynchronized reconstruction ($\gamma_\theta^{RESP} < 0.2$). In contrast, for the pulse wave reconstructions, such outliers occur to much lower extent.

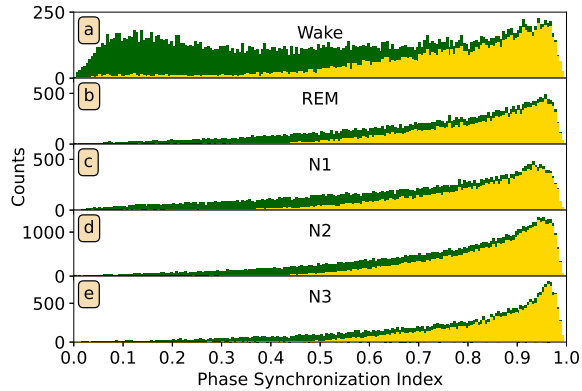


Fig. 5. Histograms for PSI values of pulse wave reconstruction γ_y^{PW} classified by sleep stages showing the values for all epochs (green) and after internal evaluation and optimization of the pulse wave reconstruction procedure with a threshold of $I_y^{PW} > 0.5$ (yellow). The results indicate that pulse wave reconstruction from accelerometer signals is much less reliable during consolidated wakefulness and that an internal evaluation and optimization procedure needs to be applied.

To illustrate the full distributions of the PSI values for the pulse wave reconstruction, Fig. 5 shows the histograms of all γ_y^{PW} values (for each epoch) during the different sleep stages. All histograms are peaked at PSI values close to 1, except for the one referring to wakefulness. In this case, another broad peak with very low PSI values indicates that pulse wave reconstructions are unreliable for about half of the 30-second epochs during wakefulness, most probably because of motion artifacts that disturb the wrist accelerometer signal during (consolidated) wakefulness but not during brief arousals. This is consistent with the recent observation that longer arousals and consolidated wakefulness lead to higher activity levels [46].

Therefore, our results suggest that the proposed approach of pulse wave (as well as respiration) reconstruction from accelerometer signals is applicable only during sleep and sedentary behaviour without significant wrist motion.

C. Effects of Sleep-Disordered Breathing on the Performance of Pulse Wave and Respiratory Signal Reconstruction

Sleep-related breathing disorders and in particular sleep apnea affect blood pressure regulation and lead to hypertension [47] and associated changes in pulse wave amplitude [48]. Therefore, it is reasonable to test the performance of pulse wave reconstruction from accelerometer signals under the condition of sleep apnea and to compare results to the obvious effect of sleep apnea on respiratory signal reconstruction. Fig. 6 shows that the largest pulse wave reconstruction PSI values γ_y^{PW} are obtained for healthy subjects with less than 5 apnea or hypopnea events per hour (i.e., $AHI < 5$). The same holds for the respiratory reconstruction γ_θ^{RESP} , however a drop in respiration reconstruction quality but not in pulse wave reconstruction quality is seen during the rare apneas and hypopneas in these subjects. The quality of both reconstructions is clearly reduced in subjects with more than 30 apnea or hypopnea events per hour, i.e., subjects suffering from severe sleep apnea. Again a further drastic decrease of γ_θ^{RESP} is seen during the actual apneas (but not hypopneas) in these patients, while this decrease is only marginal for γ_y^{PW} . When differentiating between obstructive apneas (caused by obstruction of the upper airways) and central apneas (due to absent respiratory drive from the brain stem), a slightly better reconstruction quality can be seen for the obstructive apneas, where the respiratory drive still persists.

D. Identification of Reliable Epochs for the Reconstructed Signals

Checking the consistency (similarity) of pairs of reconstructed signals can be used as internal evaluation to identify 30-second epochs with a particularly reliable reconstruction. For this purpose, we have calculated the PSIs between pairs of independently derived reconstructed signals for each epoch. Then we selected time epochs with sufficient reconstruction quality by analyzing the PSI between two reconstructions. This approach represents an internal evaluation, which does not require recordings of ECG, PPG or respiratory flow. More specifically, we have calculated, e. g., the inter-reconstruction PSI $\Gamma_{x,y}^{PW}$ according to (1) for the two reconstructed phases φ_x^{PW} and φ_y^{PW} (instead of φ^{ECG}). Then, we have taken only those 30-second epochs into account, where $\Gamma_{x,y}^{PW}$ is above a certain threshold τ , indicating good synchronization between the reconstructions A_x^{PW} and A_y^{PW} . This internal evaluation approach leads to gaps in the reconstructed time series but, on the other hand, yields a much higher quality by only using reliable epochs.

Fig. 7 (solid curves) shows how the fraction of usable 30-second epochs decreases as the threshold τ for the inter-reconstruction PSIs $\Gamma_{i,j}^{PW}$ is increased. Simultaneously, the average quality of the remaining reconstructed signals becomes higher as indicated by the increasing conditional averages of γ_j^{PW} (dash-dotted curves in Fig. 7).

For example, for reconstruction A_y^{PW} the internal evaluation yields an average $\gamma_y^{PW} = 0.81$ if $\Gamma_{y,z}^{PW} > 0.5$ is used for epoch selection (solid green curve in Fig. 7). In this case,

the reconstruction is available for 62 percent of all epochs. Hence, if a pulse wave reconstruction for nearly two thirds of all epochs during the night is sufficient in a particular application, this simple internal evaluation procedure can be used to increase the average reconstruction quality indicator from 0.70 to 0.81 (green dash-dotted curve in Fig. 7 at $\tau = 0.5$). Fig. 5 includes the histograms for the internally evaluated data with the threshold $\Gamma_{y,z}^{PW} > 0.5$ shown in yellow. One can see that the improvement is particularly effective for epochs of wakefulness, where most epochs with low reconstruction reliability (low γ_y^{PW}) are correctly identified and disregarded by the internal evaluation.

An additional improvement can be achieved by combinations of all three axes' data. Here, we developed two approaches for pulse wave reconstruction and one for respiration reconstruction:

Approach (A) Use A_x^{PW} if $\Gamma_{x,z}^{PW}$ exceeds $\Gamma_{x,y}^{PW}$, $\Gamma_{y,z}^{PW}$ and the threshold τ , or else use A_y^{PW} if $\Gamma_{x,z}^{PW}$ or $\Gamma_{y,z}^{PW}$ exceed τ . The results are shown as black curves in Fig. 7.

Approach (B) Use A_x^{PW} if $(\Gamma_{x,y}^{PW} + \Gamma_{x,z}^{PW})/2 > \tau$, or else use A_y^{PW} if $(\Gamma_{x,y}^{PW} + \Gamma_{y,z}^{PW})/2 > \tau$, or else use A_z^{PW} if $(\Gamma_{x,z}^{PW} + \Gamma_{y,z}^{PW})/2 > \tau$. The results are shown as red curves in Fig. 7.

Approach (C) Use A_ϕ^{RESP} if $\Gamma_{y,z}^{RESP}$ exceeds $\Gamma_{x,y}^{RESP}$, $\Gamma_{x,z}^{RESP}$ and the threshold τ , or else use A_θ^{RESP} if $\Gamma_{x,y}^{RESP}$ or $\Gamma_{x,z}^{RESP}$ exceed τ .

For both approaches (A) and (B) the number of 30-second epochs decreases slower with increasing threshold, see Fig. 7. For half of all 30-second epochs a PSI of 0.88 can be achieved with approach (A) and 0.87 with approach (B). These results correspond to a nearly perfect pulse wave reconstruction in the considered epochs, since they are very close to the average PSI for the PPG ($\gamma^{PPG} = 0.94$, see Fig. 4).

Fig. 8 shows our results for reconstructions optimized by internal evaluation considering only 50% of all epochs. The selection of particularly good epochs leads to generally much larger PSI values than those reported in Fig. 4 for all epochs. The improvement is much larger for the pulse wave reconstructions than for the respiratory reconstructions, however, the general sleep-stage stratification pattern as observed in Fig. 4 is preserved in both cases.

IV. DISCUSSION

We have conducted a systematic comparison between PSG-recorded cardiac dynamics and respiratory activity and corresponding signal reconstructions as derived from high-resolution wrist accelerometer data. We show that all reconstructions obtained from the accelerometer's axes and angles perform similarly well for both, pulse wave and respiration reconstruction. The overall synchronization between reconstructed signal and PSG signal is higher for the pulse waves with an average of $\gamma^{PW} \approx 0.68$ as compared to $\gamma^{RESP} \approx 0.53$ for respiration. This may be because of the different underlying phenomena giving rise to the reconstructed signals. While the 'external' respiration-triggered

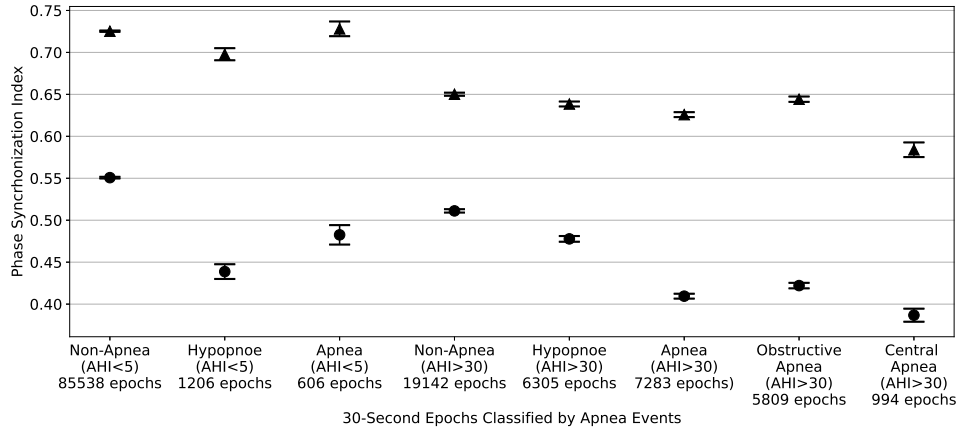


Fig. 6. Effects of sleep-related breathing disorders on the PSI for the pulse wave reconstruction γ_y^{PW} (▲) and the respiration reconstruction γ_θ^{RESP} (●) for subjects with low apnea hypopnea index (AHI) (< 5 events/h) and high AHI (> 30 events/h) averaged over all corresponding epochs (i) without apnea, (ii) with hypopnea, and (iii) with full apnea. For subjects with high AHI, PSI values for central and obstructive apnea are also reported separately. Error bars indicate the standard error. The labels include the number of epochs used for the corresponding averages. PSI values are highest for the γ_y^{PW} reconstruction for subjects with low AHI and about 10-15% lower for high AHI subjects. Interestingly, pulse wave reconstruction reliability for high AHI subjects decline only slightly when hypopnea and apnea epochs are analyzed; for central sleep apnea this decline is most pronounced. For γ_θ^{RESP} , values are consistently much lower than for γ_y^{PW} . As expected γ_θ^{RESP} shows a stronger decline when apnea epochs are analyzed. However, for obstructive apnea, γ_θ^{RESP} is only slightly better as compared to central sleep apnea.

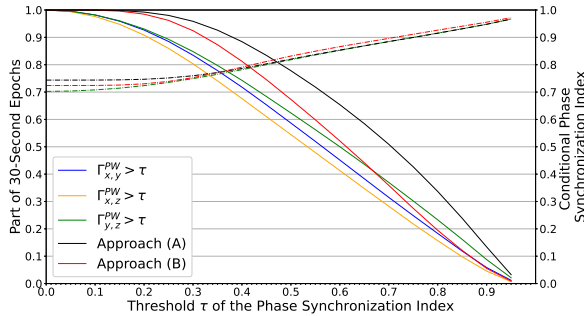


Fig. 7. Performance of internal evaluation for increasing the quality of pulse wave reconstructions. Inter-reconstruction phase synchronization indices $\Gamma_{i,j}^{PW}$ were analyzed to identify 30-seconds epochs with reliable pulse wave reconstructions. Solid curves indicate the fraction of reliable 30-seconds epochs versus the inter-reconstruction PSI threshold τ , solid blue curve for $\Gamma_{x,y}^{PW}$, green for $\Gamma_{y,z}^{PW}$, and orange for $\Gamma_{x,z}^{PW}$. Furthermore, to increase the fraction of reliable epochs and the reconstruction quality we introduced two approaches combining all three reconstructions: (A) – solid black curve and (B) – solid red curve. Dash-dotted curves show the average PSIs γ_y^{PW} (green), $\gamma_{(A)}^{PW}$ (black), and $\gamma_{(B)}^{PW}$ (red) between the selected reconstructions and our reference (ECG), calculated using only the reliable epochs. For example, the green dash-dotted curve shows γ_y^{PW} based on reliable epochs selected according to $\Gamma_{y,z}^{PW} > \tau$.

wrist rotations could be sensitive to different placements of the arm, the 'internal' pulse wave vibrations caused by the pulsatile blood flow in the wrist seem to be less affected by arm positioning.

Such interpretation could explain the stronger sleep-stage dependence we observe for the respiration reconstructions, where muscle atonia during REM sleep can diminish respiratory-triggered wrist movements. Overall, we obtain for

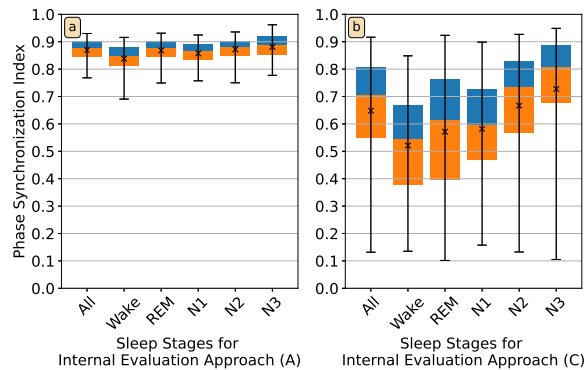


Fig. 8. Internal Evaluation Effect on Sleep Stages. Same as Fig. 4, but for signals optimized by internal evaluation with signal selection according to approach (A) and (C) (see text); 50% of all epochs are used. The inter-reconstruction PSI threshold τ is 0.7 for the pulse wave reconstructions and 0.92 for the respiration reconstructions.

the respiration reconstructions an average of $\gamma^{RESP} \approx 0.50$ for REM and $\gamma^{RESP} \approx 0.61$ for N2-N3 non-REM sleep. In contrast, average values for the pulse wave reconstructions are much higher with averages $\gamma^{PW} \approx 0.69$ and $\gamma^{PW} \approx 0.73$ for REM and N2-N3 non-REM sleep, respectively. Our analyses also show that pulse wave and respiration reconstruction from accelerometer data does not work as well during wakefulness, perhaps because of frequent body movements that are characteristic for this stage. Surprisingly, however, we find that pulse wave reconstructions are hardly affected by sleep apnea epochs per se. The reduced overall quality that we observe in patients with severe sleep apnea (during normal breathing as well as during apnea epochs) could therefore be related to a

more restless and shallow sleep that typically occurs in these patients.

Compared with seismocardiography and ballistocardiography (see Section II.B), our suggested approach using wrist accelerometers has advantages for a screening of larger population groups and general population-based cohort studies, since the sensor is worn like a normal wrist watch and can thus be handed to each subject in the study center with very brief instructions. No preparation of a bed or chair at the home of the subject, no data transmission infrastructure and no visits of care personal to the home are needed. The sensor can easily be returned to the study center by postal mail, after the pre-programmed recording period has ended. Ballistocardiography, on the other hand, has advantages for monitoring specific subjects for a long time, in particular disabled or elderly persons or children, since this method requires less compliance of the subjects but more effort from the study center or hospital.

Our proposed approach for simultaneously reconstructing pulse wave and respiration signals from wrist accelerometers has advantages and disadvantages compared to wrist or finger photoplethysmography (PPG). Certainly, pulse waves are more directly assessed by PPG. Our results show that if one has to rely on wrist actigraphy only, reliable pulse waves can only be reconstructed for parts of the night and particularly not for periods of nocturnal wakefulness. However, the reconstruction of breathing activity from a PPG is much more indirect – a double reconstruction is involved, since one must first obtain the timing of the heartbeats from the plethysmogram, and then breathing activity has to be derived based on heart rate modulations via respiratory sinus arrhythmia (RSA). In addition, respiration can also affect pulse transition times, so that the first reconstruction step becomes less reliable. Furthermore, RSA is typically weaker in elderly subjects, so that the reliability of the second reconstruction step will become age dependent and probably also be affected by cardio-respiratory impairments. In our previous work [22], we have shown that the reconstruction of breathing activity from the timing of the R peaks in the ECG is less reliable than reconstruction from wrist accelerometry. Therefore, we are convinced that PPG approaches cannot yield sufficient quality of reconstructed respiration data in large general population-based studies.

A possible next step of our research should study the relationship between the two signals reconstructed from the same wrist accelerometer. In this context, the overall question would be whether the reconstructed pulse waves and respiratory activities are sufficiently reliable so that different aspects of cardio-respiratory coupling [49]–[51] can be derived from them. Additionally, one could probe, e.g., the dependence of cardio-respiratory coupling on sleep stages (using data such as those studied here) or derive cardio-respiratory coupling in large population-based cohort studies with many thousands of participants (see below). To test how reliable different aspects of cardio-respiratory coupling can be derived from the reconstructed data, several measures of cardio-respiratory synchronization [52], [53] and cardio-respiratory coordination [44] shall be applied to the reconstructed data and the

reference PSG data.

V. CONCLUSION

Our paper introduces a novel approach for simultaneously obtaining time series of cardiac and respiratory dynamics during sleep. Unlike most previous approaches, the presented methodology relies entirely on a single wrist accelerometer, which is often used in large cohort studies, e.g., the German National Cohort study [54] with $\approx 25,000$ SOMNOWatch™ recordings up to now. Another example is the UK Biobank study, in which wrist-worn accelerometers were used to assess physical activity in 100,000 volunteers [55]. Large population-based studies often include actigraphy (accelerometry) as the only continuously measured physiological signal because it can be easily recorded by a smart watch and does not require electrodes, flow sensors, or chest belts.

Our proposed phase synchronization metric evaluates the timing of pulse waves and respiratory cycles and is independent of amplitude changes. This is adequate for our signal reconstructions since changes in wrist position with respect to the body as well as changes in the position of the device at the wrist influence the signal amplitude. Therefore, our approach may not be used for a reliable derivation of stroke or breath volume variations. Furthermore, the approach works only if no other (i.e., voluntary) movements occur and thus, is limited to the sleep period. This is consistent with our finding that the best reconstruction quality is achieved during deep sleep, followed by light sleep N2 and REM sleep, and at last nocturnal wakefulness. Nevertheless, pulse wave reconstructions are just weakly affected by apnea and hypopnea events, and their reliability can be increased by internal evaluation if the reconstructed signals are not needed for the entire sleep duration. Ultimately, our approach could be used to monitor pulse wave characteristics during sleep in combination with or as a substitute of a wrist or finger photoplethysmogram.

ACKNOWLEDGMENT

We thank Antonia Graf, Maria Kluge, and Luise Pelikan (Charité - Universitätsmedizin Berlin) for data acquisition in the sleep laboratories. We also thank Alexander Müller (Technical University of Munich) for providing R-peak detection in SOMNOWatch™ data and Yaopeng Ma (Bar-Ilan University, Ramat Gan) for discussion and data synchronization.

REFERENCES

- [1] H. R. Colten and B. M. Altevogt, Eds., *Sleep Disorders and Sleep Deprivation: An Unmet Public Health Problem*, Washington (DC), 2006.
- [2] D. R. Gold *et al.*, “Rotating shift work, sleep, and accidents related to sleepiness in hospital nurses,” *American journal of public health*, vol. 82, no. 7, pp. 1011–1014, 1992.
- [3] L. K. Barger *et al.*, “Extended work shifts and the risk of motor vehicle crashes among interns,” *The New England journal of medicine*, vol. 352, no. 2, pp. 125–134, 2005.
- [4] A. N. Vgontzas *et al.*, “Adverse effects of modest sleep restriction on sleepiness, performance, and inflammatory cytokines,” *The Journal of clinical endocrinology and metabolism*, vol. 89, no. 5, pp. 2119–2126, 2004.
- [5] L. K. Barger *et al.*, “Impact of extended-duration shifts on medical errors, adverse events, and attentional failures,” *PLoS medicine*, vol. 3, no. 12, p. e487, 2006.

- [6] A. B. Newman *et al.*, "Daytime sleepiness predicts mortality and cardiovascular disease in older adults. the cardiovascular health study research group," *Journal of the American Geriatrics Society*, vol. 48, no. 2, pp. 115–123, 2000.
- [7] H. K. Yaggi *et al.*, "Obstructive sleep apnea as a risk factor for stroke and death," *The New England journal of medicine*, vol. 353, no. 19, pp. 2034–2041, 2005.
- [8] N. Covassin and P. Singh, "Sleep duration and cardiovascular disease risk: Epidemiologic and experimental evidence," *Sleep medicine clinics*, vol. 11, no. 1, pp. 81–89, 2016.
- [9] M. Zinkhan and J. W. Kantelhardt, "Sleep assessment in large cohort studies with high-resolution accelerometers," *Sleep medicine clinics*, vol. 11, no. 4, pp. 469–488, 2016.
- [10] A. Rechtschaffen and A. Kales, *A manual of standardized terminology, techniques and scoring system for sleep stages of human subjects*. Allan Rechtschaffen and Anthony Kales, editors. ser. NIH publication no. 204. Bethesda, Md.: U. S. National Institute of Neurological Diseases and Blindness, Neurological Information Network, 1968.
- [11] R. B. Berry *et al.*, "The AASM manual for the scoring of sleep and associated events: rules, terminology and technical specifications, version 2.5," *American Academy of Sleep Medicine*. Darien, IL, 2018.
- [12] J.-H. Byun *et al.*, "The first night effect during polysomnography, and patients' estimates of sleep quality," *Psychiatry research*, vol. 274, pp. 27–29, 2019.
- [13] B. W. Riedel *et al.*, "First night effect and reverse first night effect in older adults with primary insomnia: does anxiety play a role?" *Sleep Medicine*, vol. 2, no. 2, pp. 125–133, 2001.
- [14] G. Curcio *et al.*, "Paradoxes of the first-night effect: a quantitative analysis of antero-posterior EEG topography," *Clinical neurophysiology*, vol. 115, no. 5, pp. 1178–1188, 2004.
- [15] D. J. Kupfer *et al.*, "Psychomotor activity in affective states," *Archives of general psychiatry*, vol. 30, no. 6, pp. 765–768, 1974.
- [16] T. R. Colburn *et al.*, "An ambulatory activity monitor with solid state memory," *ISA transactions*, vol. 15, no. 2, pp. 149–154, 1976.
- [17] S. Ancoli-Israel *et al.*, "The role of actigraphy in the study of sleep and circadian rhythms," *Sleep*, vol. 26, no. 3, pp. 342–392, 2003.
- [18] C. McCall and W. V. McCall, "Objective vs. subjective measurements of sleep in depressed insomniacs: first night effect or reverse first night effect?" *Journal of clinical sleep medicine*, vol. 8, no. 1, pp. 59–65, 2012.
- [19] A. Godfrey *et al.*, "Direct measurement of human movement by accelerometry," *Medical engineering & physics*, vol. 30, no. 10, pp. 1364–1386, 2008.
- [20] A. Sadeh *et al.*, "The role of actigraphy in the evaluation of sleep disorders," *Sleep*, vol. 18, no. 4, pp. 288–302, 1995.
- [21] J. Zschocke *et al.*, "Detection and analysis of pulse waves during sleep via wrist-worn actigraphy," *PLoS one*, vol. 14, no. 12, p. e0226843, 2019.
- [22] J. Leube *et al.*, "Reconstruction of the respiratory signal through ECG and wrist accelerometer data," *Scientific reports*, vol. 10, no. 1, p. 14530, 2020.
- [23] J. M. Zanetti and D. M. Salerno, "Seismocardiography: a technique for recording precordial acceleration," in *Computer-based medical systems*, I. N. Bankman and J. E. Tsitlik, Eds. Los Alamitos, CA: IEEE Computer Society Press, 1991, pp. 4–9.
- [24] O. T. Inan *et al.*, "Ballistocardiography and seismocardiography: a review of recent advances," *IEEE Journal of Biomedical and Health Informatics*, vol. 19, no. 4, pp. 1414–1427, 2015.
- [25] M. Jafari Tadi *et al.*, "A real-time approach for heart rate monitoring using a Hilbert transform in seismocardiograms," *Physiological Measurement*, vol. 37, no. 11, pp. 1885–1909, 2016.
- [26] K. Pandia *et al.*, "Extracting respiratory information from seismocardiogram signals acquired on the chest using a miniature accelerometer," *Physiological Measurement*, vol. 33, no. 10, pp. 1643–1660, 2012.
- [27] M. Jafari Tadi *et al.*, "Accelerometer-based method for extracting respiratory and cardiac gating information for dual gating during nuclear medicine imaging," *International Journal of Biomedical Imaging*, vol. 2014, p. 690124, 2014.
- [28] P. Castiglioni *et al.*, *2007 Annual International Conference of the IEEE Engineering in Medicine and Biology Society*. Piscataway, NJ: IEEE Service Center, 2007.
- [29] A. Albukhari *et al.*, "Bed-embedded heart and respiration rates detection by longitudinal ballistocardiography and pattern recognition," *Sensors*, vol. 19, p. 1451, 2019.
- [30] C. Carlson *et al.*, "Bed-based ballistocardiography: Dataset and ability to track cardiovascular parameters," *Sensors*, vol. 21, p. 156, 2021.
- [31] A. Ullal *et al.*, "Non-invasive monitoring of vital signs for older adults using recliner chair," *Health and Technology*, vol. 11, pp. 169–184, 2021.
- [32] G. Wusk and H. Gabler, "Non-invasive detection of respiration and heart rate with a vehicle seat sensor," *Sensors*, vol. 18, p. 1463, 2018.
- [33] H. Liu *et al.*, "Recent development of respiratory rate measurement technologies," *Physiological Measurement*, vol. 40, p. 07TR01, 2019.
- [34] C. Massaroni *et al.*, "Contact-based methods for measuring respiratory rate," *Sensors*, vol. 19, p. 908, 02 2019.
- [35] J. Hernandez *et al.*, "Biowatch: Estimation of heart and breathing rates from wrist motions," in *Proceedings of the 9th International Conference on Pervasive Computing Technologies for Healthcare*, B. Arrnrich *et al.*, Eds. ICST, 20.05.2015 - 23.05.2015.
- [36] J. Hernandez *et al.*, "Wearable motion-based heart-rate at rest: A workplace evaluation," *IEEE Journal of Biomedical and Health Informatics*, vol. 23, pp. 1920–1927, 2019.
- [37] M. Haescher *et al.*, "Seismotracker: Upgrade any smart wearable to enable a sensing of heart rate, respiration rate, and microvibrations," in *Proceedings of the 2016 CHI Conference Extended Abstracts on Human Factors in Computing Systems*, J. Kaye *et al.*, Eds. New York, USA: ACM Press, 2016, pp. 2209–2216.
- [38] Y. Yao *et al.*, "Unobtrusive estimation of cardiovascular parameters with limb ballistocardiography," *Sensors*, vol. 19, p. 2922, 2019.
- [39] D. Gabor, "Theory of communication. the analysis of information," *Journal of the Institution of Electrical Engineers-Part III: Radio and Communication Engineering*, vol. 93, no. 26, pp. 429–441, 1946.
- [40] B. Boashash, "Estimating and interpreting the instantaneous frequency of a signal. i - fundamentals. ii - algorithms and applications," *Proceedings of the IEEE*, vol. 80, no. 4, pp. 540–568, 1992.
- [41] M. Rosenblum *et al.*, "Chapter 9 - Phase synchronization: From theory to data analysis," in *Neuro-informatics and neural modelling*, ser. Handbook of Biological Physics, F. Moss, Ed. Elsevier, 2001, vol. 4, pp. 279–321.
- [42] P. Wohlfahrt *et al.*, "Transitions in effective scaling behavior of accelerometer time series across sleep and wake," *EPL (Europhysics Letters)*, vol. 103, no. 6, p. 68002, 2013.
- [43] R. Quian Quiroga *et al.*, "Event synchronization: A simple and fast method to measure synchronicity and time delay patterns," *Physical Review E*, vol. 66, no. 4, p. 041904, 2014.
- [44] M. Riedl *et al.*, "Cardio-respiratory coordination increases during sleep apnea," *PLoS ONE*, vol. 9, no. 4, p. e93866, 2014.
- [45] M. Rosenblum *et al.*, "Phase synchronization of chaotic oscillators," *Physical Review Letters*, vol. 76, no. 11, pp. 1804–1807, 1996.
- [46] H. Dvir *et al.*, "A biased diffusion approach to sleep dynamics reveals neuronal characteristics," *Biophysical journal*, vol. 117, no. 5, pp. 987–997, 2009.
- [47] R. P. Pedrosa *et al.*, "Obstructive sleep apnea: the most common secondary cause of hypertension associated with resistant hypertension," *Hypertension (Dallas, Tex. : 1979)*, vol. 58, no. 5, pp. 811–817, 2011.
- [48] J. Haba-Rubio *et al.*, "Obstructive sleep apnea syndrome: effect of respiratory events and arousal on pulse wave amplitude measured by photoplethysmography in NREM sleep," *Sleep & breathing*, vol. 9, no. 2, pp. 73–81, 2005.
- [49] R. Bartsch *et al.*, "Phase transitions in physiologic coupling," *Proc. Natl. Acad. Sci. USA*, vol. 109, pp. 10 181–10 186, 2012.
- [50] H. Krause *et al.*, "On the difference of cardiorespiratory synchronisation and coordination," *Chaos*, vol. 27, no. 9, p. 093933, 2017.
- [51] M. Elstad *et al.*, "Cardiorespiratory interactions in humans and animals: rhythms for life," *Am. J. Physiol. Heart Circ. Physiol.*, vol. 315, no. 1, pp. H6–H17, 2018.
- [52] R. Bartsch *et al.*, "Experimental evidence for phase synchronization transitions in the human cardio respiratory system," *Physical Review Letters*, vol. 98, no. 2, p. 054102, 1998.
- [53] A. Kuhnhold *et al.*, "Quantifying cardio-respiratory phase synchronization – a comparison of five methods using ECGs of post-infarction patients," *Physiological Measurement*, vol. 38, pp. 925–939, 2017.
- [54] GNC Consortium, "German National Cohort: aims, study design and organization," *European Journal of Epidemiology*, vol. 29, no. 5, pp. 371–382, 2014.
- [55] A. Doherty *et al.*, "Large scale population assessment of physical activity using wrist worn accelerometers: the UK Biobank study," *PLoS ONE*, vol. 12, no. 2, p. e0169649, 2017.

Supplementary Material

PREFACE

This Supplementary Material contains additional information about our studies and describe some methods in more detail, mentioned in our paper "Reconstruction of Pulse Wave and Respiration from Wrist Accelerometer During Sleep" Zschocke *et al.* 2021. The numbering follows the numbering of the original paper.

SYNCHRONIZATION OF SOMNOWATCH™ AND PSG RECORDINGS

The figure shows a photo of the SOMNOWATCH™ device placed at the wrist of a subject. Since ECGs were recorded simultaneously by SOMNOWATCH™ and the PSG systems, these time series were used for establishing synchronization between the recording devices. As first step, the temporal positions of all R-peaks were determined using the package BioSPPy in Python [56] for the PSG data and LibRasch [57] for the SOMNOWATCH™ data. Then, starting 5 minutes after the lights-off time, for each segment of 20 minutes ECG data, the SOMNOWATCH™'s R-peak positions were linearly fitted to the PSG system's R-peak positions, yielding a time shift value (offset) and a drift value (slope) of the linear fit. For each segment, the fitting procedure was repeated 2401 times: for R-peak position time series shifted with respect to each other by -20 minutes up to $+20$ minutes with 1 second increment. Only the best fit was retained for each segment of 20 minutes ECG data, and the time shift used for that fit was added to the offset. Segments with less than 500 R peaks in 20 minutes for either SOMNOWATCH™ or PSG system were disregarded, assuming insufficient ECG signal quality. A visual inspection of the best time shifts (offsets) obtained this way for all 20-minutes segments was performed to check if any time gaps occurred in the PSG data throughout the night and if the time shift increased approximately linearly with the progressing night. Then the result for the segment with the smallest fitting error was used to correct time shift and drift for the whole night.

COMPARISON OF GROUPS OF INCLUDED AND EXCLUDED SUBJECTS

Table II compares many clinical and sleep-related parameters for the group of 226 included data sets (subjects) and the group of 213 excluded data sets. As written in Subsection II.A, the procedure described in the previous section was unsuccessful for 105 subjects, and another 108 subjects had to be excluded because of noisy or corrupt respiration recordings. Only small differences in age ($\Delta\text{age} = 3.5$ y, $p = 0.009$), total sleep time ($\Delta\text{TST} = 17.5$ min, $p = 0.018$), and wake after sleep onset ($\Delta\text{WASO} = 12.9$ min, $p = 0.015$) are significant.

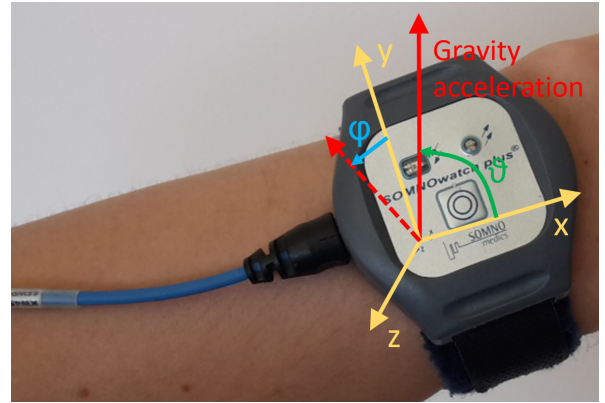


Fig. 9. Acceleration and ECG recording at the wrist. The photo shows the commercial medical device SOMNOWATCH™ plus (Somnomedics GmbH, Randersacker, Germany) placed at the wrist with the coordinate axes (x , y , and z ; yellow) according to its orientation as well as the gravity acceleration vector (red) pointing vertically upwards from the center of the earth. The device measures the three components of the gravity acceleration with respect to its coordinate axes. From this data the two orientational angles, θ = angle between x axis and gravity acceleration (see 4) and ϕ = angle between y axis and projection of the gravity acceleration into the $y - z$ plane (dashed red vector) can be calculated (see 3). In addition, the device records the ECG via the attached blue cable, using three electrodes. There is also a passive light sensor used to identify lights-off periods during the night and a LED indicating the recording period, but both are placed on the front of the device and therefore cannot be used to measure a photoplethysmogram.

We found no significant differences regarding pathologies, smoking, alcohol consumption, and snoring habits.

TABLE II
COMPARISON OF INCLUDED AND EXCLUDED DATA SETS

	included data	excluded data
male / female	117 / 109	109 / 100
Age [y]	48.6 ± 13.9	52.1 ± 13.8
Size [cm]	173.1 ± 10.1	173.2 ± 10.2
Weight [kg]	83.7 ± 18.8	85.5 ± 20.4
BMI [kg/m ²]	27.9 ± 5.7	28.4 ± 6.2
time in bed [min]	455.3 ± 46.3	452.0 ± 54.8
sleep onset latency [min]	18.4 ± 15.9	19.7 ± 20.2
total sleep time [min]	377.1 ± 72.3	359.6 ± 70.9
wake after sleep onset [min]	59.8 ± 49.1	72.7 ± 52.8
fraction of N1	0.204 ± 0.150	0.230 ± 0.149
fraction of N2	0.440 ± 0.123	0.428 ± 0.126
fraction of N3	0.186 ± 0.101	0.186 ± 0.112
fraction of REM	0.170 ± 0.081	0.157 ± 0.088
apnea hypopnea index [/h]	14.5 ± 18.7	16.6 ± 22.0
periodic limb movement ind. [/h]	13.8 ± 23.7	15.4 ± 27.4

CALCULATION OF RECONSTRUCTED PULSE WAVE PHASES

In the following, we describe the data processing from the raw acceleration signal to the pulse wave phases, corresponding to the pulse wave peaks transversing the wrist. As already mentioned in II-C*, the pulse wave information is hidden behind a high-frequency tissue vibration. Therefore we first apply a 5 to 14 Hz FFT bandpass filter on each raw acceleration axis separately (e. g., light blue curve in Fig. 1 (b)*). for the y axis) and uncover the signal by the absolute of its Hilbert transform (red curve in Fig. 1 (b)*). In order to extract only the main systolic pulse wave, we (i) subtract a moving average of 1.0 second window length and (ii) calculate a moving average over 0.43 seconds to obtain periodic signals, i.e., the pulse wave reconstructions A_x^{PW} , A_y^{PW} , and A_z^{PW} (green curve in Fig. 1 (b)*). We note that this procedure corresponds to another narrow band pass filter applied to the amplitude signal with a passband around 50 to 70 oscillations per minute, which correspond to the typical heart rate during sleep [58]. Both filter parameters, 1.0 second and 0.43 seconds, have been optimized for best phase synchronization of the pulse wave reconstructions with respect to the ECG-derived reference.

Pulse wave phases $\varphi(t)$ have been calculated by applying another Hilbert transform to the pulse wave reconstructions and using the $\arctan2$ function,

$$\varphi(t) = \arctan2(\Im(HT(A(t))), \Re(HT(A(t))), \quad (2)$$

where \Re denotes the real part and \Im the imaginary part of the Hilbert transform HT [39]*. The procedure was applied to all pulse wave reconstructions A_x^{PW} , A_y^{PW} and A_z^{PW} .

Furthermore, we derived rotation angles of the wrist from the pulse wave reconstructions,

$$\phi(t) = \arctan2(A_z^{PW}, A_y^{PW}) \quad (3)$$

$$\theta(t) = \arccos\left(\frac{A_x^{PW}}{\sqrt{(A_x^{PW})^2 + (A_y^{PW})^2 + (A_z^{PW})^2}}\right) \quad (4)$$

The acceleration axes y and z are orthogonal to the wrist, while the x axis is parallel to the lower arm. Therefore, ϕ represents the rotation angle around the lower arm axis (roll angle), and θ represents the turning angle with respect to the elbow (pitch angle). $\phi(t)$ and $\theta(t)$ are smoothed by a subtracting 1.0 second moving average and applying a moving average of 0.43 seconds. Finally, we applied Hilbert transform and calculated the corresponding phases φ_ϕ^{PW} and φ_θ^{PW} by $\arctan2$, as described above in (2).

CALCULATION OF RECONSTRUCTED RESPIRATION PHASES

Wrist acceleration data recorded during sleep contains not only pulse wave information but also respiration activity. To

derive respiration reconstructions and obtain a phase information φ^{RESP} from the raw acceleration signals, we followed six steps, separately for each axis:

- i) Apply a 1.0 second moving average. The window size of one second for the moving average was chosen such that there is typically one heartbeat in each window so that effects of heartbeats and pulse wave propagation through the wrist are systematically dampened.
- ii) Down sampling from 128 Hz to 4 Hz, since respiratory activity does not involve high-frequency components.
- iii) Calculate ϕ and θ according to (3) and (4).
- iv) Subtract a 10 seconds moving average, also for ϕ and θ .
- v) Divide by a 10 seconds moving standard deviation, also for ϕ and θ . This leads to the respiration reconstructions A_x^{RESP} , A_y^{RESP} , A_z^{RESP} , A_ϕ^{RESP} , and A_θ^{RESP} .
- vi) Apply a Hilbert transform and $\arctan2$ to calculate the respiration phases (see (2)).

A detailed explanation of this procedure can be found in [22]*.

REFERENCES

- [56] Carlos Carreiras *et al.*, "Biosppy: Biosignal processing in python," 2015. [Online]. Available: <https://github.com/PIA-Group/BioSPPy/>
- [57] R. Schneider *et al.*, "Librasch: a programming framework for signal handling," in *Institute of Electrical and Electronics Engineers 2004 – Computers in Cardiology*, 2004, pp. 53–56.
- [58] S. Patra and S. Telles, "Heart rate variability during sleep following the practice of cyclic meditation and supine rest," *Applied psychophysiology and biofeedback*, vol. 35, no. 2, pp. 135–140, 2010.

*Referenced Section, Figure or Reference can be found in Zschocke *et al.* 2021

4 | PART II: FLUCTUATION ANALYSIS STUDIES

In this part of the thesis, results of detrended fluctuation analysis (DFA) of biosignals, like heart rate and PTT, will be presented. DFA is a powerful method for the analysis of time series and the determinations of their short- and long-term auto-correlations. The method was introduced by Peng *et al.* 1994 [69] and Bunde *et al.* 2000 [70], and has been applied in thousands of studies.

In the following, the system of cardiorespiratory regulation and its investigation via DFA are introduced. Subsequently our published results on the application of DFA for studying the PTT are put into context. This chapter is concluded by unpublished results of DFA for accelerometry data.

4.1 Introduction to detrended fluctuation analysis

4.1.1 Cardiorespiratory regulation

In general, the cardiorespiratory system is regulated by the autonomic nervous system, consisting of the sympathetic and parasympathetic nervous system (an exception is the respiration, which can be controlled consciously).

The parasympathetic nervous system relaxes the body (“rest and digest”) by decreasing blood pressure, heart rate and respiration rate, and it is with its longer neuronal path ways the slower system.

The sympathetic nervous system increases the body’s performance (“fight or flight”) by increasing blood pressure, heart rate and respiration rate. Both systems act as opponents and thus enable specific adaption to different situations.

With the spectral analysis of HRV it is possible to quantify sympathetic and parasympathetic activation of the heart rate [71]. Specifically, the low-frequency components (0.04 - 0.15 Hz) reflect sympathetic activity and the high-frequency components (0.15 - 0.4 Hz) are related to parasympathetic control [8]. Nevertheless, the heart rate and its variability are not stationary over several nocturnal hours, as they change from one sleep stage to another, and are also modulated by events like apneas or waking noises. As a consequence, mean and standard deviation of the time series are changing and therefore they are not stationary.

To solve this problem this work uses DFA to investigate short- and long-term correlations in non-stationary biosignals. Fluctuations in biosignals, like changes in HRV, are better resolved by DFA than by spectral analysis [72].

4.1.2 Detrended fluctuation analysis

In the last 30 years DFA has been established as an important method to detect short and long-range correlation in non-stationary time series. In short, the idea of DFA is to decompose the signal into segments, detrend the segments and calculate the mean square fluctuations. By varying the segments' length, fluctuations on different scales can be investigated. It is done as follows in detail [73].

For a time series x_i with equidistant measuring points $i = 1, 2, \dots, N$, first the mean \bar{x} will be subtracted to obtain a time series \tilde{x}_i with zero mean, see Fig. 4.1 a. Now the global profile, i.e. the cumulative sum, is calculated

$$X(j) = \sum_{i=1}^j \tilde{x}_i, \quad j = 1, 2, \dots, N. \quad (4.1)$$

In the next step, the profile $X(j)$ is divided in $N_s = \text{int}(N/s)$ non-overlapping segments of length s , see Fig. 4.1 b and c, gray curves. In order not to neglect information at the end of the time series, the segments are divided twice, once from the beginning and once from the end, which leads to $2N_s$ segments of length s . Now each segment ν is separately detrended. Therefore each segment is approximated with a polynomial trend $p_{\nu,s}^m(j)$ by least-square fitting

$$p_{\nu,s}^m(j) = a_0 + a_1j + a_2j^2 + \dots + a_mj^m, \quad (4.2)$$

see Fig. 4.1 b and c, red dashed lines. Finally each segment of the profile $X(j)$ is detrended by subtracting the polynomial trend

$$\tilde{X}(j) = X(j) - p_{\nu,s}^m(j), \quad (4.3)$$

see Fig. 4.1 b and c, green curves. The order m of the polynomial detrending is usually mentioned in the DFA name, like DFA1 for $m = 1$ (linear detrending) or DFA2 for $m = 2$ (quadratic detrending). The mean square fluctuation of each segment ν can be calculated as follows

$$F_{\nu}^2(s) = \frac{1}{s} \sum_{j=\nu}^{s(\nu+1)} \tilde{X}^2(j), \quad (4.4)$$

see Fig. 4.1 b and c, dark red diamonds. In the last step, the mean square fluctuations are averaged over all segments of the same length s

$$F^2(s) = \frac{1}{2N_s} \sum_{\nu=1}^{2N_s} F_{\nu}^2(s). \quad (4.5)$$

This fluctuation function is now investigated in its behavior on different scales s , i.e. the different segment lengths s . Usually DFA analysis is looking into different ranges

4.1. Introduction to detrended fluctuation analysis

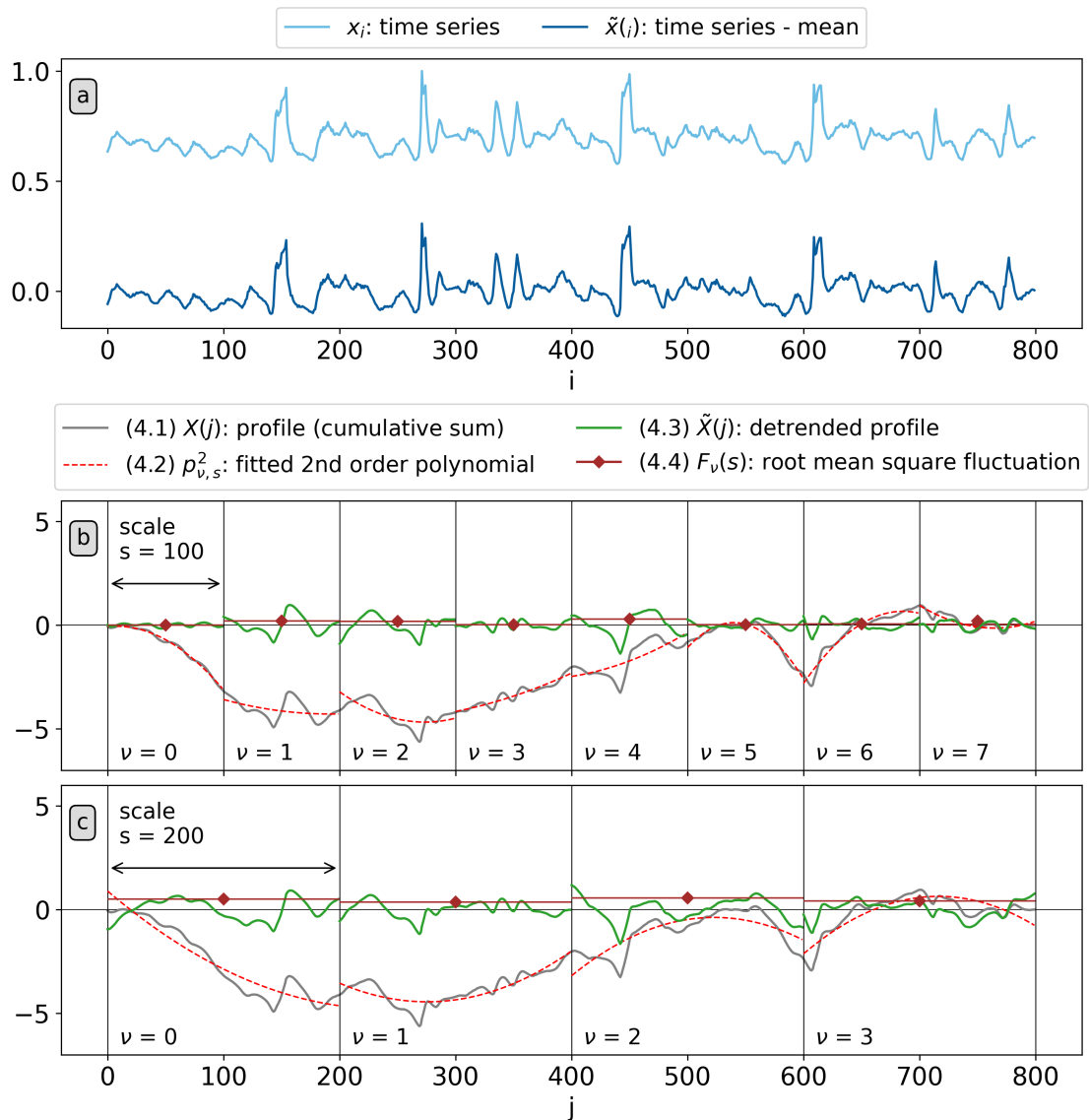


Figure 4.1: **Visualized DFA algorithm.** The upper plot (a) shows a time series of heart beat interval data (light blue) and the same time series with zero mean (dark blue). The lower plots show the single steps of the detrending algorithm, for two scales (dividing the signal in segments ν), $s = 100$ in b and $s = 200$ in c. The cumulative sum (gray) is detrended (green) by a second-order polynomial fit (red dashed lines) segment wise (ν). Finally, for each segment ν the mean square fluctuation is calculated (dark red diamonds). The numbers in the legend correspond to the equations 4.1 to 4.4

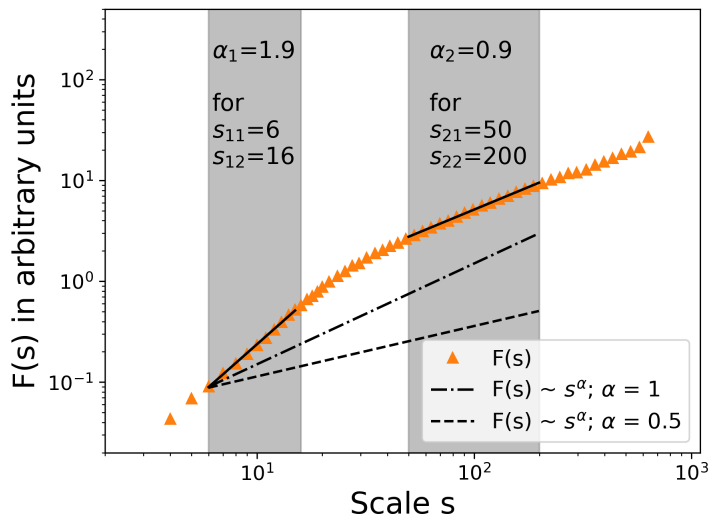


Figure 4.2: **Fluctuation function $F(s)$.** The fluctuation function $F(s)$ (orange triangles) is shown versus scale in a double-logarithmic plot. Here, two scale ranges are investigated, where we can find different power laws, indicated by different exponents α .

of scales to find power laws, which can be defined as follows:

$$F^2(s) \sim s^{2\alpha} \Rightarrow F(s) \sim s^\alpha \text{ for } s_1 < s < s_2, \quad (4.6)$$

where s_1 and s_2 define the range of scales, see Fig. 4.2. For different ranges, different power laws may be found. The mean fluctuation function $F(s)$ increases with increasing s , as the root mean square fluctuation (or the standard deviation) is larger on average with larger scales. That is why α is always positive and its values can be interpreted as follows [74], [75]:

0.0 < α < 0.5: In this case an anti-power-law correlation is present, which means small values are more likely to be followed by big values and vice versa [76].

0.5 < α < 1.0: This indicates a long-range power law correlation.

1.0 < α : The data is non-stationary, so that a correlation function cannot be defined. $\alpha = 1.5$ corresponds to a random walk.

Furthermore, α can be seen as the “roughness” of a time series, while larger α indicate smother signals.

In addition, for stationary time series, DFAs scaling behavior $F(s) \sim s^\alpha$ can be compared with the scaling behavior of autocorrelation function $C(s) \sim s^{-\gamma}$ and the scaling of a signals power spectrum $P(f) \sim f^{-\beta}$, which are established methods to

4.2. Publication: DFA of cardiorespiratory and brain signals.

describe correlation behavior.

One can find that α is related to the exponent of the power spectrum β by

$$\beta = 2\alpha - 1. \quad (4.7)$$

A relation between γ and α can only be found in the range of $0.5 < \alpha < 1.0$:

$$\gamma = 2 - 2\alpha. \quad (4.8)$$

As already mentioned, these relations are only valid in stationary time series. Therefore, the advantage of DFA over the analysis of autocorrelation functions and power spectra lies mainly in its capability of analyzing also non-stationary signals.

4.2 Publication: DFA of cardiorespiratory and brain signals.

About this publication. In the publication “Long- and short-term fluctuations compared for several organ systems across sleep stages” [JZ4] we determined and analyzed the following five time series: heart rate, pulse rate, respiration frequency, PTT, and EEG alpha-band power during different sleep stages.

In a first step we compared the age and sleep-stage dependence of the average values, the standard deviations and standard deviations of the increments for all five time series. We confirmed that they follow the physiological expectations. In a second step we applied DFA with second-order polynomial detrending (DFA2) to all five time series and investigated the scaling exponent α of the results for two regimes: short-term (6 to 16 seconds) α_1 and long-term (50 to 200 seconds) α_2 [77], separately for different sleep stages and age groups.

We studied for the first time the dynamics of PTT, from heart to finger in a similar way as previously done for inter-heart beat intervals [70], [77] respiratory intervals [77], [78] and brain-wave amplitudes [79]. Our results regarding the scaling behaviors of heart rate and respiration frequency are fully consistent with those reported in previous works [70], [77]. Their long-term (α_2) scaling patterns, reflecting the scaling behavior of EEG alpha-band amplitudes, indicate that the long-term (α_2) autonomic control system of the heart is strongly affected by cerebral activity or, alternatively, both are driven by the same regulatory process [80]. Our results for PTT are novel and thus cannot be compared with previously published results. Surprisingly, we found that there were no differences between the short- and long-term fluctuation scaling behavior (i.e., $\alpha_1 = \alpha_2$) during NREM (N2 and N3) sleep. This might indicate that only one control process is relevant for PTT during NREM sleep, and no additional short-term (α_1) correlations are introduced into PTT. This suggests that the autonomic control of short-term (α_1) variations in arterial stiffness and blood pressure seems to be not tight (variations more random than for heartbeat control). Since pronounced short-term correlations ($\alpha_1 > 1$) have been reported for blood pressure

[81], our finding implies that the short-term dynamics of blood pressure and PTT are different and that there seems to be no reliable direct relation between blood pressure and PTT.

Copyright statement

©2022 Zschocke *et al.* This publication is licensed under a Creative Commons Attribution 4.0 International (CC BY 4.0) license .

J. Zschocke, R. P. Bartsch, M. Glos, T. Penzel, R. Mikolajczyk, and J. W. Kantelhardt, „Long- and short-term fluctuations compared for several organ systems across sleep stages“, *Frontiers in Network Physiology*, vol. 2, 2022. DOI: 10.3389/fnetp.2022.937130. Reference [JZ4]



OPEN ACCESS

EDITED BY
Karin Schiecke,
Friedrich Schiller University Jena,
Germany

REVIEWED BY
Niels Wessel,
Humboldt University of Berlin, Germany
Ingo Fietze,
Charité Universitätsmedizin Berlin,
Germany

*CORRESPONDENCE
Jan W. Kantelhardt,
jan.kantelhardt@physik.uni-halle.de

SPECIALTY SECTION
This article was submitted to Systems
Interactions and Organ Networks,
a section of the journal
Frontiers in Network Physiology

RECEIVED 05 May 2022
ACCEPTED 08 August 2022
PUBLISHED 09 September 2022

CITATION
Zschocke J, Bartsch RP, Glos M,
Penzel T, Mikolajczyk R and
Kantelhardt JW (2022), Long- and
short-term fluctuations compared for
several organ systems across
sleep stages.
Front. Netw. Physiol. 2:937130.
doi: 10.3389/fnetp.2022.937130

COPYRIGHT
© 2022 Zschocke, Bartsch, Glos, Penzel,
Mikolajczyk and Kantelhardt. This is an
open-access article distributed under
the terms of the [Creative Commons
Attribution License \(CC BY\)](#). The use,
distribution or reproduction in other
forums is permitted, provided the
original author(s) and the copyright
owner(s) are credited and that the
original publication in this journal is
cited, in accordance with accepted
academic practice. No use, distribution
or reproduction is permitted which does
not comply with these terms.

Long- and short-term fluctuations compared for several organ systems across sleep stages

Johannes Zschocke^{1,2}, Ronny P. Bartsch³, Martin Glos⁴,
Thomas Penzel⁴, Rafael Mikolajczyk¹ and Jan W. Kantelhardt^{2*}

¹Institute of Medical Epidemiology, Biometrics and Informatics (IMEBI), Interdisciplinary Center for Health Sciences, Martin-Luther-University Halle-Wittenberg, Halle, Germany, ²Institute of Physics, Martin-Luther-University Halle-Wittenberg, Halle, Germany, ³Department of Physics, Bar-Ilan University, Ramat Gan, Israel, ⁴Interdisciplinary Sleep Medicine Center, Charité - Universitätsmedizin Berlin, Berlin, Germany

Some details of cardiovascular and cardio-respiratory regulation and their changes during different sleep stages remain still unknown. In this paper we compared the fluctuations of heart rate, pulse rate, respiration frequency, and pulse transit times as well as EEG alpha-band power on time scales from 6 to 200 s during different sleep stages in order to better understand regulatory pathways. The five considered time series were derived from ECG, photoplethysmogram, nasal air flow, and central electrode EEG measurements from full-night polysomnography recordings of 246 subjects with suspected sleep disorders. We applied detrended fluctuation analysis, distinguishing between short-term (6–16 s) and long-term (50–200 s) correlations, i.e., scaling behavior characterized by the fluctuation exponents α_1 and α_2 related with parasympathetic and sympathetic control, respectively. While heart rate (and pulse rate) are characterized by sex and age-dependent short-term correlations, their long-term correlations exhibit the well-known sleep stage dependence: weak long-term correlations during non-REM sleep and pronounced long-term correlations during REM sleep and wakefulness. In contrast, pulse transit times, which are believed to be mainly affected by blood pressure and arterial stiffness, do not show differences between short-term and long-term exponents. This is in contrast to previous results for blood pressure time series, where α_1 was much larger than α_2 , and therefore questions a very close relation between pulse transit times and blood pressure values. Nevertheless, very similar sleep-stage dependent differences are observed for the long-term fluctuation exponent α_2 in all considered signals including EEG alpha-band power. In conclusion, we found that the observed fluctuation exponents are very robust and hardly modified by body mass index, alcohol consumption, smoking, or sleep disorders. The long-term fluctuations of all observed systems seem to be modulated by patterns following sleep stages generated in the brain and thus regulated in a similar manner, while short-term regulations differ between the organ systems. Deviations from the reported dependence in any of the signals should be indicative of problems in the function of the particular organ system or its control mechanisms.

KEYWORDS

time series analysis, long-term correlations, persistence, scaling analysis, heartbeat, pulse-transit time, respiration, brain-wave amplitudes

1 Introduction

The regulation of quasi-periodic processes in the human body is characterized by high degree of complexity. Therefore, fluctuations in physiological signals often show nonlinear dynamics and correlation behavior with (fractal) scaling relations (Bassingthwaite and Raymond, 1994; West, 2014). For example, a scaling behavior of the power spectra similar to $1/f^\beta$ (“coloured”) noise has been observed in series of time intervals between successive heartbeats, breaths, and steps (Kobayashi and Musha, 1982; Peng et al., 1993b; Hausdorff et al., 1995; Peng et al., 2002; Ivanov et al., 2009). Their dynamics are modified by different physiological states (e.g., sleep/wake, sleep stages) and activities, aging, and under pathological conditions (Ivanov et al., 1999b; Bunde et al., 2000; Hausdorff et al., 2001; Karasik et al., 2002; Goldberger et al., 2002; Kantelhardt et al., 2003; Bartsch et al., 2007). Coloured noise is equivalent to long-term correlations as described by a slowly decaying autocorrelation function (“persistence”) (Bunde et al., 2000; Kantelhardt, 2011). Short-term correlations, on the other hand, are equivalent to exponentially (i.e., rather quickly) decaying autocorrelations and characterized by white noise fluctuations at low frequencies.

By comparing the correlation behavior of many physiological signals across different states in many subjects, hypotheses regarding the control mechanisms for the underlying physiological systems can be derived. Here, we studied, for the first time, the dynamics of pulse-transit times, from heart to finger, in a similar way as previously done for inter-heartbeat intervals (Peng et al., 1993a; Bunde et al., 2000; Schumann et al., 2010), respiratory intervals (Kantelhardt et al., 2003; Schumann et al., 2010) and brain-wave amplitudes (Kantelhardt et al., 2015). In particular, the dynamics of the control of the pulse-wave propagation—e.g., blood pressure, arterial stiffness, etc.—can potentially be studied (Guo et al., 2022). Changes of the scaling behavior in some subjects can also be used as early indicators or diagnostic tools for pathologies that affect one or many of the studied organ systems (Ivanov et al., 1999a; Goldberger et al., 2002).

Specifically, in this paper based on polysomnography (PSG) recordings from a clinical sleep laboratory, we studied the short- and long-term correlations (“persistence”) in five time series characterizing different organ systems.

- **RRI** (R-R intervals; heart): The time intervals between successive R peaks in the electrocardiogram (ECG) as an expression of autonomic cardiac control.
- **PPI** (pulse to pulse intervals; cardiovascular system): The time intervals between successive pulse wave peaks

derived from a photoplethysmogram (PPG) as an expression of autonomic cardiac control but slightly influenced by pulse wave velocity regulation mechanisms.

- **PTT** (pulse transit times, cardiovascular system): The time intervals between each R peak (in the ECG) and the corresponding pulse wave peak (in the PPG), believed to be an expression of blood pressure (Allen and Kyriacou, 2022) and arterial stiffness.
- **BBI** (breath to breath intervals; respiratory system): The time intervals between successive respiration maxima during the sleep phase as an expression of autonomic respiratory control.
- **EEG** (brain): The alpha-band amplitudes of a centrally recorded electroencephalogram (EEG, electrodes C3 or C4) as an expression of brain dynamics.

Based on previous work in the field, we address the following hypotheses for short-term (α_1) and long-term (α_2) fluctuation exponents, calculated for these five time series and probably related to parasympathetic and sympathetic control, respectively. Our implied medical hypotheses are that deviations from normal dependence should be indicative of problems in the function or control mechanisms of the particular organ system.

- 1) Short-term correlations (α_1) for RRI do slightly depend on sleep stages and have a maximum for intermediate age groups (Schumann et al., 2010).
- 2) Long-term correlations (α_2) for RRI are weaker than short-term correlations and nearly absent during non-REM sleep (N2 and N3), but pronounced during wakefulness and REM sleep (Bunde et al., 2000; Schumann et al., 2010).
- 3) The scaling behavior of RRI and PPI is very similar. This is expected because the two time series are closely linked (Schäfer and Vagedes, 2013).
- 4) The α_2 scaling behavior of BBI is similar to RRI, but the BBI correlations are generally weaker, particularly during wakefulness and REM sleep (Kantelhardt et al., 2003; Schumann et al., 2010). Different trends of α_2 with aging occur for RRI and BBI in REM sleep and wakefulness (Schumann et al., 2010).
- 5) There is no relevant influence of respiratory disorders—in particular, sleep apnea as indicated by the apnea-hypopnea index (AHI)—on the long-term scaling behavior of RRI and BBI (Penzel et al., 2003).
- 6) Average PTTs decrease with aging due to increasing arterial stiffness (Nichols, 2005).

In addition, studying the fluctuation scaling behavior in PTTs for the first time, we address the following novel hypotheses:

- 7) Long-term correlations (α_2) for PTT are similar to BBI.
- 8) Short-term correlations (α_1) for PTT are weaker than for any of the other considered time series, there is hardly any crossover (i.e., $\alpha_1 = \alpha_2$), and α_1 is only weakly changing with age. This hypothesis implies that there is no close relationship between PTT and blood pressure at short time scales, since very strong (even non-stationary, $\alpha_1 > 1$) short-term correlations have previously been reported for blood pressure time series (Galhardo et al., 2009; Fuchs et al., 2010; Castiglioni et al., 2020).
- 9) An increased body mass index (BMI) is associated with increased PTT short-term correlations (α_1) during N2 sleep. Increased alcohol consumption is associated with decreased PTT short-term correlations (α_1) during nocturnal wakefulness but not during sleep.

2 Methods

2.1 Data recordings

We analyzed single night PSG data from 246 subjects with suspected sleep disorders recorded in clinical sleep laboratories at the Charité-Universitätsmedizin Berlin, Germany, between April 2017 and March 2019. The study was approved by the ethics committee of the Charité-Universitätsmedizin Berlin and registered at the German Clinical Trial Register (DRKS) with ID DRKS00016908. All enrolled subjects gave written informed consent prior to the study. Full PSG including EEG, electrooculogram (EOG), electromyogram (EMG), ECG, PPG, oxygen saturation, and respiratory effort was recorded using either an Embla® (Natus, Pleasanton, United States) or a SOMNOscreen™ PSG system (SOMNOmedics, Randersacker, Germany). The final used data set consisted of single-night recordings of 130 female and 116 male participants with body mass index 28.3 ± 6.2 (17.0, 51.9) kg/m², age 51.2 ± 14.2 (18, 79.6) years, and time in bed 7.5 ± 0.8 (2.3, 7.9) hours [mean \pm standard deviation (minimum, maximum)].

All recordings were part of diagnostic examination and were classified by the current rules of the International Classification of Sleep Disorders (ICSD-3); multiple diagnoses are possible. The dataset includes 12 subjects without sleep disorders, 132 subjects with sleep-related breathing disorders, 70 subjects with insomnia, 32 subjects with central disorders of hypersomnolence, 37 subjects with sleep-related movement disorder, 8 subjects with parasomnias and 8 subjects with circadian rhythm sleep-wake disorders.

2.2 Data preprocessing

Each measurement was cropped to only contain data between the 'lights off' and 'lights on' time stamps, indicating beginning and end of the sleep opportunity period, respectively. Sleep stages based on 30-second epochs have been determined from the PSG data by trained experts following standard guidelines of the American Academy of Sleep Medicine (AASM) (Berry et al., 2018) to distinguish light sleep (stages N1 and N2), deep sleep (stage N3), and rapid eye movement (REM) sleep. We disregarded the N1 sleep episodes, since they were too short for the time series analysis in most subjects, hence distinguishing nocturnal wakefulness, N2, N3, and REM sleep.

Heartbeats were detected as R peaks in the ECGs using the Biosppy algorithm (Carreiras et al., 2015). Intervals between successive R peaks (RRIs) were regarded as normal if 1) $RRI_i > 330$ ms, 2) $RRI_i < 2000$ ms, and 3) $0.7 RRI_{i-1} < RRI_i < 1.6 RRI_{i-1}$. Non-normal RRIs were discarded and the remaining data segments stitched together. Chen et al. (2002) and Ma et al. (2010) have shown that cutting out and stitching together data segments obtained from discontinuous experimental recordings does not affect the outcome of the Detrended Fluctuation Analysis (DFA, see Section 2.3). From the normal RRIs, we calculated the average heartbeat interval, the standard deviation of normal-to-normal intervals (SDNN), and the standard deviations of the RRI increments (i.e., the root mean sum of squared distance, RMSSD) applying standard heart rate variability (HRV) analysis (Malik, 1996).

Pulse wave peaks were extracted from the PPGs using the intersecting tangents method (Hemon and Phillips, 2016). This approach determines the intersection between the tangent of the PPG slopes maximum and the (horizontal) tangent of its minimum, yielding the point of pulse arrival at the finger tip. We have also considered other definitions of pulse wave peaks, such as maxima or minima of the PPG signal, but—as in Hemon and Phillips, (2016)—the intersecting tangents method showed the best correspondence with R peaks. The reason behind this observation lies in the changes of pulse wave shape with aging, since the systolic peak of the pulse wave gets broader with increasing age, and therefore more inaccurate in comparison to heart beats (Kelly et al., 1989). We have also applied an offset correction (subtracting a moving average over 3 s) and a low pass filter [moving average over 0.1 s (Hemon and Phillips, 2016)] to the raw PPG signal. In order to calculate the tangent at the point of maximal slope, we used the first derivative of the PPG signal, which was high pass filtered again (moving average over 0.1 s), to reduce noise. Intervals between successive pulse wave peaks (PPIs) were regarded as normal within the same limits as for RRIs. Again, non-normal PPIs were discarded and the remaining data segments stitched together, and averages as well as statistics corresponding to SDNN and RMSSD were calculated.

Pulse transit times (PTTs) were defined as time differences between a detected R peak and the corresponding pulse wave

peak at the finger. Specifically, the pulse wave peak had to occur between 0.1 and 0.8 s after the R peak. Due to missing pulse wave peaks (temporarily low quality PPG signal, etc.) not every R peak could be matched with a corresponding pulse wave peak. All successfully derived segments of PTT series ($0.1 \text{ s} < \text{PTT}_i < 0.8 \text{ s}$) were stitched together, and averages as well as standard deviations and standard deviations of the increments were calculated.

Respiratory cycles were detected in the respiratory flow signal by identification of the maxima. The signal was preprocessed by subtracting a 10 s moving average and applying a high pass filter (1 s moving average); see Leube et al. (2020) for details. We have also considered other methods to derive respiratory intervals, but—as we focused on respiration cycles rather than the true respiration onset—the maxima methods turned out to be the most robust approach. Intervals between successive respiration peaks (BBIs) were regarded as normal if 1) $\text{BBI}_i > 2 \text{ s}$, 2) $\text{BBI}_i < 8 \text{ s}$, and 3) $0.7 \text{ BBI}_{i-1} < \text{BBI}_i < 1.6 \text{ BBI}_{i-1}$. Non-normal BBIs were discarded and the remaining data segments stitched together.

Brain-wave amplitudes for the alpha-band were derived from the C4 (or C3) electrode EEG recordings by 1) employing the Fourier filtering technique (Theiler et al., 1992) to extract the alpha-band oscillations in the range from 7 to 12 Hz, 2) applying a Hilbert transform to determine the instantaneous amplitudes for each sampling point of the recording, and 3) re-sampling to one amplitude value per second (rate 1 Hz). For a detailed description of the procedure, we refer to Kantelhardt et al. (2015).

2.3 Detrended fluctuation analysis to characterize correlation behavior

In the final step of our analysis procedure, for each subject, we split all time series according to sleep stages (wakefulness, N2, N3, REM sleep), applied DFA with second order polynomial detrending (DFA2), and averaged the fluctuation functions for each stage with statistical weights corresponding to the duration of each episode. The DFA method first introduced by Peng et al. (1994) for studying DNA sequences has been intensely applied to study persistence (auto-correlations) in noisy, non-stationary time series and later been improved for higher-order detrending (Bunde et al., 2000). The method quantifies fluctuations on different time scales s , see Kantelhardt et al. (2001) for details. In brief, for each s the integrated (cumulated) signal of length N is split into non-overlapping pieces (segments) of length s . Within each segment an n -th order polynomial fit is subtracted, and the remaining mean-square fluctuations are averaged. Repeating the procedure for many scales s yields the square of the DFA function $F(s)$, which corresponds to a detrended standard deviation on many time scales s .

In case of long-term (power-law) correlated data without trends, the scaling behavior of the fluctuation function, $F(s) \sim s^\alpha$ with scaling exponent $\alpha > 0.5$, is equivalent to a scaling of the

signal's power spectrum, $P(f) \sim f^{-\beta}$ with frequency f and $\beta = 2\alpha - 1$ (Bartsch et al., 2005). If the data is stationary, i.e., $\alpha < 1$ and $\beta < 1$, this is also equivalent to a scaling of the autocorrelation function $C(s) \sim s^{-\gamma}$ with $\gamma = 2(1 - \alpha) = 1 - \beta$ (Bashan et al., 2008). The advantage of using DFA and studying $F(s)$ instead of $P(f)$ or $C(s)$ lies mainly in the detrending capability, that allows analyzing nonstationary data. For data with only short-term correlations, the scaling exponents approach $\alpha = 0.5$ and $\beta = 0$ for asymptotically large s and small f , respectively. By determining the effective scaling exponents α_1 and α_2 for small and large scales, respectively, we can distinguish the scaling behavior of short- and long-term fluctuations.

Figure 1 shows such DFA functions on a double-logarithmic plot for an exemplary subject, the four different nocturnal sleep stages, and all five time series as described in the Introduction. In addition, we shaded in gray the areas for determining short-term scaling exponents α_1 (from 6 to 16 s) and for long-term scaling exponents α_2 (from 50 to 200 s). A scaling exponent α is, by definition, the linear slope of the fluctuation function in the double-logarithmic plot. In Figure 1 the corresponding linear fits for α_1 and α_2 are plotted as black lines.

Short-term and long-term scaling exponents were calculated for each subject, each signal, and each stage. However, to ensure the data quality, in further analysis only scaling exponents with coefficient of determination $r^2 > 0.9$ were included. Since the total durations of the sleep stages differ, we report the results for each stage separately and did not calculate weighted averages over the entire sleep period.

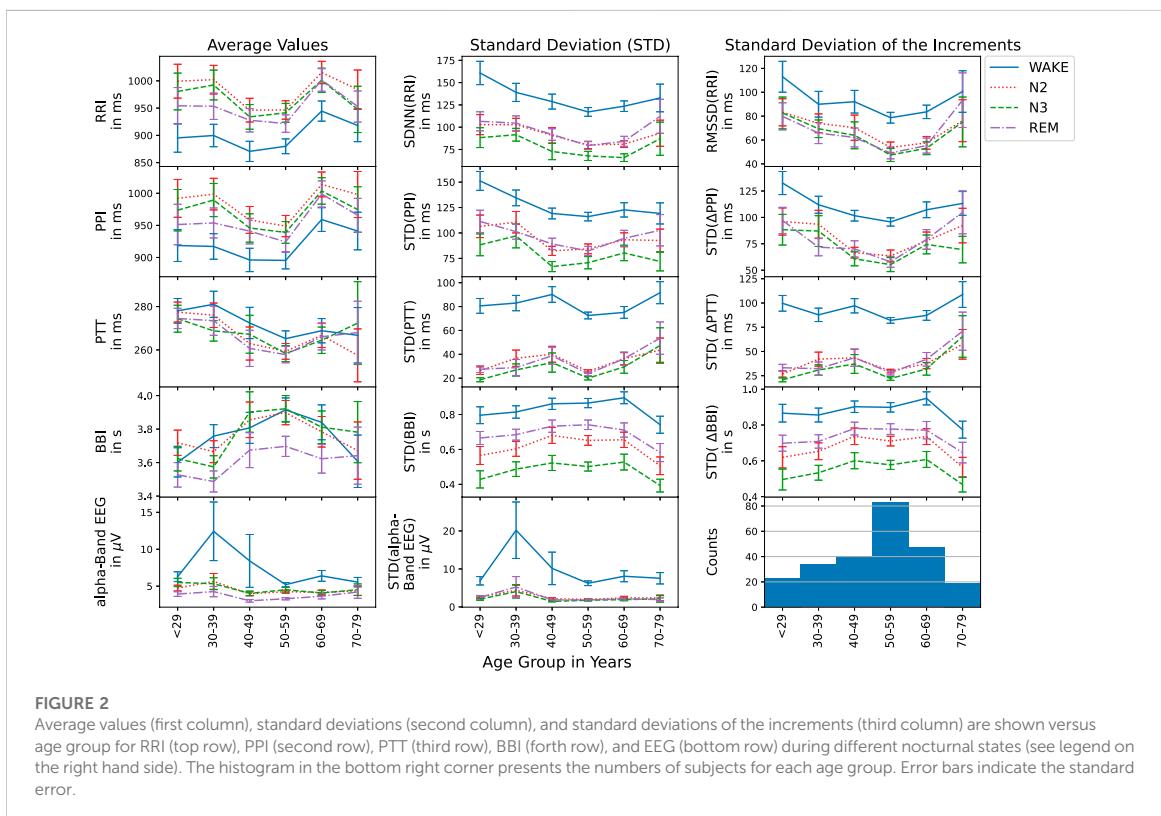
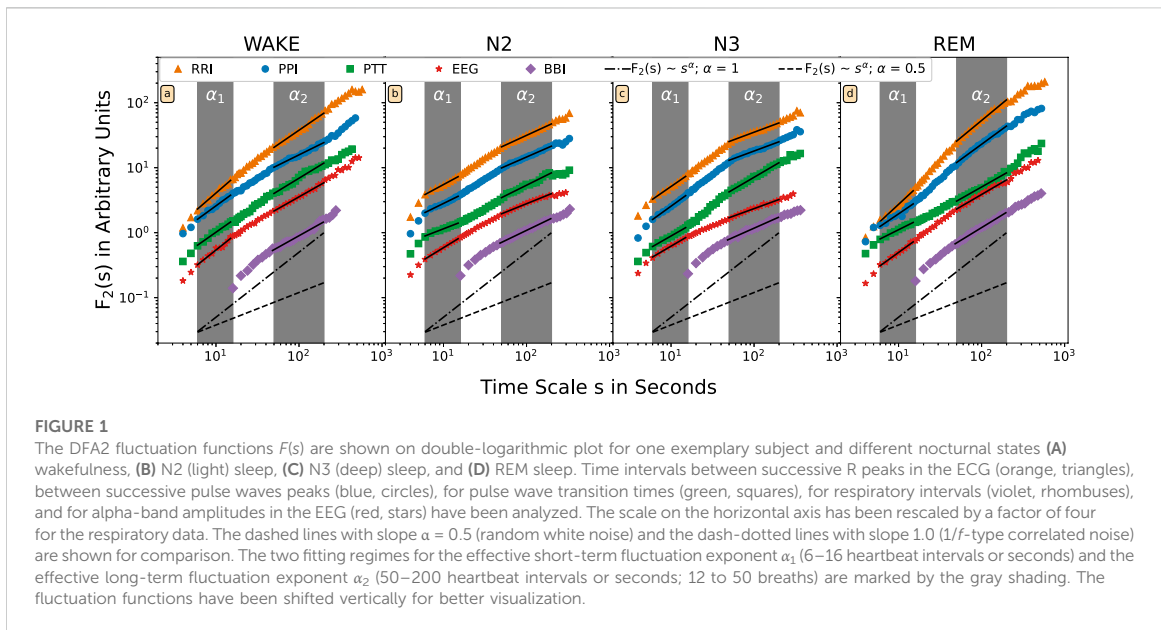
3 Results

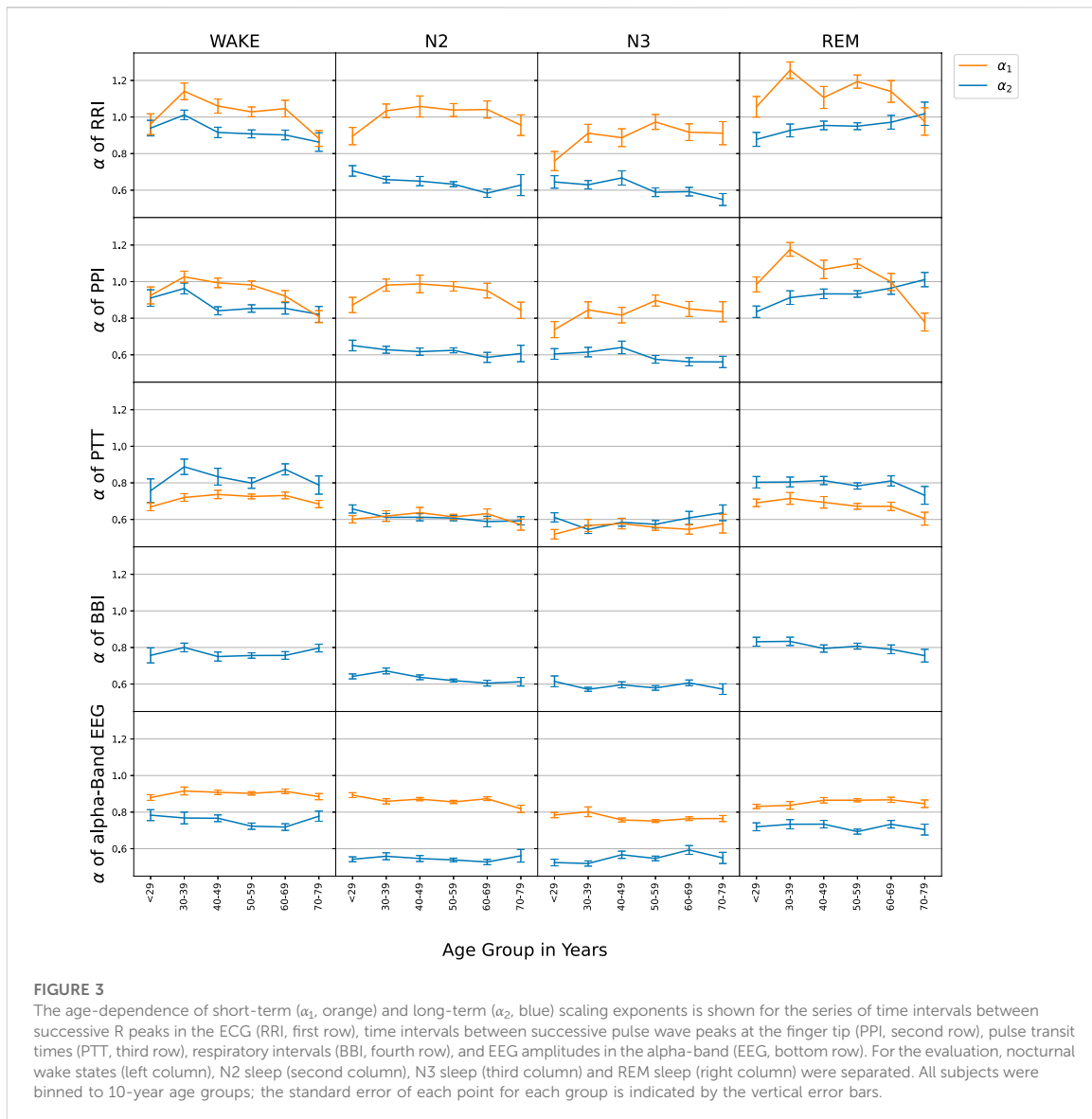
The following results are averages of each considered quantity for the whole group of subjects, often divided into 10-year age groups¹; see the bottom right histogram in Figure 2 for the age distribution in our sample. In all cases, the four nocturnal states, wakefulness, N2, N3, and REM sleep have been studied separately.

3.1 Age dependencies of averages and variabilities

First, we studied the average values, the standard deviations (corresponding to the HRV parameter SDNN for heartbeat intervals) and standard deviations of the increments (corresponding to the HRV parameter RMSSD for heartbeat intervals) for all five time series, RRI, PPI, PTT, BBI and EEG (see Introduction) to check if they follow the physiological

¹ The age group 29 years contains two subjects below 20 years; both are 18 years old.





expectations. Figure 2 shows these three standard parameters versus the age groups. As Schmitt et al. (2009) have already shown for RRI and two age groups, there is an age dependence as well as differences between the sleep stages. As expected, average RRIs were shortest during wake, while at the same time, SDNN and RMSSD showed the largest values. The parameters during N2 and REM were always very similar. For N3 (deep sleep), however, slightly lower values of SDNN were observed. For all three statistical parameters, minimum values occurred around the 50–59 years old group in all stages. As also expected (see Hypothesis 3 in the Introduction), exactly the same behavior of

the statistical parameters was observed for PPI, since RRI and PPI are closely related during rest and sleep as already reported by Schäfer and Vagedes, (2013).

The study of PTTs in the third row of Figure 2 yielded the expected behavior that generally average PTTs decrease with age (see Hypothesis 6). This occurred for all nocturnal stages, although slight deviations for the first and last age group cannot be excluded within the error bars (standard error). Standard deviations of PTT and standard deviation of PTT increments showed similarly small values during all three sleep stages, but much larger values (by a factor of

approximately three) during nocturnal wakefulness. The generally increasing but somewhat non-monotonous trend with increasing age was identical for both standard deviation parameters and all nocturnal states.

The breathing intervals exhibited the most pronounced differences between N2, N3 and REM sleep. While average BBI were shortest during REM sleep and of similar length for N2 and N3 sleep, the two standard deviation parameters were smallest during N3, followed by N2 and REM as expected. Wakefulness yielded the largest BBI standard deviations. Each standard deviation parameter showed the same age dependence for all sleep stages. However, for the average respiration period, BBI, a slightly different age dependence was observed during wakefulness.

EEG alpha-band brain wave amplitudes, also showed the expected behavior with clearly much larger values during wakefulness as compared to sleep. These differences seem to become slightly weaker with increasing age.

3.2 Age dependences of short- and long-term correlations

Figure 3 summarizes the results of the DFA2 fluctuation scaling analysis for the five considered time series during different sleep stages. The results for short-term correlations of RRI (α_1) in the first row confirmed our Hypothesis 1, although the maximum for intermediate age groups was a bit broader than in Schumann et al. (2010) and reached the largest values at lower ages (≈ 35 instead of ≈ 55 years). The long-term correlations of RRI (α_2) in the first row together with the results for brain-wave amplitudes in the bottom row clearly confirmed our Hypothesis 2. Since the results for PPI (second row) were—within the error bars—identical with those for RRI (first row), our Hypothesis 3 was also confirmed.

The results regarding BBI were also in agreement with Schumann et al. (2010). Since we observed decreasing (increasing) α_2 exponents with aging for RRI and PPI during wakefulness (REM sleep), but slightly decreasing α_2 exponents with aging for BBI during REM sleep, Hypothesis 4 was also confirmed. Note however, that the observed age dependence of BBI during wakefulness was not the same as in Schumann et al. (2010).

Our main findings for PTT confirmed hypotheses (7), long-term correlations (α_2) for PTT were similar to BBI and (8), short-term correlations (α_1) were weaker than for any of the other considered time series. It is important to note that for PTT particularly during non-REM sleep (N2 and N3) short and long-term correlations became identical ($\alpha_1 = \alpha_2$), so that the crossover disappeared. Furthermore, there was no change of PTT α_1 with aging. Such behavior was not observed for any of the other signals. PTT and EEG data did not seem to have a relevant age dependence, except for a possible slight decay of PTT short-term

correlations (α_1) with age above 40 years during wakefulness and REM sleep.

3.3 Influences of sex, BMI, smoking, alcohol consumption, and sleep apnea

Figure 4 shows how the short- and long-term scaling exponents for RRI and PTT depend on sex, BMI, smoking status and alcohol consumption. Interestingly, we found a strong (highly significant, $p < 0.001$) sex dependence of the short-term (α_1) correlations in RRI (as well as those in PPI), which were consistently higher in males than in females across all sleep stages. In contrast, the long-term (α_2) correlations in RRI were not sex depended. For short- and long-term correlation in PTT only marginal differences between males and females were seen, with some significance reached for α_1 during N2, N3, and REM sleep ($p = 0.020, 0.008, 0.032$, respectively).

An increasing BMI led to slightly increasing short-term correlations (α_1) in PTT but not in RRI or any of the other considered signals. Multivariable regression analysis², adjusted for age (in categories of 10 years as shown before) and sex, showed a significant increase of α_1 for PTT with BMI during N2 sleep ($p = 0.010$). The same trend was observed for breathing intervals (BBI, not shown). Body size was associated with short-term correlations (α_1) of the heart (also not shown). However, this effect was mainly due to the increase of male population with increasing body size and therefore not relevant.

Smoking led to a slightly higher heart rate (not shown), but hardly affected SDNN and RMSSD over all sleep stages. In the multivariable regression analysis, short-term correlations (α_1) were significantly decreased for smokers during wakefulness regarding RRI ($p = 0.038$) and during REM sleep regarding PTT ($p = 0.012$), while long-term correlations (α_2) for PTT were significantly increased for smokers during wakefulness ($p = 0.007$) and N3 ($p = 0.021$) sleep (see also Figure 4).

While the mean values of RRI and PPI increased (slower heartbeat) with habitual alcohol consumption, PTT, BBI and EEG amplitudes stayed rather constant. We also saw a decline of PTT and EEG averages and possibly an increase in the average BBI associated with a large increase of BBI standard deviations. Regarding the short- and long-term correlations, only a slight decline of α_1 (short-term correlations) for RRI during N3 sleep ($p = 0.048$) and for PTT with increasing alcohol consumption was significant during wakefulness ($p = 0.029$).

Among the many possible disorders, our sample is most suitable for addressing the effects of sleep apnea. This sleep-related breathing disorder can be classified by the apnea hypopnea index (AHI), which is defined as the average

² Multivariable regression analysis was done in python using the package *statsmodels* from Seabold and Perktold, (2010).

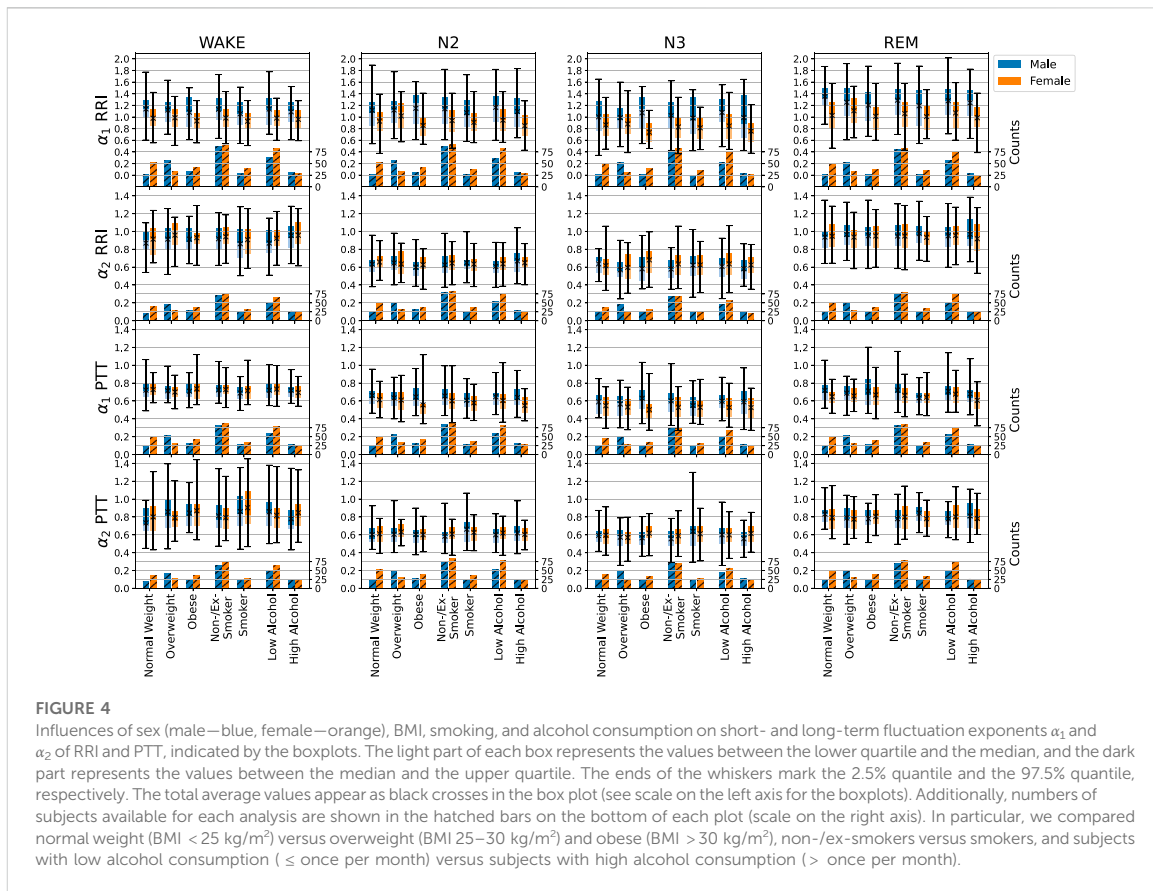


FIGURE 4

Influences of sex (male—blue, female—orange), BMI, smoking, and alcohol consumption on short- and long-term fluctuation exponents α_1 and α_2 of RRI and PTT, indicated by the boxplots. The light part of each box represents the values between the lower quartile and the median, and the dark part represents the values between the median and the upper quartile. The ends of the whiskers mark the 2.5% quantile and the 97.5% quantile, respectively. The total average values appear as black crosses in the box plot (see scale on the left axis for the boxplots). Additionally, numbers of subjects available for each analysis are shown in the hatched bars on the bottom of each plot (scale on the right axis). In particular, we compared normal weight (BMI < 25 kg/m²) versus overweight (BMI 25–30 kg/m²) and obese (BMI > 30 kg/m²) versus non-/ex-smokers versus smokers, and subjects with low alcohol consumption (\leq once per month) versus subjects with high alcohol consumption ($>$ once per month).

number of apneas and hypopneas per hour of sleep. We distinguished healthy subjects (AHI < 5/h), mild apnea (5–15/h), moderate apnea (15–30/h), and severe apnea ($>$ 30/h). While the mean values of RRI, PPI, and PTT clearly decreased with increasing AHI during all four considered states, their standard deviations were clearly decreasing only during wakefulness. For BBI, we observed an increase of the standard deviation with AHI as expected, since the apneas represent a stopping of respiration. Mean respiratory intervals seemed to peak for the moderate apnea group. Regarding the short- and long-term correlations, however, we did not observe any relevant changes with increasing AHI. This finding is consistent with Penzel et al. (2003) and confirmed our Hypothesis 5. A detailed analysis of five-minute epochs before apneas, after apneas, and far from apneas did not reveal any significant differences in the short- and long-term fluctuation exponents, even if we studied central apneas, obstructive apneas, mixed apneas and hypopneas separately.

Furthermore, we did not see any significant effect of the ICSD-3 classifications on the scaling behavior of RRI, PPI, PTT, BBI, and EEG. This could be due to the small numbers of patients

in some of the subgroups. In particular, we had only 12 subjects without sleep related disease in our control group. As sleep disorders (sleep-related breathing disorders and insomnia) can have several causes and show very large variability, a systematic manifestation in the examined signals (heart rate, pulse transit time, respiration and EEG) is not visible in our method of analysis.

4 Discussion

Our results in Figure 2 showed that the average values, standard deviations and standard deviations of increments for RRI, PPI, PTT, and BBI depend on sleep stages, while some of them change non-linearly with aging. Regarding RRI, i.e., for HRV parameters, similar changes have previously been reported by Schmitt et al. (2009) for young and elderly subjects. For 24 h averages, Umetani et al. (1998) reported that the HRV parameters SDNN and RMSSD decreased till the age of 50–60 years and then stabilized. This is consistent with our observations. Other studies reported decreases of heart rate

and HRV parameters with aging (Voss et al., 2012; Xhyheri et al., 2012; Jensen-Urstad et al., 1997). Since a decreasing heart rate corresponds to increasing average RRI values, these observations are not really coinciding with ours, see Figure 2 top left panel. A reason could be that we focused on subjects with sleep related disorders instead of healthy subjects. Hence, a study with better statistics and a focus on healthy subjects as well as sleep stage distinction is needed for a full clarification.

Furthermore, we found a close similarity between HRV parameters (from RRI, top row in Figure 2) and pulse rate variability parameters (from PPI, second row in Figure 2), confirming our Hypothesis 3 from the Introduction. Chen et al. (2015) and Khandoker et al. (2011) have reported differences between these two kinds of parameters during apnea events, but no differences during normal breathing. Compared with our work, they studied shorter episodes (2–3 min) of apnea or non-apnea data, while we averaged over all identical sleep stages for the whole night, so that the influence of apneas is probably averaged out in our results. We note that Constant et al. (1999) have shown that pulse rate variability can solely be induced by respiratory modulations as in their study on children with a fixed cardiac pace maker rhythm, possible effects of heart rate variability on PPI have been excluded.

To our knowledge, this is the first paper that analyzes long nocturnal series of PTT values, defined by the time intervals between R peaks and corresponding pulse wave peaks at the finger. We confirmed Hypothesis 6 based on Nichols, (2005) that average PTT decreases with aging, likely due to increasing arterial stiffness. There was hardly any sleep-stage dependence of the average PTT values. However, like HRV (i.e., SDNN and RMSSD), the two PTT variability parameters clearly decreased during sleep as compared to wakefulness (see Figure 2 center and right panels). Hardly any further decay in the PTT variabilities occurred from REM to N2 to N3 sleep, although respiratory variability clearly followed this decaying order. No clear age dependence could be observed for PTT or BBI variabilities. More statistics and a focus on healthy subjects is needed for a full clarification of these dependencies.

The results for the correlation behavior on short and long time scales, i.e., the exponents α_1 and α_2 of RRI, PPI, PTT, BBI, and EEG alpha-band amplitude data were presented in Figure 3. Our results regarding RRI and BBI are fully consistent with those reported in previous work (Bunde et al., 2000; Kantelhardt et al., 2003; Schumann et al., 2008; Schumann et al., 2010). In particular, short-term correlations (α_1) for RRI did only weakly depend on sleep stages and had a maximum for intermediate age groups, confirming our Hypothesis 1. This suggests that the short-term autonomic control system of the heart is not strongly affected by sleep-stage related brain activity and that it ages in a non-monotonous way. Further research is needed to clarify the reasons behind this unusual age dependence.

Long-term correlations (α_2) for RRI were weaker than short-term correlations and nearly absent during non-REM sleep (N2 and N3), but pronounced during wakefulness and REM sleep, confirming our Hypothesis 2. This pattern, reflecting the scaling behavior of EEG alpha-band amplitudes, indicates that the long-term autonomic control system of the heart is significantly affected by cerebral activity via sympathetic control, or, alternatively, both are driven by the same regulatory process (Günther et al., 2022). Since the type of long-term correlations strongly differs between non-REM sleep on the one hand and REM sleep or wakefulness on the other hand, this dependence strongly indicates that an influence from the brain is involved, because sleep stages originate in the brain. In our opinion, it is not plausible that an organ or organ system would independently from the brain create correlations that simultaneously change with those in brain dynamics following exactly the same sleep-stage stratification pattern. Again, we observed a very similar behavior for PPIs (cp. first and second row in Figure 3), also confirming our Hypothesis 3 from the Introduction (Schäfer and Vagedes, 2013).

Nevertheless, a comparison of the results for males and females in Figure 4 revealed significant differences, which had not been observed in previous studies of healthy subjects (Schumann et al., 2008; Schumann et al., 2010). In particular, α_1 values were higher in men than in women, while α_2 values were similar. This finding may be related with differences in parasympathetic control in men and women. However, since most of our subjects had some kind of sleep-related disorder (see end of Section 2.1), we cannot exclude an effect of these disorders on our results, and suggest that a scaling analysis of data from a larger group of healthy subjects is needed for a clarification. Possibly, HRV parameters reported to be higher in men than in women (Umetani et al., 1998) may be related with this observation.

Our medical hypothesis is that organ-specific alternations in the long-term fluctuation pattern (which seems to originate in the brain) or short-term fluctuation pattern (with a more local origin) can indicate medical problems related with this organ. For example, if short-term fluctuations of RRI are described by a lower exponent α_1 than expected for the age of the subject, this could be a hint towards premature aging of the cardiovascular system. Or if long-term RRI fluctuations follow a nearly random behavior (low α_2) not only during non-REM sleep, but also during REM sleep and/or wakefulness, this could indicate a diminished sympathetic input. On the other hand, a high α_2 also during non-REM sleep could indicate insufficiency of the cardiovascular system to relax, which in turn may negatively affect sleep quality. However, since we do not have data from subjects with specific cardiac problems or diagnoses, such hypotheses cannot be tested in this study.

Comparing the long-term (α_2) scaling behaviors of RRI and BBI, we confirmed previous reports of a very similar sleep-stage dependence, but somewhat weaker correlations in BBI,

particularly during wakefulness and REM sleep (Kantelhardt et al., 2003; Schumann et al., 2010) (Figure 3), indicating that cerebral activity also influences respiration during sleep. Different trends of α_2 with aging occurred for RRI and BBI in wakefulness and REM sleep, confirming our Hypothesis 4. This suggests that aging affects autonomic cardiac and respiratory control in somewhat different ways. While our results regarding RRI were fully in agreement with Schumann et al. (2010), the trends for aging were less clear for BBI, so that a study with more data and of healthy subjects would be needed for a clarification of this detail.

Our results for the nonlinear dynamics of PTT series on short and long time scales, i.e., their exponents α_1 and α_2 , are novel and thus cannot be directly compared with previously published results. Surprisingly, we found that there were no differences between the short- and long-term fluctuation scaling behavior (i.e., $\alpha_1 = \alpha_2$) during non-REM (N2 and N3) sleep, so that no crossover occurs, see Figure 3. This might indicate that only one control process is relevant for PTT during non-REM sleep, and no additional short-term correlations are introduced into PTT. An alternative interpretation is that the parasympathetic and sympathetic control of PTT are well and identically balanced during the different sleep and wake stages so that practically no crossover occurs. During wakefulness and REM sleep, slight differences between α_1 and α_2 were observed, but—contrary to the behavior of RRI, PPI and EEG amplitude data— α_1 was smaller than α_2 for all age groups.

According to a standard textbook (Allen and Kyriacou, 2022) PTT intervals are mainly affected by blood pressure, although varying levels of arterial stiffness and body and limb positions do also play a certain role. Since body and limb positions do not often change during the sleep phase, their influence does probably not yield a relevant contribution to the observed PTT fluctuations. Moreover, the stroke volume mainly affects the pulse wave amplitude (which we do not study here), but not the timing. Regarding arterial stiffness, we are not aware of specific studies that address their short- and long-term fluctuation behavior, so that currently no conclusions regarding its (sleep-stage or age-dependent) influence on PTT seems possible. Blood pressure, on the other hand, is known to be strongly correlated on short time scales with α_1 values of 1.4 for mice (Galhardo et al., 2009) and 1.2 for humans (Fuchs et al., 2010) during wakefulness, increasing to 1.3–1.4 during the night (Castiglioni et al., 2020). We are not aware of published data regarding differences between the sleep stages. Hence, if the fluctuations of PTT intervals would mainly reflect blood pressure changes, a similarly large α_1 value would have to occur for PTT, which is not the case. Therefore, our result seems to indicate that PTT is only reflecting long-term fluctuations of blood pressure, while short-term correlations of PTT must be dominated by faster and much closer to random fluctuations of arterial stiffness. It thus suggests that the parasympathetic control of short-term variations in arterial stiffness has no short-term memory (variations close to random) and is not directly linked to autonomic cardiac and respiratory control.

The sleep stage dependence of α_2 for PTT is very similar to BBI. This suggests that long-term PTT fluctuations are similarly controlled via the sympathetic nervous system as long-term respiratory fluctuations and also linked to cerebral activity. We did not observe pronounced changes of PTT scaling behavior with aging and only a marginally significant sex dependence, see Figure 3 (third row) and Figure 4 (third and fourth row).

An increased body mass index (BMI) was associated with slightly increased PTT short-term correlations (α_1) during N2 sleep. Increased alcohol consumption was associated with decreased PTT short-term correlations (α_1) during nocturnal wakefulness but not during sleep. For smokers, short-term correlations (α_1) in RRI decreased during wakefulness, while those in PTT decreased during REM sleep; long-term correlations (α_2) in PTT increased during wakefulness and N3 sleep. We think that a study with more subjects is needed to confirm these apparently not very systematic effects, before a medical interpretation can be provided. Nevertheless, the observation of changes for PTT but (in most cases) not for the other considered signals suggests that PTTs yield independent information, probably related with changes in arterial stiffness control and should be included in subsequent work.

Consistent with previous reports [see, e.g., Penzel et al. (2003)] we did not observe any relevant changes of the scaling behaviors of either RRI, PPI, PTT, BBI, or EEG alpha-band amplitudes with increasing disease severity of apnea (i. e., AHI) nor with other sleep disorders. This suggests that the observed scaling behaviors of these signals and their long-term autonomic control are very robust. However, studies with a larger samples are needed for clarification.

Limitations of our study include our sample size of just 246 subjects, mainly with sleep related disorders, while most previous studies regarding temporal correlations in biosignals and HRV focused on healthy subjects.

5 Summary and conclusion

We confirmed the sleep-stage and age dependence of basic statistical parameters characterizing cardiovascular, respiratory, and brain dynamics, including mean RRI and its deviations (SDNN, RMSSD), mean PPI and its deviations, mean PTT and its deviations, mean BBI and its deviations and mean EEG alpha-band amplitude and its deviation during different sleep stages. Additionally, we investigated systematically aspects of nonlinear dynamics and the correlation behavior of these time series by calculating the DFA exponents α_1 and α_2 . While the long-term correlations (α_2) of all analyzed physiological systems follow the same sleep-stage stratification pattern, indicating a common regulatory mechanism, short-term correlations do hardly vary across sleep stages and may be governed by organ-specific physiological processes. Surprisingly, PTT is an exception from this rule, since

we have observed a complete absence of additional short-term fluctuations, i.e., $\alpha_1 \approx \alpha_2$ across all age groups and sleep stages. This result indicates that short-term PTT fluctuations do not reflect short-term blood pressure fluctuations, which are rather characterized by very different exponents $\alpha_1 > 1$.

Data availability statement

The data are available from the project “Long- and short-term fluctuations compared for several organ systems across sleep stages” at OSFHOME (osf.io; location Frankfurt, Germany) under the doi [10.17605/OSF.IO/3R4PU](https://doi.org/10.17605/OSF.IO/3R4PU).

Ethics statement

The studies involving human participants were reviewed and approved by Ethics Committee of the Charité-Universitätsmedizin Berlin. The patients/participants provided their written informed consent to participate in this study.

Author contributions

JZ and JK implemented the methodology, analyzed the data, and wrote the first draft of the manuscript. JZ prepared all figures; JK supervised the work of JZ. MG, and TP acquired the data in their sleep laboratories. All authors participated in discussions and in writing the manuscript. RM, RB, and TP acquired funding for the project.

References

- Allen, J., and Kyriacou, P. (2022). *Photoplethysmography*. Academic Press.
- Bartsch, R., Hennig, T., Heinen, A., Heinrichs, S., and Maass, P. (2005). Statistical analysis of fluctuations in the ECG morphology. *Phys. A* 354, 415–431. doi:10.1016/j.physa.2005.03.019
- Bartsch, R., Plotnik, M., Kantelhardt, J. W., Havlin, S., Giladi, N., and Hausdorff, J. M. (2007). Fluctuation and synchronization of gait intervals and gait force profiles distinguish stages of Parkinson's disease. *Phys. A* 383, 455–465. doi:10.1016/j.physa.2007.04.120
- Bashan, A., Bartsch, R., Kantelhardt, J. W., and Havlin, S. (2008). Comparison of detrending methods for fluctuation analysis. *Phys. A* 387, 5080–5090. doi:10.1016/j.physa.2008.04.023
- Bassingthwaite, J. B., and Raymond, G. M. (1994). Evaluating rescaled ranged analysis for time series. *Ann. Biomed. Eng.* 22, 432–444. doi:10.1007/BF02368250
- Berry, R. B., Albertario, C. L., Harding, S. M., Lloyd, R. M., Plante, D. T., Quan, S. F., et al. (2018). Darien, IL. The AASM manual for the scoring of sleep and associated events: Rules, terminology and technical specifications, version 2.5. *Am. Acad. Sleep Med.*
- Bunde, A., Havlin, S., Kantelhardt, J. W., Penzel, T., Peter, J. H., and Voigt, K. (2000). Correlated and uncorrelated regions in heart-rate fluctuations during sleep. *Phys. Rev. Lett.* 85, 3736–3739. doi:10.1103/PhysRevLett.85.3736
- Carreiras, C., Lourenço, A., Canento, F., Silva, H., and Fred, A. (2015). *Biosppy: Biosignal processing in python*. Available at: <https://github.com/PIA-Group/BioSPpy/> (Accessed March, 2022).
- Castiglioni, P., Omboni, S., Parati, G., and Faini, A. (2020). Day and night changes of cardiovascular complexity: A multi-fractal multi-scale analysis. *Entropy* 22, 462. doi:10.3390/e22040462
- Chen, Z., Ivanov, P. C., Hu, K., and Stanley, H. E. (2002). Effect of nonstationarities on detrended fluctuation analysis. *Phys. Rev. E* 65, 041107. doi:10.1103/PhysRevE.65.041107
- Chen, X., Huang, Y.-Y., Yun, F., Chen, T.-J., and Li, J. (2015). Effect of changes in sympathovagal balance on the accuracy of heart rate variability obtained from photoplethysmography. *Exp. Ther. Med.* 10, 2311–2318. doi:10.3892/etm.2015.2784
- Constant, I., Laude, D., Murat, I., and Elghozi, J.-L. (1999). Pulse rate variability is not a surrogate for heart rate variability. *Clin. Sci.* 97, 391. doi:10.1042/CS19990062
- Fuchs, K., Schumann, A. Y., Kuhnhold, A., Guzik, P., Piskorski, J., Schmidt, G., et al. (2010). “Comparing analysis of heart rate and blood pressure fluctuations in healthy subjects,” in Proc. 6th Conference of the European Study Group on Cardiovascular Oscillations, Berlin, Germany.
- Galhardo, C. E. C., Penna, T. J. P., Argollo de Menezes, M., and Soares, P. P. S. (2009). Detrended fluctuation analysis of a systolic blood pressure control loop. *New J. Phys.* 11, 103005. doi:10.1088/1367-2630/11/10/103005
- Goldberger, A. L., Amaral, L. A. N., Hausdorff, J. M., Ivanov, P. C., Peng, C.-K., and Stanley, H. E. (2002). Fractal dynamics in physiology: Alterations with disease and aging. *Proc. Natl. Acad. Sci. U. S. A.* 99 (1), 2466–2472. doi:10.1073/pnas.012579499

Funding

This work was supported in part by German Israeli Foundation (GIF) Grant no I-1372-303.7/2016 and by the German National Cohort (GNC) (www.nako.de), funded by the Federal Ministry of Education and Research (BMBF) and the Helmholtz Association.

Acknowledgments

The authors would like to thank Antonia Graf, Maria Kluge, Luise Pelikan (Charité-Universitätsmedizin Berlin) for data acquisition in the sleep laboratories.

Conflict of interest

The authors declare that the research was conducted in the absence of any commercial or financial relationships that could be construed as a potential conflict of interest.

Publisher's note

All claims expressed in this article are solely those of the authors and do not necessarily represent those of their affiliated organizations, or those of the publisher, the editors and the reviewers. Any product that may be evaluated in this article, or claim that may be made by its manufacturer, is not guaranteed or endorsed by the publisher.

- Günther, M., Kantelhardt, J. W., and Bartsch, R. P. (2022). The reconstruction of causal networks in physiology. *Front. Netw. Physiol.* 2. doi:10.3389/fnetp.2022.893743
- Guo, C., Jiang, Z., He, H., Liao, Y., and Zhang, D. (2022). Wrist pulse signal acquisition and analysis for disease diagnosis: A review. *Comput. Biol. Med.* 143, 105312. doi:10.1016/j.combiomed.2022.105312
- Hausdorff, J. M., Peng, C.-K., Ladin, Z., Wei, J. Y., and Goldberger, A. L. (1995). Is walking a random walk? Evidence for long-range correlations in stride interval of human gait. *J. Appl. Physiol.* 78, 349–358. doi:10.1152/jappl.1995.78.1.349
- Hausdorff, J. M., Ashkenazy, Y., Peng, C.-K., Ivanov, P. C., Stanley, H. E., and Goldberger, A. L. (2001). When human walking becomes random walking: Fractal analysis and modeling of gait rhythm fluctuations. *Phys. A* 302, 138–147. doi:10.1016/s0378-4371(01)00460-5
- Hemon, M. C., and Phillips, J. P. (2016). Comparison of foot finding methods for deriving instantaneous pulse rates from photoplethysmographic signals. *J. Clin. Monit. Comput.* 30, 157–168. doi:10.1007/s10877-015-9695-6
- Ivanov, P. C., Amaral, L. A., Goldberger, A. L., Havlin, S., Rosenblum, M. G., Struzik, Z. R., et al. (1999a). Multifractality in human heartbeat dynamics. *Nature* 399, 461–465. doi:10.1038/20924
- Ivanov, P. C., Bunde, A., Amaral, L. N., Havlin, S., Fritsch-Yelle, J., Baevsy, R. M., et al. (1999b). Sleep-wake differences in scaling behavior of the human heartbeat: Analysis of terrestrial and long-term space flight data. *Europhys. Lett.* 48, 594–600. doi:10.1209/epl/1999-00525-0
- Ivanov, P. C., Ma, Q. D., Bartsch, R. P., Hausdorff, J. M., Amaral, L. A. N., Schulte-Frohlinde, V., et al. (2009). Levels of complexity in scale-invariant neural signals. *Phys. Rev. E* 79, 041920. doi:10.1103/PhysRevE.79.041920
- Jensen-Urstad, K., Storck, N., Bouvier, F., Ericson, M., Lindblad, L. E., and Jensen-Urstad, M. (1997). Heart rate variability in healthy subjects is related to age and gender. *Acta Physiol. Scand.* 160, 235–241. doi:10.1046/j.1365-201X.1997.00142.x
- Kantelhardt, J. W., Koscielny-Bunde, E., Rego, H. H., Havlin, S., and Bunde, A. (2001). Detecting long-range correlations with detrended fluctuation analysis. *Phys. A* 295, 441–454. doi:10.1016/S0378-4371(01)00144-3
- Kantelhardt, J. W., Penzel, T., Rostig, S., Becker, H. F., Havlin, S., and Bunde, A. (2003). Breathing during rem and non-rem sleep: Correlated versus uncorrelated behaviour. *Phys. A* 319, 447–457. doi:10.1016/S0378-4371(02)01502-9
- Kantelhardt, J. W., Tismer, S., Gans, F., Schumann, A. Y., and Penzel, T. (2015). Scaling behavior of eeg amplitude and frequency time series across sleep stages. *EPL Europhys. Lett.* 112, 18001. doi:10.1209/0295-5075/112/18001
- Kantelhardt, J. W. (2011). "Fractal and multifractal time series," in *Mathematics of complexity and dynamical systems*. Editor R. Meyers (New York, NY: Springer). doi:10.1007/978-1-4614-1806-1_30
- Karasik, R., Sapir, N., Ashkenazy, Y., Ivanov, P. C., Dvir, I., Lavie, P., et al. (2002). Correlation differences in heartbeat fluctuations during rest and exercise. *Phys. Rev. E* 66, 062902. doi:10.1103/PhysRevE.66.062902
- Kelly, R., Hayward, C., Avolio, A., and O'Rourke, M. (1989). Noninvasive determination of age-related changes in the human arterial pulse. *Circulation* 80, 1652–1659. doi:10.1161/01.cir.80.6.1652
- Khandoker, A. H., Karmakar, C. K., and Palaniswami, M. (2011). Comparison of pulse rate variability with heart rate variability during obstructive sleep apnea. *Med. Eng. Phys.* 33, 204–209. doi:10.1016/j.medengphy.2010.09.020
- Kobayashi, M., and Musha, T. (1982). 1/f fluctuation of heartbeat period. *IEEE Trans. Biomed. Eng.* 29, 456–457. doi:10.1109/TBME.1982.324972
- Leube, J., Zschocke, J., Kluge, M., Pelikan, L., Graf, A., Glos, M., et al. (2020). Reconstruction of the respiratory signal through eeg and wrist accelerometer data. *Sci. Rep.* 10, 14530. doi:10.1038/s41598-020-71539-0
- Ma, Q. D., Bartsch, R. P., Bernal-Galván, P., Yoneyama, M., and Ivanov, P. C. (2010). Effect of extreme data loss on long-range correlated and anticorrelated signals quantified by detrended fluctuation analysis. *Phys. Rev. E* 81, 031101. doi:10.1103/PhysRevE.81.031101
- Malik, M. (1996). Heart rate variability. *Ann. Noninvasive Electrocardiol.* 1, 151–181. doi:10.1111/j.1542-474X.1996.tb00275.x
- Nichols, W. W. (2005). Clinical measurement of arterial stiffness obtained from noninvasive pressure waveforms. *Am. J. Hypertens.* 18, 3S–10S. doi:10.1016/j.amjhyper.2004.10.009
- Peng, C.-K., Buldyrev, S. V., Goldberger, A. L., Havlin, S., Simons, M., and Stanley, H. E. (1993a). Finite-size effects on long-range correlations: Implications for analyzing dna sequences. *Phys. Rev. E* 47, 3730–3733. doi:10.1103/PhysRevE.47.3730
- Peng, C.-K., Mietus, J., Hausdorff, J., Havlin, S., Stanley, H. E., and Goldberger, A. L. (1993b). Long-range anticorrelations and non-Gaussian behavior of the heartbeat. *Phys. Rev. Lett.* 70, 1343–1346. doi:10.1103/PhysRevLett.70.1343
- Peng, C. K., Buldyrev, S. V., Havlin, S., Simons, M., Stanley, H. E., and Goldberger, A. L. (1994). Mosaic organization of dna nucleotides. *Phys. Rev. E* 49, 1685–1689. doi:10.1103/PhysRevE.49.1685
- Peng, C.-K., Mietus, J. E., Liu, Y., Lee, C., Hausdorff, J. M., Stanley, H. E., et al. (2002). Quantifying fractal dynamics of human respiration: Age and gender effects. *Ann. Biomed. Eng.* 30, 683–692. doi:10.1114/1.1481053
- Penzel, T., Kantelhardt, J. W., Grote, L., Peter, J.-H., and Bunde, A. (2003). Comparison of detrended fluctuation analysis and spectral analysis for heart rate variability in sleep and sleep apnea. *IEEE Trans. Biomed. Eng.* 50, 1143–1151. doi:10.1109/TBME.2003.817636
- Schäfer, A., and Vagedes, J. (2013). How accurate is pulse rate variability as an estimate of heart rate variability? A review on studies comparing photoplethysmographic technology with an electrocardiogram. *Int. J. Cardiol.* 166, 15–29. doi:10.1016/j.ijcard.2012.03.119
- Schmitt, D. T., Stein, P. K., and Ivanov, P. C. (2009). Stratification pattern of static and scale-invariant dynamic measures of heartbeat fluctuations across sleep stages in young and elderly. *IEEE Trans. Biomed. Eng.* 56, 1564–1573. doi:10.1109/TBME.2009.2014819
- Schumann, A. Y., Bauer, A., Penzel, T., Schmidt, G., and Kantelhardt, J. W. (2008). "Cardiovascular oscillations and correlations during sleep," in Proc. 5th Conference of the European Study Group on Cardiovascular Oscillations (Parma Italy).
- Schumann, A. Y., Bartsch, R. P., Penzel, T., Ivanov, P. C., and Kantelhardt, J. W. (2010). Aging effects on cardiac and respiratory dynamics in healthy subjects across sleep stages. *Sleep* 33, 943–955. doi:10.1093/sleep/33.7.943
- Seabold, S., and Perktold, J. (2010). Statsmodels: Econometric and statistical modeling with python. *Proc. Python Sci. Conf.*, 92–96. doi:10.25080/Majora-92bf1922-011
- Theiler, J., Eubank, S., Longtin, A., Galdrikian, B., and Farmer, J. D. (1992). Testing for nonlinearity in time series: The method of surrogate data. *Phys. D. Nonlinear Phenom.* 58, 77–94. doi:10.1016/0167-2789(92)90102-S
- Umetani, K., Singer, D. H., McCraty, R., and Atkinson, M. (1998). Twenty-four hour time domain heart rate variability and heart rate: Relations to age and gender over nine decades. *J. Am. Coll. Cardiol.* 31, 593–601. doi:10.1016/S0735-1097(97)00554-8
- Voss, A., Heitmann, A., Schroeder, R., Peters, A., and Perz, S. (2012). Short-term heart rate variability-age dependence in healthy subjects. *Physiol. Meas.* 33, 1289–1311. doi:10.1088/0967-3334/33/8/1289
- West, B. J. (2014). A mathematics for medicine: The network effect. *Front. Physiol.* 5, 456. doi:10.3389/fphys.2014.00456
- Xhyheri, B., Manfrini, O., Mazzolini, M., Pizzi, C., and Bugiardini, R. (2012). Heart rate variability today. *Prog. Cardiovasc. Dis.* 55, 321–331. doi:10.1016/j.pcad.2012.09.001

4.3 Preliminary results of DFA in accelerometry data

Finally preliminary results based on accelerometry data are presented. We investigated the scaling behavior of simultaneously measured hip and wrist accelerometry in different activity categories.

4.3.1 Preprocessing of accelerometry data

The NAKO Gesundheitsstudie provided us with a subsample of 3000 datasets, where subjects wore an accelerometer at the wrist (SOMNOwatch) and one at the hip (ActiGraph). While the hip data were recorded for 7 days, the wrist recording was only about 24 hours. From previous analysis, we had already calculated the 5 second MAD values (5s-MAD, see Eq. 2.3) of the hip data, with the GGIR package [50]. Thus, we had only to calculate the 5s-MAD of the wrists' datasets. In order to assure synchronicity, in a first step, time series of hip and wrist were synchronized by their timestamps. As a second step, cross-correlation were calculated in the 5s-MAD time series in blocks of two hours, to identify offsets and drifts. Recordings with little drift (less than 5 seconds) were used and corrected based on the offset. Furthermore, the 7 day hip measurement was shortened to the matching 24 hour recording from the wrist. In total, 2798 datasets could be successfully matched and analyzed.

4.3.2 Classification of accelerometry data

Wrist and hip accelerometry differ because of their wearing places. The wrist is moved more frequently and with higher intensity in comparison to the hip. That leads to a better usability of wrist accelerometry for sleep and low activity classification, while hip accelerometry is better suited for scoring physical activity [83], [84].

As already mentioned, we used the 5s-MAD values, which agglomerate the 3D data to one time series, and also reduce storage space and computing time. In Fig. 4.3 5s-MAD of the wrist is plotted versus the 5s-MAD of the hip in a double logarithmic plot. The resulting curve reminds of a boomerang, and was introduced in the author's master thesis [85]. For low hip activity (1 to 10 mg) the wrist activity varies by a factor of ten (0.5 to 100 mg). On the other hand, for higher wrist activity (50 to 200 mg), the hip activity varies from 2 to 500 mg. Therefore, wrist accelerometer measurements provide more accurate results for sleep and sedentary activity, while hip measurements provide better resolution for more intense physical activity. In addition, the curve contains also example activities, like standing still, sweeping etc, reported by [82].

As shown in Fig. 4.3 the data was ad-hoc divided in to four activity classes and an outlier area. Values are scored as outliers, if

- $5s\text{-MAD Wrist} < 5s\text{-MAD Hip} \cdot 0.05$ or
- $5s\text{-MAD Wrist} > 5s\text{-MAD Hip} \cdot 100$

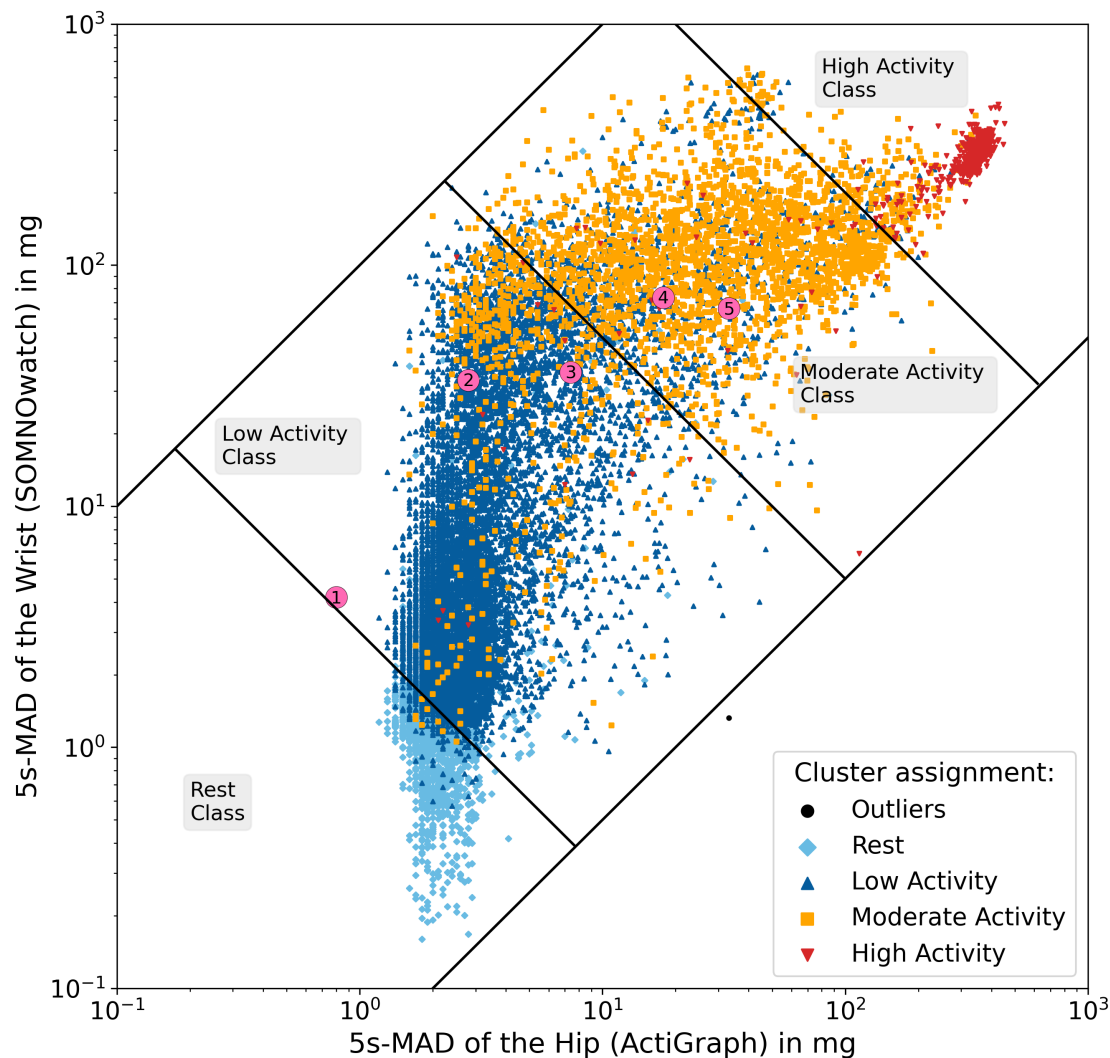


Figure 4.3: **Boomerang curve.** 5s-MAD values for hip (ActiGraph) and wrist (SOMNOwatch) are plotted against each other. Four activity classes were defined based on hip and wrist values (see gray labels). For further analysis, 12 consecutive data points were always combined and assigned to the majority's activity class, which is why there are deviations between the classes and the cluster assignment. Magenta numbered dots are example activities: (1) standing still, (2) washing pots, (3) dusting, (4) sweeping floor, (5) self-paced free-living walk, as reported in [82]. Accelerometry data is from a subject of the NAKO Gesundheitsstudie, see Subsection 2.3.1.

4.3. Preliminary results of DFA in accelerometry data

After all outliers were removed for further analysis, the following terms were applied:

- **Rest:** $5s\text{-MAD Wrist} \cdot 5s\text{-MAD Hip} < 3 \text{ mg}^2$
- **Low activity:** $3 \text{ mg}^2 \leq 5s\text{-MAD Wrist} \cdot 5s\text{-MAD Hip} < 500 \text{ mg}^2$
- **Moderate activity:** $500 \text{ mg}^2 \leq 5s\text{-MAD Wrist} \cdot 5s\text{-MAD Hip} < 20000 \text{ mg}^2$
- **High activity:** $20000 \text{ mg}^2 \leq 5s\text{-MAD Wrist} \cdot 5s\text{-MAD Hip}$

In order to have longer uninterrupted activity clusters and to apply DFA to these activity clusters, we looked into 12 consecutive data points (1 minute) and assigned all 12 data points to the majorities' class. For this reason, the activity scoring in Fig. 4.3 differs from the defined classes.

4.3.3 Results and discussion of accelerometry DFA

DFA2 was applied to hip and wrist 5s-MAD time series. In addition, time series snippets of the same activity cluster type were stitched together. The scaling exponent was investigated in three regimes: α_2 (50 to 200 seconds), α_3 (5 to 20 minutes) and α_4 (0.5 to 2 hours)¹. The exponent α was calculated in the same way as described in the publication in Section 4.2 [JZ4].

In Fig. 4.4 the three scaling exponents of hip and wrist accelerometry are shown for different activity clusters. The exponents α are plotted versus age, in bins of 10 years, and split by sex. An age dependency can hardly be seen. For the analysis combining all activity levels we see a slight decrease of α_2 with age and an increase of α_4 with age. While the wrist data hardly exhibits crossovers ($\alpha_i \approx 1$, for $i = 2, 3, 4$), the hip data shows a crossover from $\alpha_2 > 1$ to $\alpha_4 < 1$ in all age groups. In contrast, Hu *et. al* found a slight decrease of α with age on very long time scales (> 1.5 hours). In general, we found no sex dependencies either. Whereas Raichlen *et. al* [86] found for α in the range of 10 minutes to 7 hours a slight, but clear age and sex dependency.

However, we can see clear differences between the activity clusters. Rest has the lowest exponents, followed by low and moderate activity. Both are very similar, and the highest exponent is observed for the high activity cluster. This can also be found in literature [86]–[88].

DFA2 for the whole 24 hour time series reveals exponents close to 1.0, which can also be found in literature, where Hu *et. al* reported $\alpha = 0.93$ for a time scale of minutes to hours for wrist actigraphy, but this value seems to be dependent on week days [89]. Besides Ivanov *et. al* report a similar value of $\alpha = 0.9$ [90]. Higher activities will dominate the DFA results and therefore, we generally find higher exponents α , in the analysis combining all activity clusters.

Comparing the hip and wrist accelerometry, we can see, a higher exponent in hip accelerometry, in time ranges of a few minutes (α_2), except for the rest cluster. In the time range of 5 to 20 minutes (α_3), only differences for low and moderate activity

¹The scaling exponents start with α_2 , to be consistent with [JZ4].

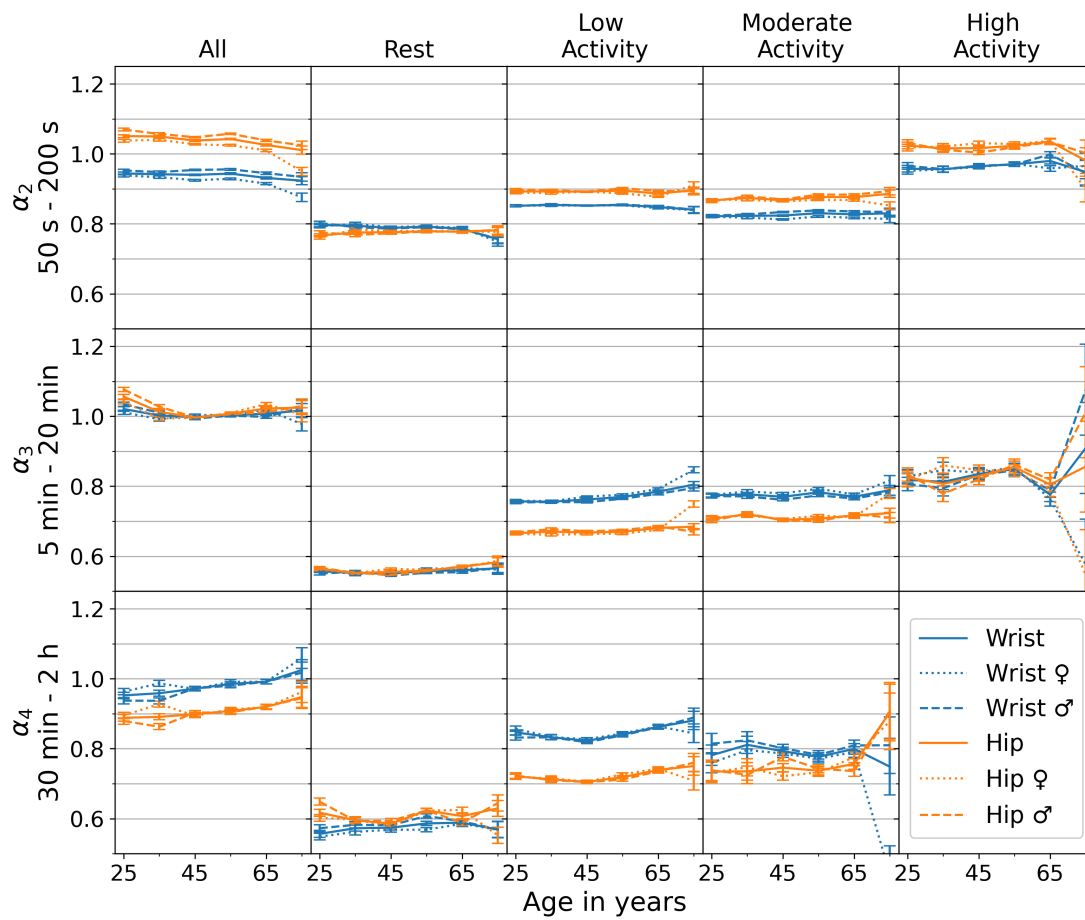


Figure 4.4: **DFA2 of accelerometry data.** The behavior of scaling exponents α of DFA2 of hip (orange) and wrist (blue) accelerometry is plotted versus age, in bins of 10 years, and in addition split into females (dotted) and males (dashed). Three scaling exponents are shown: α_2 , α_3 , and α_4 (rows), each for different activity clusters (columns). The error bars indicating the standard error of each bin. The high activity cluster has too few data for α_4 .

4.3. Preliminary results of DFA in accelerometry data

exists, where now wrist activity has higher values than hip. A similar picture emerges in α_4 , except for all, where wrist has higher values than hip.

Movement patterns can be identified more easily in hip accelerometry than in wrist accelerometry [91], because the wrist rotates a lot more frequently, but less strongly. Hence, we can expect a larger DFA slope in hip accelerometry on time scales of a few minutes (α_2), as we see in Fig. 4.4. On longer time scales (>5 minutes), movement episodes, like walking, are more likely to be interrupted by sitting etc., and the DFA exponent drops in hip accelerometry. On the other hand, the DFA slope in wrist accelerometry seems more stable for different time scales, as even in sitting the wrist is moved a lot. A special case is the rest cluster. For larger time scales, the exponents α_3 and α_4 during rest become close to 0.6, which is near the random noise ($\alpha = 0.5$). As the rest cluster is closely related to sleeping or just lying, it is consistent with expectations that there is no long term (>5 minute) correlation. Besides, for shorter time scales, we have $\alpha_2 \approx 0.8$, indicating correlation of movements in the range of a few minutes.

Finally, it should be mentioned, that we compared two different devices with different specifications. The SOMNOwatch at the wrist has a better signal to noise ratio, which can be seen in Fig. 4.3. For a comparison of smaller scales, e.g. 1s-MAD can be used, but only for identical devices, since device differences are more important in MAD values for shorter intervals.

5 | CONCLUSION AND OUTLOOK

This thesis explored in the first part the mostly hidden potential of accelerometry data to estimate pulse waves and respiration at the wrist. Methods and algorithms to extract pulse wave peaks and respiration have been introduced, described and discussed.

In the second part, the scaling behavior of biosignals and accelerometry was examined. Especially, the short- and long-term correlations of PTT were investigated for the first time. Furthermore, hip and wrist actigraphy scaling behavior was analyzed and compared for different activity levels.

According to the goals (i - v) formulated in the Introduction, the following main findings have been achieved:

- (I) An algorithm to detect pulse wave peaks and estimate pulse wave rate via wrist accelerometry was developed and successfully applied (Section 3.2 [JZ1]):
 - It could be shown that the pulse waves traversing the wrist cause tiny movements, which can be detected by accelerometers during sleep, and can therefore be used to investigate pulse to pulse intervals and also pulse transit times.
 - The values of the PTT estimated between R peak and reconstructed pulse wave peak are in agreement with literature.
 - Pulse rate variability (PRV) derived from wrist accelerometry is slightly higher than HRV, so that it is not a perfect surrogate.
 - PRV is more strongly influenced by respiration (respiratory sinus arrhythmia), which could explain the larger PRV.
- (II) It has been shown, that respiration movements could be extracted from wrist accelerometry in order to estimate respiratory activities (Section 3.3 [JZ2]):
 - During sleep and in the absence of motion artifacts, wrist accelerometry is able to capture the respiration-induced movements.
 - Comparing respiration estimates from ECG and wrist accelerometry, the latter one is superior.
- (III) Methods from (I), pulse wave peak reconstruction, and (II), respiration estimation from wrist accelerometry, have been successfully evaluated and investigated in the context of sleep stages (Section 3.4 [JZ3]):
 - During sleep, respiration and pulse wave signals can be reconstructed simultaneously.

5. CONCLUSION AND OUTLOOK

- Pulse waves can be better reconstructed than respiration.
 - Best results could be reached during N3 with hardly any movement artifacts, followed by N2 and REM sleep, while the synchronization drops during epochs of wakefulness, which are associated with movements.
 - Phase synchronization between pre-filtered accelerometry data from multiple axes, can be used as a performance predictor of the 30 second episodes. Discarding episodes based on this prediction could increase synchronization with the real signal, and therefore the reliability of the reconstructed signals, at the cost of less reconstructed data.
 - Apnea events affects the reconstruction of respiration negatively, but hardly affects pulse wave reconstruction.
- (IV) The scaling behavior of heart rate, pulse rate, respiration frequency, PTT and EEG alpha-band power during different sleep stages was studied and compared.
- Heart and pulse rates are characterized by sex- and age-dependent short-term (6 to 16 seconds) fluctuations, while their long-term (50 to 200 seconds) fluctuations exhibit a clear sleep stage dependence: weak long-term correlations during NREM sleep and pronounced long-term correlations during REM sleep and wakefulness.
 - In contrast, PTTs do not show differences between short-term and long-term scaling behavior; their short-term fluctuations are less correlated and hardly depend on age or sex.
 - Very similar sleep-stage dependent differences, are observed for respiration frequency, EEG alpha-band power and PTT.
 - The long-term scaling of all five observed signals seems to be modulated by sleep stage patterns generated in the brain, while short-term control differs between the organ systems.
- (V) In our scaling analysis of accelerometry data we have, for the first time, compared results for two different wearing locations (wrist and hip) and for four activity classes, while simultaneously studying many (≈ 2800) subjects and distinguishing scaling behaviors on three different time scale ranges.
- We could clearly show that activity clusters and wearing location of the sensor have a stronger effect on the results than sex or age (except during rest).
 - Weak trends with aging are opposite for short-term and long-term correlations when we combine data from all activity clusters.
 - Our results that hardly show any age dependencies in the separate activity classes suggest that the previously reported slight drop of the fluctuation scaling exponent with aging [86] is probably due to a reduction of high activity in the elderly and not due to an independent decrease of motion complexity with aging.

-
- No sex dependency could be observed in the long-term correlations.
 - It was found that, with increasing activity, the scaling exponents increase.
 - During rest, autocorrelations can be found on time scales of a few minutes (α_2 , 50 - 200 seconds), while they vanish on longer scales.
 - On time scales of a few minutes (α_2), the scaling exponent of hip accelerometry is larger than the one for wrist accelerometry, but vice-versa on long time scales (α_3 and α_4), except for rest, where all exponents are similar.

As a follow-up investigation connected to Part I of this thesis, the stronger influence of the respiratory sinus arrhythmia on the pulse wave peak signal needs further investigations. Here, we only investigated wrist accelerometry, but recent investigations of our group indicate that the algorithms are transferable to hip accelerometry, where respiration reconstructions seem to perform better. The combination of wrist and hip accelerometry is suggested, since it matches to a smartwatch (wrist) and smartphone (in a pocket at the hip) setup, leading to first algorithms for costumer applications.

Certainly the reconstructed signals cannot replace a PSG setup. But even if the reconstructed signals themselves are not reliable from a medical point of view, they can be used to distinguish non-wear time and sleep [44], [45].

In connection to the results presented in Part II, the scaling behavior of human accelerometry data deserves further investigation. We used the 5s-MAD value to compare 24 hour measurements from wrist and hip, finding no age and sex dependencies in scaling ranges of minutes to hours, while the scaling exponent increases with increasing activity. The comparison of the scaling behavior in accelerometry and biosignals could be improved by using accelerometry data with sleep stage scoring, together with 24 hour heart rate, respiration and PPG data. For further research, the scaling behavior of the reconstructed pulse waves and respiration rates could be investigated and compared.

Another approach to investigate cardiorespiratory signals and regulation, is the examination of the coupling between respiration and heart rate, or in terms of this work, the coupling between the reconstructed signals. This coupling could be described by synchronization or coordination.

In this work we have given a small insight into the advanced application of accelerometry data. On the one hand we showed how to derive cardiorespiratory information and on the other hand we dealt with the scaling behavior on different time scales. This opens further possibilities for future research projects and costumer applications.

6 | BIBLIOGRAPHY

6.1 Publication List

- [JZ1] **J. Zschocke**, M. Kluge, L. Pelikan, A. Graf, M. Glos, A. Müller, R. Mikolajczyk, R. P. Bartsch, T. Penzel, and J. W. Kantelhardt, „Detection and analysis of pulse waves during sleep via wrist-worn actigraphy“, *PloS one*, vol. 14, no. 12, e0226843, 2019. DOI: 10.1371/journal.pone.0226843.
- [JZ2] J. Leube, **J. Zschocke**, M. Kluge, L. Pelikan, A. Graf, M. Glos, A. Müller, R. P. Bartsch, T. Penzel, and J. W. Kantelhardt, „Reconstruction of the respiratory signal through ECG and wrist accelerometer data“, *Scientific Reports*, vol. 10, no. 1, p. 14530, 2020. DOI: 10.1038/s41598-020-71539-0.
- [JZ3] **J. Zschocke**, J. Leube, M. Glos, O. Semyachkina-Glushkovskaya, T. Penzel, R. Bartsch, and J. Kantelhardt, „Reconstruction of pulse wave and respiration from wrist accelerometer during sleep“, *IEEE Transactions on Bio-Medical Engineering*, vol. 69, no. 2, pp. 830–839, 2022. DOI: 10.1109/TBME.2021.3107978.
- [JZ4] **J. Zschocke**, R. P. Bartsch, M. Glos, T. Penzel, R. Mikolajczyk, and J. W. Kantelhardt, „Long- and short-term fluctuations compared for several organ systems across sleep stages“, *Frontiers in Network Physiology*, vol. 2, 2022. DOI: 10.3389/fnetp.2022.937130.
- [JZ5] Y. Ma, **J. Zschocke**, M. Glos, T. Penzel, J. W. Kantelhardt, and R. P. Bartsch, „Automatic sleep-stage classification in wearable data using deep and transfer learning approaches“, *Manuscript submitted for publication*, 2022.
- [JZ6] A. Peters, K. H. Greiser, S. Göttlicher, W. Ahrens, M. Albrecht, F. Bamberg, T. Bärnighausen, H. Becher, K. Berger, A. Beule, H. Boeing, B. Bohn, K. Bohnert, B. Braun, H. Brenner, R. Bülow, S. Castell, A. Damms-Machado, M. Dörr, N. Ebert, M. Ecker, C. Emmel, B. Fischer, C.-W. Franzke, S. Gastell, G. Giani, M. Günther, K. Günther, K.-P. Günther, J. Haerting, U. Haug, I. M. Heid, M. Heier, D. Heinemeyer, T. Hendel, F. Herbolsheimer, J. Hirsch, W. Hoffmann, B. Holleczeck, H. Hölling, A. Hörlein, K.-H. Jöckel, R. Kaaks, A. Karch, S. Karrasch, N. Kartschmit, H.-U. Kauczor, T. Keil, Y. Kemmling, B. Klee, B. Klüppelholz, A. Kluttig, L. Kofink, A. Köttgen, D. Kraft, G. Krause, L. Kretz, L. Krist, J. Kühnisch, O. Kuß, N. Legath, A.-T. Lehnich, M. Leitzmann, W. Lieb, J. Linseisen,

6. BIBLIOGRAPHY

- M. Loeffler, A. Macdonald, K. H. Maier-Hein, N. Mangold, C. Meinke-Franze, C. Meisinger, J. Melzer, B. Mergarten, K. B. Michels, R. Mikolajczyk, S. Moebus, U. Mueller, M. Nauck, T. Niendorf, K. Nikolaou, N. Obi, S. Ostrzinski, L. Panreck, I. Pigeot, T. Pischon, I. Pschibul-Thamm, W. Rathmann, A. Reineke, S. Roloff, D. Rujescu, S. Rupf, O. Sander, T. Schikowski, S. Schipf, P. Schirmacher, C. L. Schlett, B. Schmidt, G. Schmidt, M. Schmidt, G. Schöne, H. Schulz, M. B. Schulze, A. Schweig, A. M. Sedlmeier, S. Selder, J. Six-Merker, R. Sowade, A. Stang, O. Stegle, K. Steindorf, G. Stübs, E. Swart, H. Teismann, I. Thiele, S. Thierry, M. Ueffing, H. Völzke, S. Waniek, A. Weber, N. Werner, H.-E. Wichmann, S. N. Willich, K. Wirkner, K. Wolf, R. Wolff, H. Zeeb, M. Zinkhan, and **J. Zschocke**, „Framework and baseline examination of the German National Cohort (NAKO)“, *European Journal of Epidemiology*, vol. 37, no. 10, pp. 1107–1124, 2022. DOI: 10.1007/s10654-022-00890-5.
- [JZ7] A. Kluttig, **J. Zschocke**, J. Haerting, A. Schmermund, S. Gastell, K. Steindorf, F. Herbolsheimer, A. Hillreiner, C. Jochem, S. Baumeister, O. Sprengeler, T. Pischon, L. Jaeschke, K. B. Michels, L. Krist, H. Greiser, G. Schmidt, W. Lieb, S. Waniek, H. Becher, A. Jagodzinski, S. Schipf, H. Völzke, W. Ahrens, K. Günther, S. Castell, Y. Kemmling, N. Legath, K. Berger, T. Keil, J. Fricke, M. B. Schulze, M. Loeffler, K. Wirkner, O. Kuß, T. Schikowski, S. Kalinowski, A. Stang, R. Kaaks, A. Damms Machado, M. Hoffmeister, B. Weber, C.-W. Franzke, S. Thierry, A. Peters, N. Kartschmit, R. Mikolajczyk, B. Fischer, M. Leitzmann, and M. Brandes, „Messung der körperlichen Fitness in der NAKO Gesundheitsstudie – Methoden, Qualitätssicherung und erste deskriptive Ergebnisse“, *Bundesgesundheitsblatt, Gesundheitsforschung, Gesundheitsschutz*, vol. 63, no. 3, pp. 312–321, 2020. DOI: 10.1007/s00103-020-03100-3.
- [JZ8] K. Wolf, U. Kraus, M. Dzolan, G. Bolte, T. Lakes, T. Schikowski, K. H. Greiser, O. Kuß, W. Ahrens, F. Bamberg, H. Becher, K. Berger, H. Brenner, S. Castell, A. Damms-Machado, B. Fischer, C.-W. Franzke, S. Gastell, K. Günther, B. Holleczeck, L. Jaeschke, R. Kaaks, T. Keil, Y. Kemmling, L. Krist, N. Legath, M. Leitzmann, W. Lieb, M. Loeffler, C. Meinke-Franze, K. B. Michels, R. Mikolajczyk, S. Moebus, U. Mueller, N. Obi, T. Pischon, W. Rathmann, S. Schipf, B. Schmidt, M. Schulze, I. Thiele, S. Thierry, S. Waniek, C. Wigmann, K. Wirkner, **J. Zschocke**, A. Peters, and A. Schneider, „Nächtliche Verkehrslärmbelästigung in Deutschland: Individuelle und regionale Unterschiede in der NAKO Gesundheitsstudie“, *Bundesgesundheitsblatt, Gesundheitsforschung, Gesundheitsschutz*, vol. 63, no. 3, pp. 332–343, 2020. DOI: 10.1007/s00103-020-03094-y.
- [JZ9] M. Leitzmann, S. Gastell, A. Hillreiner, F. Herbolsheimer, S. E. Baumeister, B. Bohn, M. Brandes, H. Greiser, L. Jaeschke, C. Jochem, A. Kluttig, L. Krist, K. B. Michels, T. Pischon, A. Schmermund, O. Sprengeler, **J. Zschocke**, W. Ahrens, H. Baurecht, H. Becher, K. Berger, H. Brenner, S.

Castell, B. Fischer, C.-W. Franzke, J. Fricke, W. Hoffmann, B. Holleczeck, R. Kaaks, S. Kalinowski, T. Keil, Y. Kemmling, O. Kuß, N. Legath, W. Lieb, J. Linseisen, M. Löffler, R. Mikolajczyk, N. Obi, A. Peters, I. Ratjen, T. Schikowski, M. B. Schulze, A. Stang, S. Thierry, H. Völzke, K. Wirkner, and K. Steindorf, „Körperliche Aktivität in der NAKO Gesundheitsstudie: erste Ergebnisse des multimodalen Erhebungskonzepts“, *Bundesgesundheitsblatt, Gesundheitsforschung, Gesundheitsschutz*, vol. 63, no. 3, pp. 301–311, 2020. DOI: 10.1007/s00103-020-03099-7.

6.2 References

- [1] „The German National Cohort: aims, study design and organization“, *European Journal of Epidemiology*, vol. 29, no. 5, pp. 371–382, 2014. DOI: 10.1007/s10654-014-9890-7.
- [2] H. Völzke, J. Schössow, C. O. Schmidt, *et al.*, „Cohort profile update: the study of health in Pomerania (SHIP)“, *International Journal of Epidemiology*, 2022. DOI: 10.1093/ije/dyac034.
- [3] A. Doherty, D. Jackson, N. Hammerla, *et al.*, „Large scale population assessment of physical activity using wrist worn accelerometers: the UK biobank study“, *PloS one*, vol. 12, no. 2, e0169649, 2017. DOI: 10.1371/journal.pone.0169649.
- [4] K. Sundararajan, S. Georgievska, B. H. W. Te Lindert, *et al.*, „Sleep classification from wrist-worn accelerometer data using random forests“, *Scientific Reports*, vol. 11, no. 1, p. 24, 2021. DOI: 10.1038/s41598-020-79217-x.
- [5] M. Ermes, J. Pärkka, J. Mantyjarvi, *et al.*, „Detection of daily activities and sports with wearable sensors in controlled and uncontrolled conditions“, *IEEE Transactions on Information Technology in Biomedicine : a publication of the IEEE Engineering in Medicine and Biology Society*, vol. 12, no. 1, pp. 20–26, 2008, ISSN: 1089-7771. DOI: 10.1109/TITB.2007.899496.
- [6] J. Margarito, R. Helaoui, A. M. Bianchi, *et al.*, „User-independent recognition of sports activities from a single wrist-worn accelerometer: A template-matching-based approach“, *IEEE Transactions on Bio-Medical Engineering*, vol. 63, no. 4, pp. 788–796, 2016. DOI: 10.1109/TBME.2015.2471094.
- [7] M. S. Tremblay, S. Aubert, J. D. Barnes, *et al.*, „Sedentary behavior research network (SBRN) - terminology consensus project process and outcome“, *The International Journal of Behavioral Nutrition and Physical Activity*, vol. 14, no. 1, p. 75, 2017. DOI: 10.1186/s12966-017-0525-8.
- [8] Electrophysiology, Task Force of the European Society of Cardiology the North A., „Heart rate variability“, *Circulation*, vol. 93, no. 5, pp. 1043–1065, 1996, ISSN: 0009-7322. DOI: 10.1161/01.CIR.93.5.1043.
- [9] H. Ernst, M. Scherpf, H. Malberg, *et al.*, „Pulse arrival time - a sensitive vital parameter for the detection of mental stress“, *Current Directions in Biomedical Engineering*, vol. 7, no. 2, pp. 419–422, 2021. DOI: 10.1515/cdbme-2021-2106.
- [10] G. Zhang, M. Gao, Da Xu, *et al.*, „Pulse arrival time is not an adequate surrogate for pulse transit time as a marker of blood pressure“, *Journal of Applied Physiology*, vol. 111, no. 6, pp. 1681–1686, 2011. DOI: 10.1152/japplphysiol.00980.2011.

- [11] M. Nitzan, B. Khanokh, and Y. Slovik, „The difference in pulse transit time to the toe and finger measured by photoplethysmography“, *Physiological Measurement*, vol. 23, no. 1, pp. 85–93, 2002. DOI: 10.1088/0967-3334/23/1/308.
- [12] M. J. Drinnan, J. Allen, and A. Murray, „Relation between heart rate and pulse transit time during paced respiration“, *Physiological Measurement*, vol. 22, no. 3, pp. 425–432, 2001. DOI: 10.1088/0967-3334/22/3/301.
- [13] M. Deak and L. J. Epstein, „The history of polysomnography“, *Sleep Medicine Clinics*, vol. 4, no. 3, pp. 313–321, 2009. DOI: 10.1016/j.jsmc.2009.04.001.
- [14] H. Berger, „Über das Elektrenkephalogramm des Menschen“, *Archiv für Psychiatrie und Nervenkrankheiten*, vol. 87, pp. 527–570, 1929. [Online]. Available: <https://cir.nii.ac.jp/crid/1572543024156905856>.
- [15] W. Dement and N. Kleitman, „Cyclic variations in EEG during sleep and their relation to eye movements, body motility, and dreaming“, *Electroencephalography and Clinical Neurophysiology*, vol. 9, no. 4, pp. 673–690, 1957, ISSN: 00134694. DOI: 10.1016/0013-4694(57)90088-3.
- [16] L. J. Monroe, „Inter-rater reliability and the role of experience in scoring EEG sleep records: Phase 1“, *Psychophysiology*, vol. 5, no. 4, pp. 376–384, 1969, ISSN: 0048-5772. DOI: 10.1111/j.1469-8986.1969.tb02836.x.
- [17] A. Rechtschaffen and A. Kales, *A manual of standardized terminology, techniques and scoring system for sleep stages of human subjects*. (NIH publication no. 204). Bethesda, Md.: U. S. National Institute of Neurological Diseases and Blindness, Neurological Information Network, 1968.
- [18] J. W. Atkinson, „The evolution of polysomnographic technology.“, in *Fundamentals of Sleep Technology*, N. Butkov and T. Lee-Chiong, Eds., Philadelphia, Pa: Lippincott Williams & Wilkins, 2007, pp. 1–5, ISBN: 978-0-7817-9287-5.
- [19] C. Iber, S. Ancoli-Israel, A. Chesson, *et al.*, „The AASM manual for the scoring of sleep and associated events rules, terminology and technical specifications. 1st edition. Westchester (IL)“, 2007.
- [20] R. B. Berry, R. Budhiraja, D. J. Gottlieb, *et al.*, „Rules for scoring respiratory events in sleep: update of the 2007 AASM Manual for the Scoring of Sleep and Associated Events. Deliberations of the sleep apnea definitions task force of the American Academy of Sleep Medicine“, *Journal of Clinical Sleep Medicine*, vol. 8, no. 5, pp. 597–619, 2012. DOI: 10.5664/jcsm.2172.
- [21] R. B. Berry, C. L. Albertario, S. M. Harding, *et al.*, „The AASM manual for the scoring of sleep and associated events: rules, terminology and technical specifications, version 2.5.“, *American Academy of Sleep Medicine, Darien, IL*, 2018.

6. BIBLIOGRAPHY

- [22] H. Jasper, „Report of the committee on methods of clinical examination in electroencephalography“, *Electroencephalography Clinical Neurophysiology*, vol. 10, pp. 370–375, 1958.
- [23] S. R. Pandi-Perumal, D. W. Spence, and A. S. BaHammam, „Polysomnography: an overview“, in *Primary Care Sleep Medicine*, J. F. Pagel and S. R. Pandi-Perumal, Eds., New York, NY: Springer New York, 2014, pp. 29–42, ISBN: 978-1-4939-1184-4. DOI: 10.1007/978-1-4939-1185-1_4.
- [24] A. Sadeh, „Sleep assessment methods“, *Monographs of the Society for Research in Child Development*, vol. 80, no. 1, pp. 33–48, 2015. DOI: 10.1111/mono.12143.
- [25] J.-H. Byun, K. T. Kim, H.-J. Moon, *et al.*, „The first night effect during polysomnography, and patients’ estimates of sleep quality“, *Psychiatry Research*, vol. 274, pp. 27–29, 2019. DOI: 10.1016/j.psychres.2019.02.011.
- [26] B. W. Riedel, C. F. Winfield, and K. L. Lichstein, „First night effect and reverse first night effect in older adults with primary insomnia: does anxiety play a role?“, *Sleep Medicine*, vol. 2, no. 2, pp. 125–133, 2001, ISSN: 13899457. DOI: 10.1016/S1389-9457(00)00054-X.
- [27] G. Curcio, M. Ferrara, A. Piergianni, *et al.*, „Paradoxes of the first-night effect: a quantitative analysis of antero-posterior EEG topography“, *Clinical Neurophysiology*, vol. 115, no. 5, pp. 1178–1188, 2004, ISSN: 1388-2457. DOI: 10.1016/j.clinph.2003.12.018.
- [28] S. L. Verhulst, N. Schrauwen, W. A. de Backer, *et al.*, „First night effect for polysomnographic data in children and adolescents with suspected sleep disordered breathing“, *Archives of Disease in Childhood*, vol. 91, no. 3, pp. 233–237, 2006. DOI: 10.1136/adc.2005.085365.
- [29] S. Kwon, H. Kim, and W.-H. Yeo, „Recent advances in wearable sensors and portable electronics for sleep monitoring“, *iScience*, vol. 24, no. 5, p. 102461, 2021. DOI: 10.1016/j.isci.2021.102461.
- [30] E. Wischmeyer, „Integrative Funktionen des Gehirns: Wachen und Schlafen“, in *Taschenlehrbuch Physiologie*, Stuttgart: Thieme, 2010, pp. 787–794, ISBN: 978-3-13-144981-8.
- [31] A. K. Patel, V. Reddy, K. R. Shumway, *et al.*, „Physiology, sleep stages“, in *StatPearls*, Online; accessed 10.10.2022, Treasure Island (FL), 2022.
- [32] F. G. Foster, D. Kupfer, G. Weiss, *et al.*, „Mobility recording and cycle research in neuropsychiatry“, *Journal of Interdisciplinary Cycle Research*, vol. 3, no. 1, pp. 61–72, 1972, ISSN: 0022-1945. DOI: 10.1080/09291017209359298.

- [33] D. J. Kupfer, T. P. Detre, G. Foster, *et al.*, „The application of delgado’s telemetric mobility recorder for human studies“, *Behavioral Biology*, vol. 7, no. 4, pp. 585–590, 1972, ISSN: 0091-6773. DOI: 10.1016/s0091-6773(72)80220-7.
- [34] D. F. Kripke, D. J. Mullaney, S. Messin, *et al.*, „Wrist actigraphic measures of sleep and rhythms“, *Electroencephalography and Clinical Neurophysiology*, vol. 44, no. 5, pp. 674–676, 1978, ISSN: 00134694. DOI: 10.1016/0013-4694(78)90133-5.
- [35] D. J. Mullaney, D. F. Kripke, and S. Messin, „Wrist-actigraphic estimation of sleep time“, *Sleep*, vol. 3, no. 1, pp. 83–92, 1980, ISSN: 0161-8105. DOI: 10.1093/sleep/3.1.83.
- [36] J. B. Webster, D. F. Kripke, S. Messin, *et al.*, „An activity-based sleep monitor system for ambulatory use“, *Sleep*, vol. 5, no. 4, pp. 389–399, 1982, ISSN: 0161-8105. DOI: 10.1093/sleep/5.4.389.
- [37] R. J. Cole, D. F. Kripke, W. Gruen, *et al.*, „Automatic sleep/wake identification from wrist activity“, *Sleep*, vol. 15, no. 5, pp. 461–469, 1992, ISSN: 0161-8105. DOI: 10.1093/sleep/15.5.461.
- [38] J. Paquet, A. Kawinska, and J. Carrier, „Wake detection capacity of actigraphy during sleep“, *Sleep*, vol. 30, no. 10, pp. 1362–1369, 2007, ISSN: 0161-8105. DOI: 10.1093/sleep/30.10.1362.
- [39] A. Sadeh, P. J. Hauri, D. F. Kripke, *et al.*, „The role of actigraphy in the evaluation of sleep disorders“, *Sleep*, vol. 18, no. 4, pp. 288–302, 1995, ISSN: 0161-8105. DOI: 10.1093/sleep/18.4.288.
- [40] A. Sadeh, „The role and validity of actigraphy in sleep medicine: an update“, *Sleep Medicine Reviews*, vol. 15, no. 4, pp. 259–267, 2011, ISSN: 1087-0792. DOI: 10.1016/j.smr.2010.10.001.
- [41] P. J. Hauri and J. Wisbey, „Wrist actigraphy in insomnia“, *Sleep*, vol. 15, no. 4, pp. 293–301, 1992, ISSN: 0161-8105. DOI: 10.1093/sleep/15.4.293.
- [42] G. Jean-Louis, D. F. Kripke, W. J. Mason, *et al.*, „Sleep estimation from wrist movement quantified by different actigraphic modalities“, *Journal of Neuroscience Methods*, vol. 105, no. 2, pp. 185–191, 2001, ISSN: 0165-0270. DOI: 10.1016/s0165-0270(00)00364-2.
- [43] P. I. Terrill, D. G. Mason, and S. J. Wilson, „Development of a continuous multisite accelerometry system for studying movements during sleep“, *Annual International Conference of the IEEE Engineering in Medicine and Biology Society.*, vol. 2010, pp. 6150–6153, 2010, ISSN: 2375-7477. DOI: 10.1109/IEMBS.2010.5627780.
- [44] P. Wohlfahrt, J. W. Kantelhardt, M. Zinkhan, *et al.*, „Transitions in effective scaling behavior of accelerometric time series across sleep and wake“, *EPL (Europhysics Letters)*, vol. 103, no. 6, p. 68002, 2013, ISSN: 0295-5075. DOI: 10.1209/0295-5075/103/68002.

6. BIBLIOGRAPHY

- [45] M. Zinkhan and J. W. Kantelhardt, „Sleep assessment in large cohort studies with high-resolution accelerometers“, *Sleep Medicine Clinics*, vol. 11, no. 4, pp. 469–488, 2016. DOI: 10.1016/j.jsmc.2016.08.006.
- [46] J. Fraden, *AIP handbook of modern sensors: Physics, designs and applications* (AIP series in modern instrumentation and measurements in physics & engineering), 3. print. Woodbury, NY: AIP Press, 1995, ISBN: 1563961083.
- [47] C. Aszkler, „Acceleration, shock and vibration sensors“, in *Sensor Technology Handbook*, Elsevier, 2005, pp. 137–159, ISBN: 9780750677295. DOI: 10.1016/B978-075067729-5/50045-8.
- [48] H. Vähä-Ypyä, T. Vasankari, P. Husu, *et al.*, „A universal, accurate intensity-based classification of different physical activities using raw data of accelerometer“, *Clinical Physiology and Functional Imaging*, vol. 35, no. 1, pp. 64–70, 2015. DOI: 10.1111/cpf.12127.
- [49] V. T. van Hees, L. Gorzelniak, E. C. Dean León, *et al.*, „Separating movement and gravity components in an acceleration signal and implications for the assessment of human daily physical activity“, *PloS one*, vol. 8, no. 4, e61691, 2013. DOI: 10.1371/journal.pone.0061691.
- [50] J. H. Migueles, A. V. Rowlands, F. Huber, *et al.*, „GGIR: a research community-driven open source R package for generating physical activity and sleep outcomes from multi-day raw accelerometer data“, *Journal for the Measurement of Physical Behaviour*, vol. 2, no. 3, pp. 188–196, 2019, ISSN: 2575-6605. DOI: 10.1123/jmpb.2018-0063.
- [51] H. Vähä-Ypyä, T. Vasankari, P. Husu, *et al.*, „Validation of cut-points for evaluating the intensity of physical activity with accelerometry-based mean amplitude deviation (MAD)“, *PloS one*, vol. 10, no. 8, e0134813, 2015. DOI: 10.1371/journal.pone.0134813.
- [52] W. W. Tryon, „Issues of validity in actigraphic sleep assessment“, *Sleep*, vol. 27, no. 1, pp. 158–165, 2004, ISSN: 0161-8105. DOI: 10.1093/sleep/27.1.158.
- [53] Y. J. Lee, J. Y. Lee, J. H. Cho, *et al.*, „Interrater reliability of sleep stage scoring: a meta-analysis“, *Journal of Clinical Sleep Medicine*, vol. 18, no. 1, pp. 193–202, 2022. DOI: 10.5664/jcsm.9538.
- [54] S. Schipf, G. Schöne, B. Schmidt, *et al.*, „Die Basiserhebung der NAKO Gesundheitsstudie: Teilnahme an den Untersuchungsmodulen, Qualitätssicherung und Nutzung von Sekundärdaten“, *Bundesgesundheitsblatt, Gesundheitsforschung, Gesundheitsschutz*, vol. 63, no. 3, pp. 254–266, 2020. DOI: 10.1007/s00103-020-03093-z.
- [55] E. A. Schäfer, „On the rhythm of muscular response to volitional impulses in man“, *The Journal of Physiology*, vol. 7, no. 2, pp. 111–117, 1886, ISSN: 0022-3751. DOI: 10.1113/jphysiol.1886.sp000210.

- [56] F. Peterson, „A contribution to the study of muscular tremor“, *Journal of Nervous and Mental Disease*, vol. 16, pp. 99–112, 1889.
- [57] A. A. Eshner, „A graphic study of tremor“, *The Journal of Experimental Medicine*, vol. 2, no. 3, pp. 301–312, 1897, ISSN: 0022-1007. DOI: 10.1084/jem.2.3.301.
- [58] O. C. Lippold, „Oscillation in the stretch reflex arc and the origin of the rhythmical, 8-12 C-S component of physiological tremor“, *The Journal of Physiology*, vol. 206, no. 2, pp. 359–382, 1970, ISSN: 0022-3751. DOI: 10.1113/jphysiol.1970.sp009018.
- [59] R. Durbaba, A. Taylor, C. A. Manu, *et al.*, „Stretch reflex instability compared in three different human muscles“, *Experimental Brain Research*, vol. 163, no. 3, pp. 295–305, 2005, ISSN: 0014-4819. DOI: 10.1007/s00221-004-2165-x.
- [60] R. J. Elble, „Central mechanisms of tremor“, *Journal of Clinical Neurophysiology*, vol. 13, no. 2, 1996, ISSN: 0736-0258.
- [61] M. Lakie, C. A. Vernooij, T. M. Osborne, *et al.*, „The resonant component of human physiological hand tremor is altered by slow voluntary movements“, *The Journal of Physiology*, vol. 590, no. 10, pp. 2471–2483, 2012, ISSN: 0022-3751. DOI: 10.1113/jphysiol.2011.226449.
- [62] J. Raethjen, F. Pawlas, M. Lindemann, *et al.*, „Determinants of physiologic tremor in a large normal population“, *Clinical Neurophysiology*, vol. 111, no. 10, pp. 1825–1837, 2000, ISSN: 13882457. DOI: 10.1016/S1388-2457(00)00384-9.
- [63] C. Marsden, J. Meadows, G. Lange, *et al.*, „The relation between physiological tremor of the two hands in healthy subjects“, *Electroencephalography and Clinical Neurophysiology*, vol. 27, no. 2, pp. 179–185, 1969, ISSN: 00134694. DOI: 10.1016/0013-4694(69)90171-0.
- [64] H. Rohracher, „Permanente rhythmische Mikrobewegungen des Warmblüter-Organismus (Mikrovibration)“, *Die Naturwissenschaften*, vol. 49, no. 7, pp. 145–150, 1962, ISSN: 0028-1042. DOI: 10.1007/BF00640123.
- [65] E. Gallasch and T. Kenner, „Characterisation of arm microvibration recorded on an accelerometer“, *European Journal of Applied Physiology and Occupational Physiology*, vol. 75, no. 3, pp. 226–232, 1997, ISSN: 0301-5548. DOI: 10.1007/s004210050152.
- [66] D. Gabor, „Theory of communication. The analysis of information“, *Journal of the Institution of Electrical Engineers-Part III: Radio and Communication Engineering*, vol. 93, no. 26, pp. 429–441, 1946, ISSN: 2054-0604.
- [67] M. Rosenblum, A. Pikovsky, J. Kurths, *et al.*, „Phase synchronization: from theory to data analysis“, in *Neuro-Informatics and Neural Modelling*, F. Moss, Ed., vol. 4, Elsevier, 2001, pp. 279–321, ISBN: 9780444502841. DOI: 10.1016/S1383-8121(01)80012-9.

6. BIBLIOGRAPHY

- [68] P. H. Charlton, T. Bonnici, L. Tarassenko, *et al.*, „Extraction of respiratory signals from the electrocardiogram and photoplethysmogram: technical and physiological determinants“, *Physiological Measurement*, vol. 38, no. 5, pp. 669–690, 2017. DOI: 10.1088/1361-6579/aa670e.
- [69] C. K. Peng, S. V. Buldyrev, S. Havlin, *et al.*, „Mosaic organization of DNA nucleotides“, *Physical review. E, Statistical physics, plasmas, fluids, and related interdisciplinary topics*, vol. 49, no. 2, pp. 1685–1689, 1994, ISSN: 1063-651X. DOI: 10.1103/PhysRevE.49.1685.
- [70] A. Bunde, S. Havlin, J. W. Kantelhardt, *et al.*, „Correlated and uncorrelated regions in heart-rate fluctuations during sleep“, *Physical Review Letters*, vol. 85, no. 17, pp. 3736–3739, 2000, ISSN: 0031-9007. DOI: 10.1103/PhysRevLett.85.3736.
- [71] S. Akselrod, D. Gordon, F. A. Ubel, *et al.*, „Power spectrum analysis of heart rate fluctuation: a quantitative probe of beat-to-beat cardiovascular control“, *Science*, vol. 213, no. 4504, pp. 220–222, 1981, ISSN: 0036-8075. DOI: 10.1126/science.6166045.
- [72] T. Penzel, J. W. Kantelhardt, C.-C. Lo, *et al.*, „Dynamics of heart rate and sleep stages in normals and patients with sleep apnea“, *Neuropsychopharmacology*, vol. 28 Suppl 1, S48–53, 2003, ISSN: 0893-133X. DOI: 10.1038/sj.npp.1300146.
- [73] J. W. Kantelhardt, „Fractal and multifractal time series“, in *Encyclopedia of Complexity and Systems Science*, R. A. Meyers, Ed., New York, NY: Springer, 2009, pp. 3754–3779, ISBN: 978-0-387-75888-6. DOI: 10.1007/978-0-387-30440-3_221.
- [74] C. K. Peng, S. Havlin, H. E. Stanley, *et al.*, „Quantification of scaling exponents and crossover phenomena in nonstationary heartbeat time series“, *Chaos*, vol. 5, no. 1, pp. 82–87, 1995. DOI: 10.1063/1.166141.
- [75] A. L. Goldberger, L. A. Amaral, L. Glass, *et al.*, „PhysioBank, PhysioToolkit, and PhysioNet: components of a new research resource for complex physiologic signals“, *Circulation*, vol. 101, no. 23, E215–20, 2000, ISSN: 0009-7322. DOI: 10.1161/01.cir.101.23.e215.
- [76] J. Beran, *Statistics for long-memory processes*. Boca Raton and London: Chapman & Hall/CRC, 1994. DOI: 10.1201/9780203738481.
- [77] A. Y. Schumann, R. P. Bartsch, T. Penzel, *et al.*, „Aging effects on cardiac and respiratory dynamics in healthy subjects across sleep stages“, *Sleep*, vol. 33, no. 7, pp. 943–955, 2010, ISSN: 0161-8105. DOI: 10.1093/sleep/33.7.943.
- [78] J. W. Kantelhardt, T. Penzel, S. Rostig, *et al.*, „Breathing during REM and non-REM sleep: correlated versus uncorrelated behaviour“, *Physica A: Statistical Mechanics and its Applications*, vol. 319, pp. 447–457, 2003, ISSN: 03784371. DOI: 10.1016/S0378-4371(02)01502-9.

- [79] J. W. Kantelhardt, S. Tismer, F. Gans, *et al.*, „Scaling behavior of EEG amplitude and frequency time series across sleep stages“, *EPL (Europhysics Letters)*, vol. 112, no. 1, p. 18001, 2015, ISSN: 0295-5075. DOI: 10.1209/0295-5075/112/18001.
- [80] M. Günther, J. W. Kantelhardt, and R. P. Bartsch, „The reconstruction of causal networks in physiology“, *Frontiers in Network Physiology*, vol. 2, p. 893743, 2022, ISSN: 2674-0109. DOI: 10.3389/fnetp.2022.893743.
- [81] P. Castiglioni, S. Omboni, G. Parati, *et al.*, „Day and night changes of cardiovascular complexity: a multi-fractal multi-scale analysis“, *Entropy*, vol. 22, no. 4, 2020, ISSN: 1099-4300. DOI: 10.3390/e22040462.
- [82] K. Bakrania, T. Yates, A. V. Rowlands, *et al.*, „Intensity thresholds on raw acceleration data: euclidean norm minus one (ENMO) and mean amplitude deviation (MAD) approaches“, *PloS one*, vol. 11, no. 10, e0164045, 2016. DOI: 10.1371/journal.pone.0164045.
- [83] M. Zinkhan, K. Berger, S. Hense, *et al.*, „Agreement of different methods for assessing sleep characteristics: a comparison of two actigraphs, wrist and hip placement, and self-report with polysomnography“, *Sleep Medicine*, vol. 15, no. 9, pp. 1107–1114, 2014, ISSN: 13899457. DOI: 10.1016/j.sleep.2014.04.015.
- [84] H. Sievänen and U. M. Kujala, „Accelerometry - simple, but challenging“, *Scandinavian Journal of Medicine & Science in Sports*, vol. 27, no. 6, pp. 574–578, 2017. DOI: 10.1111/sms.12887.
- [85] J. Zschocke, „Bi- und trivariate Analyse von Langzeit-EKG- und Beschleunigungsmessungen“, Masterarbeit, Martin-Luther-Universität Halle-Wittenberg, Halle (Saale), Germany, 2017. [Online]. Available: http://www.physik.uni-halle.de/Fachgruppen/kantel/Masterarbeit_Zschocke.pdf.
- [86] D. A. Raichlen, Y. C. Klimentidis, C.-H. Hsu, *et al.*, „Fractal Complexity of Daily Physical Activity Patterns Differs With Age Over the Life Span and Is Associated With Mortality in Older Adults“, *The journals of gerontology. Series A, Biological sciences and medical sciences*, vol. 74, no. 9, pp. 1461–1467, 2019. DOI: 10.1093/gerona/gly247.
- [87] J.-H. Lee, S. Goh, S. Ho Kim, *et al.*, „Statistical properties of human activity and criticality in active behavior“, *EPL (Europhysics Letters)*, vol. 126, no. 6, p. 68001, 2019, ISSN: 0295-5075. DOI: 10.1209/0295-5075/126/68001.
- [88] L. A. N. Amaral, D. J. B. Soares, L. R. Da Silva, *et al.*, „Power law temporal auto-correlations in day-long records of human physical activity and their alteration with disease“, *Europhysics Letters (EPL)*, vol. 66, no. 3, pp. 448–454, 2004, ISSN: 0295-5075. DOI: 10.1209/epl/i2003-10227-7.

6. BIBLIOGRAPHY

- [89] K. Hu, P. C. Ivanov, Z. Chen, *et al.*, „Non-random fluctuations and multi-scale dynamics regulation of human activity“, *Physica A*, vol. 337, no. 1-2, pp. 307–318, 2004, ISSN: 0378-4371. DOI: 10.1016/j.physa.2004.01.042.
- [90] P. C. Ivanov, K. Hu, M. F. Hilton, *et al.*, „Endogenous circadian rhythm in human motor activity uncoupled from circadian influences on cardiac dynamics“, *Proceedings of the National Academy of Sciences of the United States of America*, vol. 104, no. 52, pp. 20 702–20 707, 2007. DOI: 10.1073/pnas.0709957104.
- [91] S. G. Trost, Y. Zheng, and W.-K. Wong, „Machine learning for activity recognition: hip versus wrist data“, *Physiological Measurement*, vol. 35, no. 11, pp. 2183–2189, 2014. DOI: 10.1088/0967-3334/35/11/2183.

7 | CURRICULUM VITAE

PERSONAL DATA

NAME: Johannes Zschocke

WORK EXPERIENCE

- since 12/2022 Full Stack Engineer
Kialo GmbH
Berlin, Germany
- 01/2019 - 12/2022 Scientific Assistant at the Institute of Epidemiology,
Biostatistics and Informatics (IMEBI),
Interdisciplinary Center for Health Science,
Martin-Luther-Universität Halle-Wittenberg
Halle (Saale), Germany
- 10/2017 - 12/2018 Scientific Assistant at the Department of Physics,
Cardiovascular Physics
Humboldt-Universität zu Berlin
Berlin, Germany
- 12/2014 - 09/2017 Student Assistant at Physics Schools Laboratory,
Institut of Physics,
Martin-Luther-Universität Halle-Wittenberg
Halle (Saale), Germany

EDUCATION

- since 10/2017 **PhD studies**
Martin-Luther-Universität Halle-Wittenberg
Halle (Saale), Germany
Supervisor: Priv. Doz.-Dr. Jan W. Kantelhardt
- 01/2018 - 02/2018 **Minerva Short-Term Research Grant**
Department of Physics, Bar-Ilan University
Ramat Gan, Israel
- 10/2015 - 09/2017 **Master of Science in Medical Physics**
Martin-Luther-Universität Halle-Wittenberg
Halle (Saale), Germany
Thesis: "Bi- and Trivariate Analysis of Long-Term ECG and Acceleration Measurements"
- 10/2016 Internship "Rheology of FLOPAAM"
Institut Laue-Langevin - Large Scale Structures
Grenoble, France
- 10/2011 - 09/2015 **Bachelor of Science in Medical Physics**
Martin-Luther-Universität Halle-Wittenberg
Halle (Saale), Germany
Thesis: "Examination of Volume-Dependent Anion Channels of Macrophagen with Iodide-Sensitive YFP"
- 10/2013 - 09/2014 ERASMUS Exchange, Physics
Université Joseph Fourier
Grenoble, France
- 09/2008 - 07/2011 **Allgemeine Hochschulreife**
(general qualification for university entrance)
Johannes-Kepler-Gymnasium
Chemnitz, Germany

Halle (Saale), November 9, 2023

Johannes Zschocke

8 | DECLARATION UNDER OATH EIDESSTATTLICHE ERKLÄRUNG

I declare under penalty of perjury that this thesis is my own work entirely and has been written without any help from other people. I used only the sources mentioned and included all the citations correctly both in word or content.

Ich erkläre an Eides statt, dass ich die Arbeit selbstständig und ohne fremde Hilfe verfasst, keine anderen als die von mir angegebenen Quellen und Hilfsmittel benutzt und die den benutzten Werken wörtlich oder inhaltlich entnommenen Stellen als solche kenntlich gemacht habe.

Date (*Datum*)

Signature of the applicant (*Unterschrift des Antragstellers*)

9 | ACKNOWLEDGEMENTS

Ich möchte mich bei allen bedanke, die mich in den letzten fünf Jahren bei meiner Promotion begleitet und unterstützt haben.

Ein besonderer Dank gilt an dieser Stelle meinem Doktorvater PD Dr. Jan W. Kantelhardt, der mir diese Arbeit erst ermöglicht hat. Jederzeit konnte ich bei Ihm Rat und Unterstützung finden. Zudem hat er mir den Zugang zu Forschungsgruppen und vielen wichtigen Kontakten eröffnet.

Bei Dr. Ronny Bartsch bedanke ich mich für den wissenschaftlichen Austausch und die freundliche Aufnahme in Israel während meines Forschungsaufenthaltes. I would like to take the opportunity to thank Yaopeng Ma for the scientific cooperation, exchange and inspiration.

Weiterhin möchte ich mich bei der NAKO-Expertengruppe Schlaf und seinen Mitgliedern (Prof. Stang, PD Dr. Kantelhardt, Dr. Greiser, Dr. Lehnich, Dr. Kantermann, Prof. Weinreich, Dr. Bartsch, Prof. Pillmann, Prof. Penzel, Dr. Glos, Dr. Steger, Dr. Schöbel, Prof. Schmidt und Dipl.-Ing Müller) bedanken. Der wissenschaftliche Austausch hat mich immer wieder inspiriert und motiviert, weiteren Projekten nach zu gehen.

Ich möchte mich auch bei meinen Kollegen am IMEBI, im NAKO Studienzentrum Halle für die schöne Zusammenarbeit bedanken. Hier möchte ich besonders Prof. Rafael Mikolajczyk und Dr. Alexander Kluttig für die Finanzierung meiner Stelle, die Einführung in die Epidemiologie und Unterstützung bei technischen Fragen danken.

Ich danke Sebastian Meier und Dr. Stefan Förster für das Korrekturlesen meiner Arbeit.

Zuletzt möchte ich mich auch bei meiner Familie für ihre Geduld und Unterstützung bei meiner Promotion bedanken. Insbesondere danke ich meiner Frau für ihre Vertrauen und Motivation in allen Phasen meiner Arbeit.

In dieser Disseratationsarbeit wurden Daten der NAKO Gesundheitsstudie verwendet. (www.nako.de). Die NAKO Gesundheitsstudie wird durch das Bundesministerium für Bildung und Forschung (BMBF) [Förderkennzeichen 01ER1301A/B/C und 01ER1511D], die Bundesländer und die Helmholtz Gemeinschaft gefördert sowie durch die beteiligten Universitäten und Institute der Leibniz- Gemeinschaft finanziell unterstützt. Ich danke allen Teilnehmerinnen und Teilnehmern der NAKO Gesundheitsstudie sowie den Mitarbeiterinnen und Mitarbeitern der NAKO Gesundheitsstudie.

Ich möchte mich bei der Minerva Stiftung für mein Short-Term Research Grant

9. ACKNOWLEDGEMENTS

bedanken, der mir einen längeren Forschungsaufenthalt in Israel ermöglicht hat.

Weiterhin möchte ich mich auch bei der German-Israeli Foundation für den finanziellen Support unserer Studien bedanken.